Late Quaternary Sedimentation
and Stratigraphy in
the Strait of Sicily

*Andrés Maldonado
and Daniel Jean Stanley*

ABSTRACT

Maldonado, Andrés, and Daniel Jean Stanley. Late Quaternary Sedimentation and Stratigraphy in the Strait of Sicily. *Smithsonian Contributions to the Earth Sciences,* number 16, 73 pages, 39 figures, 5 tables, 1976.—The Strait of Sicily, a broad, elongate, topographically complex platform in the central Mediterranean, separates the deep Ionian Basin from the Algéro-Balearic and Tyrrhenian basins to the west. A detailed core analysis shows that the late Quaternary sections in the different sectors of the Strait are distinct from those in the deep Mediterranean basins. Strait lithofacies are characteristically uniform, highly bioturbated, and contain significant amounts of coarse calcareous sediment. Five major sediment types (coarse calcareous sand, sand- to silt-size sediment, ash, mud, and sapropel) are grouped into natural vertical successions termed sequences. The three major sequences defined in the Strait are upward-coarsening and upward-fining, uniform, and turbiditic (including both mud and sand-silt turbidites); sapropel sequences are recovered in cores on the Ionian slope east of the Strait.

The direct relation between sediment type, lateral lithofacies distribution, water depth, and structural displacement is demonstrated. For example, the proportion of turbiditic mud increases while that of hemipelagic mud and bioturbated strata decreases with depth. The effects of regional Quaternary events, particularly climatic changes and eustatic sea level oscillations, are well recorded in cores collected in shallow platform and neritic-bathyal environments; here the upper sediment sequences are truncated and fining- and coarsening-upward sequences, which include coarse calcareous sand layers interbedded with mud and sandy lutite, prevail. In contrast, well stratified units comprising sand (including gravity flow units and volcanic ash) alternating with hemipelagic and turbiditic mud form the surficial deposits in the deep (>1000 m) elongate Linosa, Pantelleria, and Malta basins. Homogeneous bioturbated light olive gray to dusty yellow muddy sequences predominate in the intermediate depth neritic-bathyal environments.

Stratigraphic correlation of cores based on carbon-14 analyses shows that individual units or sequences are not correlatable across the Strait or even within small basins, although it is possible to recognize a general vertical succession of depositional patterns. Sedimentation rates generally decrease with increasing depth. Rates in the deep basins have been relatively uniform from the late Quaternary to the present, while upper (Holocene) sequences in the shallow platform and neritic-bathyal environments have been truncated. Correlation of reflectors on high-resolution subbottom profiles indicates that faulting in many sectors of the Strait is of recent or subrecent origin and that the vertical displacement rate is locally in excess of the average sedimentation rate (i.e., greater than 20 cm per 1000 years).

The absence of sapropel layers in the Strait basins indicates that these depressions remained ventilated during periods when anaerobic conditions prevailed in the deep basins in the eastern and central Mediterranean. An early Holocene paleooceanographic model depicting a possible reversal of currents in the Strait of Sicily region is postulated.

Contents

Late Quaternary Sedimentation and Stratigraphy in the Strait of Sicily

Andrés Maldonado
and Daniel Jean Stanley

Introduction

GENERAL

The Strait of Sicily is the submerged surface of the large topographic high which separates the Ionian Sea in the eastern Mediterranean from the Tyrrhenian and Algéro-Balearic seas in the western Mediterranean. This morphologically complex platform lying between Sicily and Tunisia is long, broad, and trapezoid-shaped (Figure 1). The Strait comprises shallow banks, ridges, volcanoes (including submerged mounts and islands), gentle depressions, and deep basins, and its relief (which locally exceeds 1000 m) and morphologic configuration are considerably more irregular than those of most shelves and continental borderlands.

A sedimentological investigation of this region is warranted for several reasons: the Strait includes a series of highly varied environments; it is geologically and hydrographically distinct from the large, deep basins bordering the Strait; and, to date, comprehensive regional studies have not been made relating processes and deposits in time and space. Earlier studies of the Strait of Sicily have emphasized sediments in the shallower en-

vironments (Blanc, 1958, 1972; Poizat, 1970; Akal, 1972; Emelyanov, 1972; Colantoni and Borsetti, 1973). The sedimentation patterns in the deeper environments have received less attention (Blanc, 1958; U.S. Naval Oceanographic Office, 1965, 1967; Emelyanov, 1972; Chassefière and Monaco, 1973; and an ongoing investigation of the "Campagne Gesite 1973" materials collected by the Station de Géodynamique de Villefranche of the University of Paris, Blanc-Vernet et al., 1975 and C. Bobier, personal communication).

The present study defines the major Quaternary lithologic facies in the various Strait environments and compares the sedimentation patterns in this region with those of the adjacent, but much deeper, Balearic and Ionian basins. More specifically, this investigation establishes the relationship between sedimentary processes, associated facies, and sedimentary environments of the Strait. Sedimentary sequences, defined on the basis of recently collected core data, are interpreted in light of the Quaternary dynamics which affected the Mediterranean region.

ACKNOWLEDGMENTS

Andrés Maldonado, Sección de Estratigrafía y Sedimentología, C.S.I.C., Universidad de Barcelona, Avenida de José Antonio, 585, Barcelona, Spain. Daniel Jean Stanley, Division of Sedimentology, National Museum of Natural History, Smithsonian Institution, Washington, D.C. 20560.

FIGURE 1.—Strait of Sicily showing major physiographic features discussed in text and position of cores and bottom camera data used in study. (Chart base is Mediterranean Sea chart N.O. 310, Defense Mapping Agency Hydrographic Center; depth in fathoms: 1 fm = 1.829 m.)

This study was made possible primarily with the aid of the following: Smithsonian Research Foundation; Consejo Superior de Investigaciones Cientificas (CSIC); Laboratoire de Géodynamique Marine, Villefranche-sur-Mer (CNRS); Lamont-Doherty Geological Observatory of Columbia University; Marine Geology and Geophysics Laboratory, National Oceanic and Atmospheric Administration, Miami; Program of Cultural Cooperation between the United States of America and Spain; Rosenstiel School of Marine and Atmos-pheric Science of the University of Miami; U.S. Naval Oceanographic Office (NAVOCEANO); and Woods Hole Oceanographic Institution.

Bottom and subbottom profiles, core samples and bottom photographs were collected on the R/V *Atlantic* (AS 6), 1965–1967; R/V *Chain 61;* USNS *Lynch II,* 1972; R/V *Vema 14;* R/V *Pillsbury,* 6510; R/V *San Pablo* and N/O *Charcot,* 1973. The captains, officers, and crew of these ships are thanked for support so efficiently given in the work at sea. We thank Dr. R. Stuckenrath of the Smith-

STRUCTURAL-STRATIGRAPHIC FRAMEWORK

The Strait of Sicily platform occupies a geologically strategic position between the deep, fault-bounded basins of the Balearic, Tyrrhenian, and Ionian seas and the emerged North African and southern European regions bounding it. Most workers envision this shallow area as a prolongation of the Tunisian-Southern Sicilian land mass and as a link between the North African Atlas chain and the Sicilian-Italian Apennine chain. The different tectonic provinces of the Strait region have been defined and mapped by Burollet (1967) and Zarudzki (1972). Seismic reflection exploration has provided both deep penetration (excellent Flexotir records of Finetti and Morelli, 1972a, b) and shallower subbottom coverage (Woods Hole Oceanographic Institution sparker and air gun profiles, Zarudzki, 1972).

Flexotir records show that this zone, separating the distinct eastern and western Mediterranean geodynamic sections, consists of thick continental crust comprising a generally thin Pliocene-Quaternary unconsolidated section above a thick sequence of Triassic to Miocene rock units (Finetti and Morelli, 1972a). The reduced thickness of unconsolidated Pliocene and Quaternary sediments (except in some depressions such as the Malta Graben where these exceed 1 second, penetration two-way travel time) can be contrasted with the thick sections in the Balearic Basin west of the Strait. The underlying Upper Miocene units, correlated with limestone and dolomite sequences in cores and land sections, thicken toward Tunisia (Burollet, 1967).

There is ample evidence of geologically recent (post-Miocene) structural displacement, and the different morphological-tectonic sectors of the Strait can be related to major fault patterns. Magnetic and gravity studies reveal that the main structural trends are oriented west northwest-east southeast, i.e., parallel to the major orientation of the Sicily Channel (Allan and Morelli, 1971; Morelli, 1972; Colantoni and Zarudzki, 1973; and others). A northeast-southwest trend predominates at the westernmost sector of the Strait (Auzende, 1971; Auzende et al., 1974). The largely vertical structural displacement gives rise to a complex configuration of horsts (shallow tabular-shaped banks) and grabens (narrow, deep linear basins). Seismic profiles clearly display the vertical and subvertical offset of reflectors. The intensity of structural offset and seismicity (shallow earthquake epicenters), and the concentration of vol-

canoes (most are submarine cones) increase in the northern sector of the Strait.

The islands of Linosa and Pantelleria reflect the importance of Pliocene and Quaternary eruptions in this part of the Mediterranean. Pantelleria, interpreted as a composite stratovolcano, rises from the 1300-m-deep Pantelleria Basin. The position of other volcanic deposits, including some which accumulated in historic time, are plotted by Zarudzki (1972, fig. 3) and Finetti and Morelli (1972a, fig. 5); these are concentrated mostly in the northern sector of the Strait. The presence of dike swarms or narrow lava streams are also suggested on the basis of magnetic anomalies and appear aligned parallel to the principal tectonic provinces. Some Mesozoic and early Tertiary intrusions also have been penetrated by petroleum exploratory wells.

In terms of regional Mediterranean-Alpine tectonics, the thick crustal sections of the platform are considered part of the African Plate, which underthrusts the Euro-Asiatic plate in the Ustica-Lipari region of Sicily (Caputo et al., 1970). Finetti and Morelli (1972b, fig. 19) also emphasize the role of compression but prefer to relate plate motion to subduction of the African Plate below what they define as the Mediterranean Plate. Like most geophysicists, these latter authors tend to agree that much of the Mediterranean—in particular the deep basins bounding the Strait—has undergone considerable subsidence since the end of the Miocene. Benson (1972) has proposed that the Strait platform was deeper during the Pliocene than at present. The development of vertical faults with offsets to 1000 m in the upper crust is believed to reflect isostatic adjustment following the main Alpine orogeny. Additional structural offset may also be due to alternating phases of compression and distension. Zarudzki (1972) relates the gentle folding of the more than 300 m of section in the northwest end of the Pantelleria Trough, as observed in continuous seismic profiles, to the above-cited recent, postorogenic tectonic activity. The fault development, volcanism, and seismicity of this region are not unlike those postulated in some subduction models (tension and rifting behind the leading edge of a subducted plate margin, cf. Isacks et al., 1968, fig. 7; Ninkovich and Hays, 1972, fig. 12, and others). An interpretative diagram showing the origin of this modern rift-tension relief in

the Strait and associated volcanism in relation to subduction is presented by Akal (1972, fig. 16).

That volcanic activity, fault displacement, and sedimentation have been concurrent is clearly of importance in this study. These Quaternary neotectonic factors will be emphasized in the context of sedimentary processes and sedimentation rates in the Strait region. Physiographic and structural considerations are considered in greater detail in later sections.

HYDROGRAPHY

The general hydrographic and current trends in the central Mediterranean and Strait of Sicily region are reasonably well known (cf. Lacombe and Tchernia, 1960, 1972; Wüst, 1961.) The dominant pattern is one of exchange of two well-defined water masses, one flowing above the other in opposite directions. This exchange across the broad, shallow platform is similar to, but not as intense as, the one measured in the narrower Strait of Gibraltar some 1280 km to the west. The water flowing across the Strait of Sicily must pass over a series of sills (eastern and western sills at opposite ends of the Strait) and across a much longer and broader area than that at Gibraltar.

Surface waters, primarily of Atlantic origin, move toward the east-southeast at velocities of 10 to 90 cm/sec (Frassetto, 1972). The lower part of this water mass extends to depths of 200 to 300 m (depths increase in winter) and has a salinity of approximately 37.4‰; temperatures are seasonably variable (13° to over 23°C). Below this lies the Intermediate or Levantine water, which originates by convective sinking of cooled surface water in the Levantine Basin east of the Strait. The Intermediate water, with an average salinity of 38.7‰ and temperature of about 14°C, flows from the Ionian Basin across the sill toward the western Mediterranean. This water mass fills the deep Strait basins and is renewed rapidly as a result of the undercurrent (Morel, 1972). The exchange between Surface and Intermediate water is related to the higher evaporation rates in the eastern Mediterranean which entrain the less saline waters as a replacement (outgoing versus ingoing flux calculations are provided by Morel, 1972). Deep waters in the Ionian and Balearic basins are
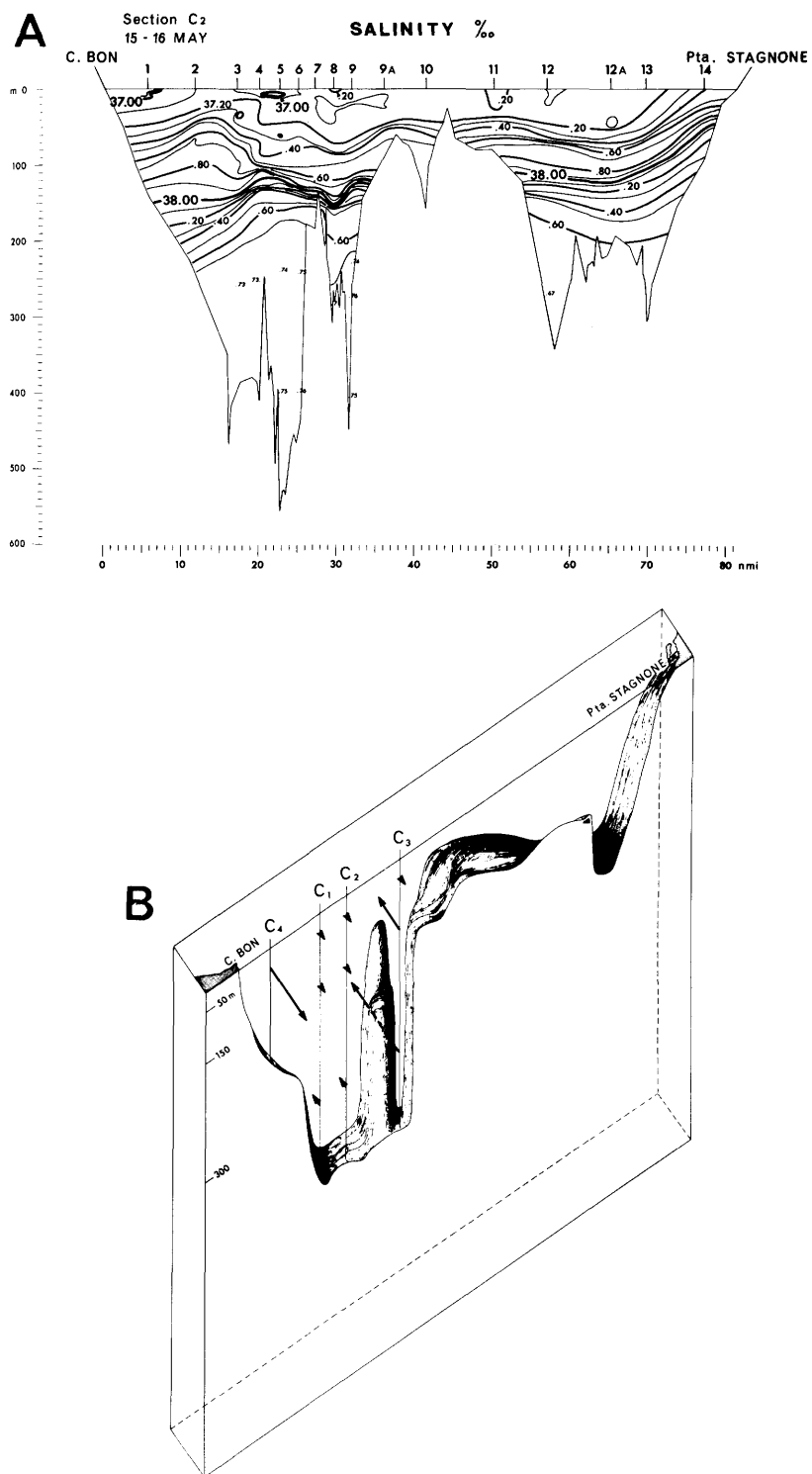
FIGURE 2.—Profiles across the Strait of Sicily Narrows between Punta Stagnone near Marsala, Sicily, and Cape Bon, Tunisia: A, salinity profile in May 1970; B, opposite current flow patterns of the Levantine and less saline surface water masses. (From Molcard, 1972.)
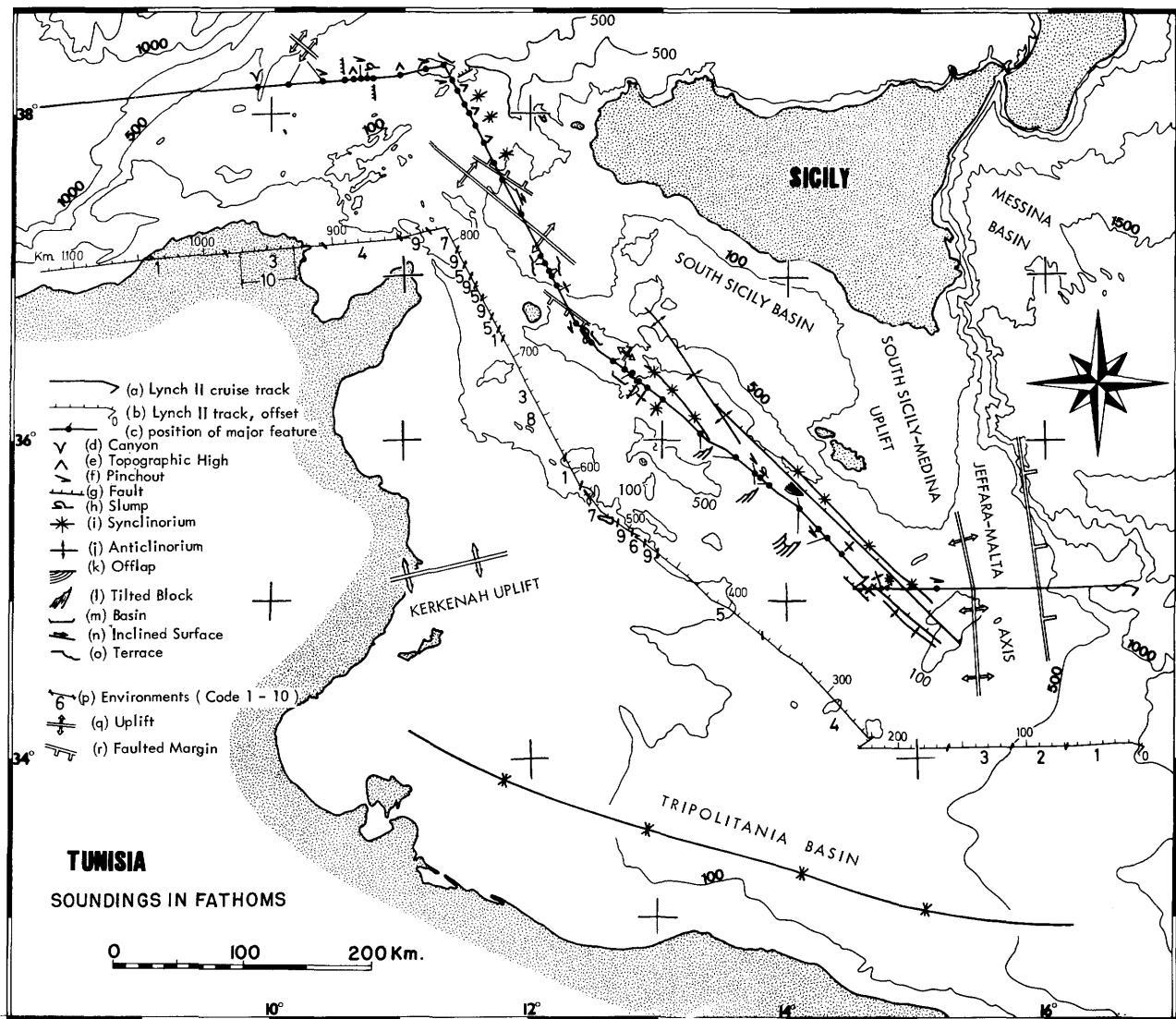
FIGURE 3.—Track (dark solid line) of the USNS *Lynch* (cruise II, 1972) in the Strait of Sicily region. The dominant structural features observed on 3.5 kHz and 30,000 J sparker are depicted (explanation in text). The specific topographic environments (code 1 to 10) are displayed on the thin line (offset from the track line); these are defined in the text. The scale on this line is shown in kilometers (a total of about 1100 km between the Ionian slope east of the Strait and the Algéro-Balearic Basin). The major structural trends of the Strait are also depicted (modified after Burollet, 1967; Finetti and Morelli, 1972a, b; Zarudzki, 1972).

blocked by the sill and do not cross from the eastern to western Mediterranean.

The surface waters are a source of suspended sediment in the form of pelagic tests (planktonic foraminifera, etc.) and terrigenous fraction (over 1.0 mg/1, according to Emelyanov and Shimkus, 1972). The influence of this Atlantic water should

be more intense on the Tunisian margin inasmuch as the flow is thicker and less saline in this sector than on the Sicilian side. On the other hand, Levantine water flows along the sea floor and is thus an agent of transport and erosion as we shall demonstrate in later sections (Pierce and Stanley, 1975). Further transport is perhaps also related to

TABLE 1.—Position, water depth, and length of Strait of Sicily cores analyzed in this study (specific environment, defined in text, and geographical location of each core also listed)

CRUISE	CORE NO.	LATITUDE	LONGITUDE	WATER DEPTH (in m)	CORE LENGTH (in cm)	ENVIRONMENT	GEOGRAPHIC LOCATION
Lynch II	3	35°02'N	16°42'E	2432	575	(1)	Ionian Slope
	4	35°05'N	14°30'E	604	380	(4)	Pelagian Shelf
	5	36°25.3'N	12°46'E	1089	332	(6)	Pantelleria Intermedian Basin
	5A	35°34'N	12°30'E	1257	600	(7)	Pantelleria Trough
	6	38°16.8'N	11°19.8'E	1217	500	(7)	North Marittimo
	6A	38°13.2'N	10°57.2'E	755	610	(5-4)	Galite
	7	38°02.7'N	8°09.2'E	2588	342	(1)	Tyrrhenian-Balearic Slope
Pillsbury 6510	34	36°22'N	12°33'E	1294	109	(7)	Pantelleria Trough
	33	36°27.5'N	13°28.5'E	1549	119	(7)	Malta Trough
Atlantic Seal 6	8	36°22'N	11°13'E	93	555	(8)	Tunisian Shelf
	7	37°19.6'N	12°39.5'E	183	770	(8)	Adventure Bank
San Pablo 8	7	37°56'N	11°09.9'E	350	540	(8-4)	Strait Narrows
Vema 14	138	36°19'N	14°48'E	124	245	(8)	South Sicily Uplift
	139	36°28'N	13°31'E	1703	576	(7)	Malta Trough
	140	37°10.5'N	11°47.5'E	166	420	(8)	Strait Narrows
Chain 61	19	35°46.6'N	13°05.8'E	1475	1030	(7)	Linosa Trough
Gesite 73	KS 12	37°33.2'N	11°29.0'E	956	700	(6)	Strait Narrows
	KS 23	37°26.5'N	11°24.5'E	1200	725	(7)	Pantelleria Trough
	KS 33	36°37.0'N	12°05.0'E	1164	715	(7)	Pantelleria Trough
	KS 53	36°08.4'N	12°51.7'E	805	678	(4-5)	Linosa Platform
	KS 63	35°42.8'N	13°14.9'E	1428	850	(7)	Linosa Trough
	KS 69	35°50.4'N	13°02.3'E	1484	608	(7)	Linosa Trough
	KS 76	35°50.6'N	13°03.2'E	1463	740	(7)	Linosa Trough
	KS 78	35°29.2'N	13°42.9'E	769	659	(5-4)	Pelagian Shelf
	KS 100	35°58.7'N	13°52.8'E	1088	669	(6)	Malta (Intermediate) Basin
	KS 104	36°31.6'N	13°26.6'E	1087	208	(6)	Malta (Intermediate) Basin
	KS 105	35°47.7'N	13°18.5'E	580	626	(4)	South Sicily Basin
	KS 109	36°27.3'N	13°12.2'E	1688	732	(7)	Malta Trough
	KS 110	36°27.9'N	13°08.0'E	1492	110	(7)	Malta Trough
	KS 118	35°46.9'N	13°09.7'E	1493	825	(7)	Linosa Trough
	KS 120	35°51.1'N	13°02.8'E	1454	701	(7)	Linosa Trough
	KS 125	35°59.6'N	12°36.0'E	785	785	(5-4)	Linosa Platform

turbulence, vertical mixing, and internal waves formed along the shear zone between the two water masses.

Short-term current-measurements above the bottom at the western end of the Strait (Figure 2) between Cape Bon (Tunisia) and Punta Stagnone (Sicily) revealed currents in excess of 30 cm per second (Molcard, 1972). Velocities to 50 cm per second have been recorded by other workers (Lacombe and Tchernia, 1972). Bottom photographs in the same region, which show crinoids heeling over (cf., Akal, 1972, fig. 8, upper right), provide further evidence of the strong current flow above the sea floor.

METHODOLOGY

The basic material for this study was collected during the March-April 1972 cruise of the USNS *Lynch* (LY II–72). Positioning of the ship was

made with satellite and radar navigation. Seven Ewing piston cores were retrieved along a transect between the Ionian and Balearic basins crossing different environments of the Strait. Continuous (*3.5* kHz) echo-sounding and sparker (*30,000* Joules) records were obtained along the ship track (Figure 3). These subbottom profiles have been reduced photographically to the same horizontal scale (Figures 5–15).

Additional core data have been obtained from the following organizations (Figure 1, Table 1): United States Naval Marine Geophysical Survey Program 1965–1967, Area 6, cores AS 6–7 and AS 6–8 (U.S. Naval Oceanographic Office, 1967); University of Miami cores P 6510–G33 and P 6510–G34; Groupe des Géologues Marins Mediterranéens, Campagne "Gesite"–1973, cores KS 12, KS 23, KS 33, KS 53, KS 63, KS 69, KS 76, KS 78, KS 100, KS 104, KS 105, KS 109, KS 110, KS 118, KS 120 and KS 125; Lamont-Doherty Geological Observatory, cores *Vema 14,* 138, 139, and 140, and *San Pablo 8,* 7; Woods Hole Oceanographic Institution, core *Chain 61,* 19. A total of 32 cores have been analyzed by us for this study (Figure 1). A set of deep-sea camera station photographs (Figure 1) was provided by the Lamont-Doherty Geological Observatory (station *Vema 14,* K 53) and six camera stations from Woods Hole Oceanographic Institution (stations *Atlantis 151,* 56, 58, 59, 60, 61, and 62). The camera station positions are listed in Table 2.

The *Gesite* cores were X-radiographed before splitting, while *Lynch* and *Pillsbury* cores were radiographed (half cores) after splitting and before sampling. Detailed core logs record texture, sedimentary and biogenic structures, color, and other characteristics observed visually and on X-radiographs. Gross texture and composition of the sand and lutite fraction of over 200 selected samples have been processed for mineralogical analysis. The relative percentages of 14 compositional components of the sand fraction in 48 of these samples have been calculated. The lutite fraction (silt plus clay) was examined by means of the Scanning Electron Microscope; samples prepared for SEM analysis were soaked in 30% hydrogen peroxide for at least 24 hours to destroy organic matter. The core thickness sampled ranged from 4 to 12 mm.

Large samples of mud (comprising between 15

TABLE 2.—Position and water depth of camera stations in the Strait of Sicily

CRUISE	CAMERA STATION	LATITUDE	LONGITUDE	WATER DEPTH (in m)
Vema 14	K-53	36°29'N	13°23'E	1588
Atlantis 151	56	36°25'N	11°43'E	119
	58	37°12'N	11°34'E	567
	59	37°18'N	11°33'E	88
	60	37°18'N	11°07'E	106
	61	38°22'N	11°23'E	381
	62	38°14'N	11°31'E	134

to 45 cm of core section) were sieved and the fraction coarser than 63 microns extracted for radiocarbon dating. Carbon-14 age determinations also have been made on bulk samples of about 15 cm-long sections of cores. Our tests have shown that dates obtained with the total (or bulk) core samples provide comparable dates to those obtained with the coarse fraction. We favor dating with bulk samples inasmuch as it allows us to use much less core for dating. A total of 40 samples were age-dated (R. Stuckenrath, Smithsonian Radiocarbon Laboratory, pers. comm.).

In calculating sediment thicknesses on subbottom profiles we have assumed an average velocity of 1800 m per second (Finetti and Morelli, 1972a, b); the scales in the figures are given in two-way travel time.

Defining the Major Strait Environments

GENERAL

In this study "Strait of Sicily" is the general geographic term applicable to the entire region between Tunisia and Sicily. The term "Strait Narrows" is applied to the narrowest passage (about 160 km in width) between Cape Bon (Tunisia) and Punta Stagnone or Marsala (southwest coast of Sicily). The Strait trends in a northeast-southwest direction and is approximately 450 to 700 km in length. It is broadest (over 500 km) along a north-south transect between southeast Sicily and Libya. Recent charts (Carter et al., 1972; Finetti and Morelli, 1972a) of the central Mediterranean show that the total area exceeds 175,000 km², and that over one-third of this surface (approximately 80,000 km²) is shallower than
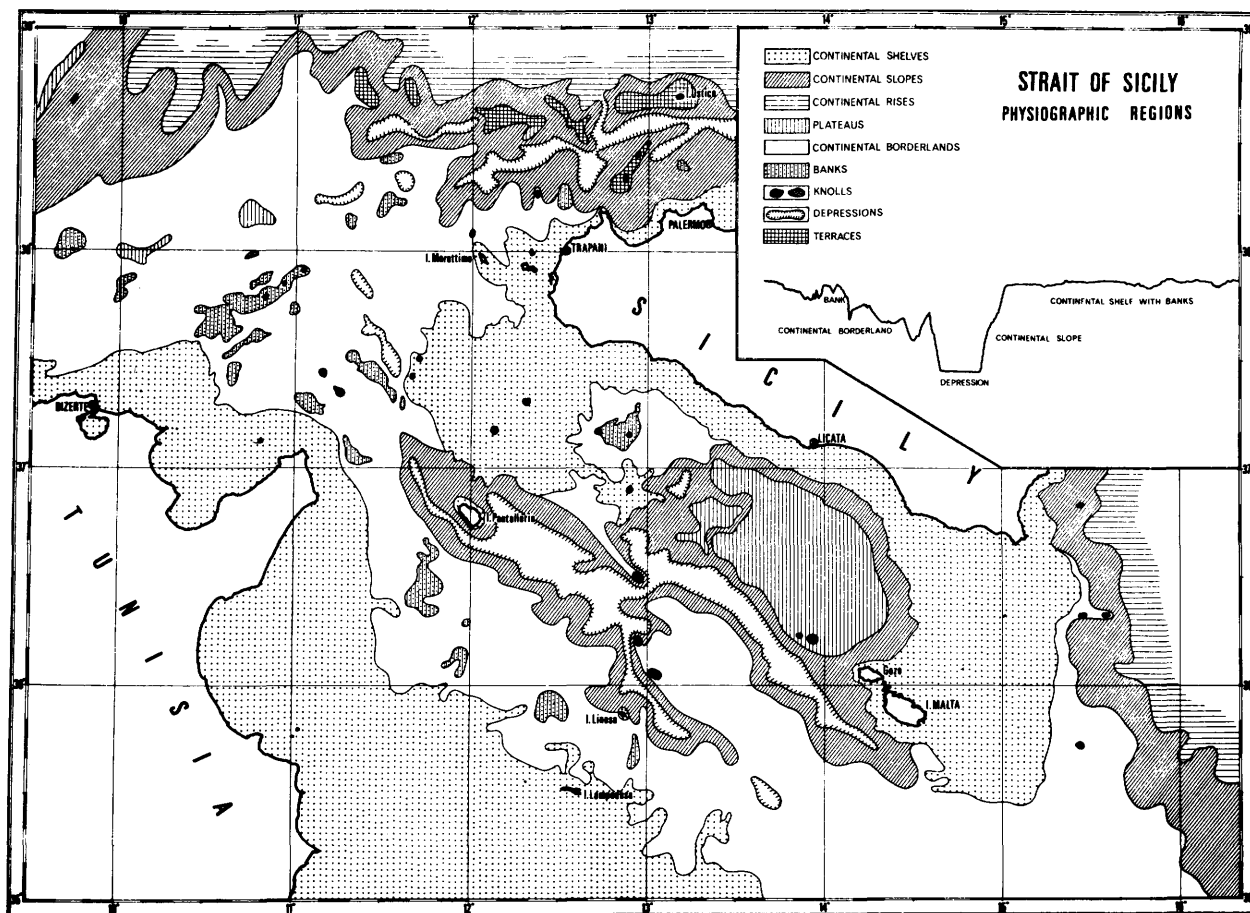
FIGURE 4.—Physiographic chart of the Strait of Sicily showing highly irregular topography of this region. (From Akal, 1972.)

200 m (shown as shelf on Figure 4). The deeper, elongate regions, including deep basins, known by some authors as the Sicily Channel, parallel the main trend of the Strait platform, i.e., northwest–southeast. Three narrow, steep-walled, elongate basins (Malta, Pantelleria, and Linosa) are 1700, 1300, and 1600 m in depth, respectively. These three distinct depressions are separated from each other by a neritic bathyal platform. The Gela or South Sicily Basin is a shallower but much larger basin lying south of Sicily and northwest of Malta. The larger islands include Malta and Gozo, Pantelleria, Linosa, Lampedusa, Kerkennah, Galite, Marettimo, and Djerba south of the Gulf of Gabes.

The region is characterized by some extensive, shallow, generally flat-topped or tabular, platforms of which the one east of Tunisia and the South

Sicily-Medina and Adventure Banks south of Sicily are the largest (Figure 1).

Of particular interest are the two shallow banks at both ends of the Strait Platform: Skerki Bank (Blanc, 1958), north-northwest of Cape Bon, and Medina Bank, southeast of Malta. These elongate topographic highs serve as important barriers to water masses flowing across the platform. These shallow platforms at opposite ends of the Strait platform are also called Eastern Sill and Western Sill.

Names assigned to the various other morphological features depicted in Figures 1 and 3 are shown on charts in Blanc (1958), Burollet (1967), Allan and Morelli (1971), and Carter et al. (1972).

In the Strait six major physiographic units or morphological-sedimentary environments are rec-
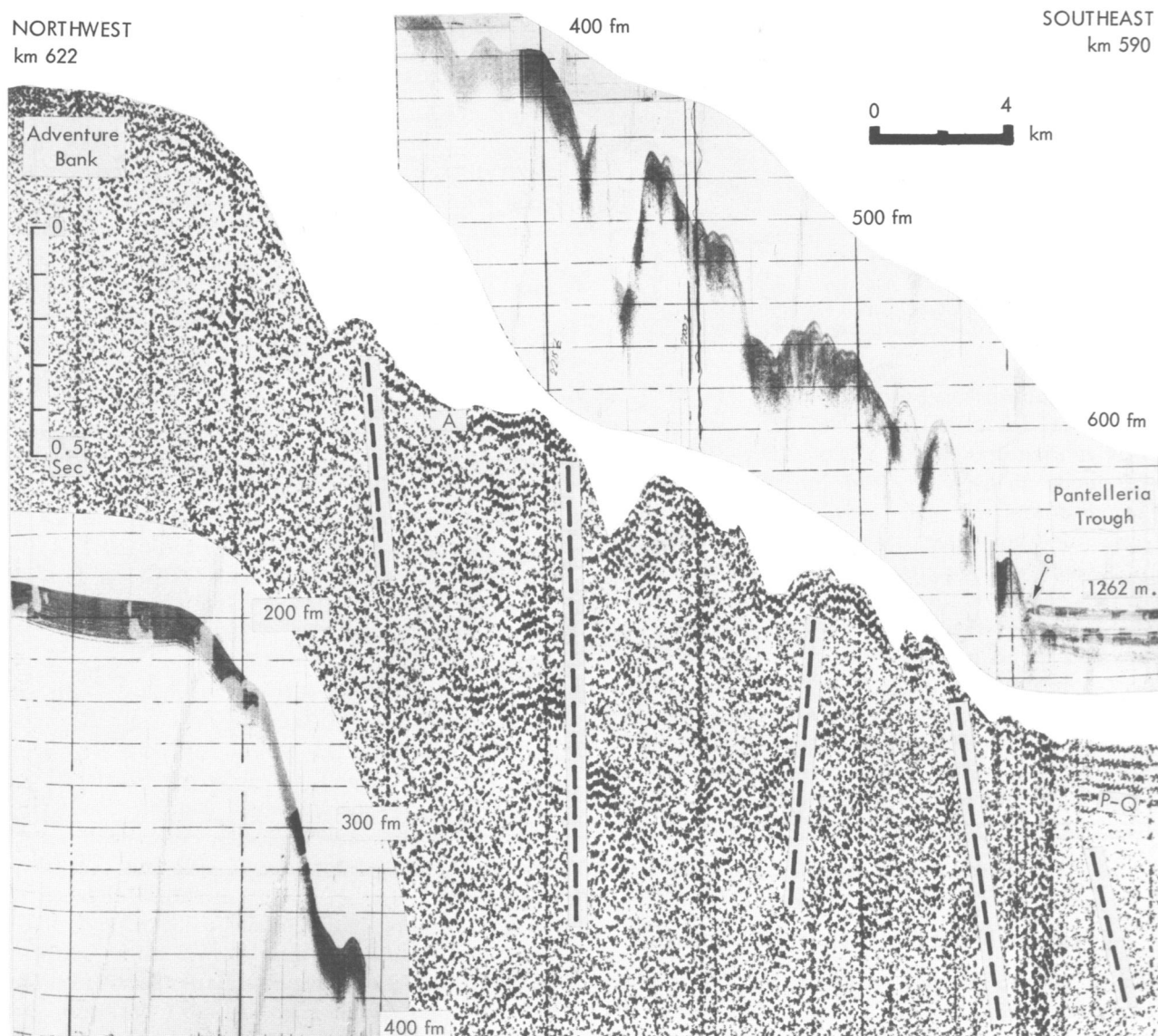
FIGURE 5.—Sparker (30,000 Joules) and 3.5 kHz profiles (spacing between horizontal lines is 20 fms, or 37 m, in all 3.5 kHz records) reproduced at the same horizontal scale showing slope transect from Pantelleria Trough to Adventure Bank. Near-horizontal Pliocene and Quaternary (P–Q) sediment of the basin distinct in both records is shown abutting against the base of the slope, which appears relatively free of sediment cover. (Some of the normal faults are indicated by the dashed lines. Depth in seconds, two-way travel time.)

ognized: (a) slope; (b) neritic-bathyal borderland; (c) basin; (d) shallow platform (shelf and bank); (e) marked topographic high (submarine mounts, volcanoes, diapirs, etc.); and (f) canyon. Two of these units (b, c) can be subdivided. In addition, the Strait Narrows (g) between Cape Bon and Marsala is considered as a separate entity. A total of 11 environments (Figure 3) are identified, and these are defined in following sections.

These sections also describe the structural configuration of the unconsolidated sediment sequences (largely Pliocene and Quaternary, P–Q) that lie above Miocene and older units as observed in seismic records. The top of the consolidated

Miocene is identified and correlated with sequence A of Finetti and Morelli (1972a, b).

Environments

Slope (Environment 1).—The slopes considered here are those that flank the Strait of Sicily on the east (Ionian) margin and the west (Algéro-Balearic) margin, and steep slopes which bound the major deep basins of the Strait. A transect from Pantelleria Trough to the Adventure Bank (km 590 to 615, on Figure 3) crossing a slope of the type discussed here is shown in Figure 5. This highly irregular slope appears on 3.5 kHz records as a series of single or multiple hyperbolic patterns. Poor definition of stratification or sediment ponding is in part an acoustic artifact (roughness and steepness of the slope); poor penetration also may be due to a reduction of the unconsolidated sediment cover.

Outcrops of older Tertiary deposits have been reported from slopes bounding the major basins of the Strait (Colantoni and Borsetti, 1973). Such slopes average about 2.5°, but attain much higher values locally; they commonly display a steplike configuration as a result of fault offsets (Figure 5).

Two cores retrieved from this environment show rather distinct lithofacies: core LY II–7 on the Algéro-Balearic margin includes an alternating sequence of turbidites and hemipelagic mud, while core LY II–3 on the Ionian Basin margin comprises distinctive gray to black organic-rich sapropel layers as well as turbidites and hemipelagic mud.

Neritic-Bathyal Borderland (Environments 2, 3, 4, 5).—Somewhat more than half of the Strait area lies within a depth range of 200 to 700 m. This zone is morphologically complex and the sparker profiles reveal the importance of vertical structural displacement that has broken the sea floor into a complex net of horsts and grabens. Four subzones are recognized.

Outer Margin, Faulted (Environment 2): An outer margin, faulted zone, distinguished at the eastern end of the Strait (km 68–115, Figures 3, 6A), comprises the transitional area between the Strait proper and the margin slopes. The sea floor on the 3.5 kHz records presents an irregular, rugged topography with a reduced sediment cover. This area corresponds to the faulted and flexured

zone defined by Burollet (1967) and Finetti and Morelli (1972a).

Broad Uplift (Environment 3): This zone includes those areas occupying positive structural axes (Burollet, 1967); e.g., the South-Sicily Medina Uplift, Jeffara-Malta axis (km 110–160, Figure 6c), and the northeastern extension of the Galite Archipelago (km 908–983, Figure 6B_1, B_2). The latter is deeply cut by a canyon. These areas are characterized by a broad, convex-up topography (probably gentle anticlinal-like folds) and small distinct valleys. Faulting is not as prominent a feature in this zone as in the other outer margin environments of the Strait. The reduced sediment cover on the convex-up topography suggests a slow, uniform rate of sediment accumulation, or erosion by bottom currents (Pierce and Stanley, 1975), or both.

Neritic-Bathyal Platform (Environment 4): The neritic-bathyal platform includes essentially flat, depressed areas although the sea floor in this zone is not completely confined as are the basins. Depositional processes dominate here. Two platform sectors are traversed: the Pelagian Shelf, km 160–365 (Figures 7, 8), and the Galite Platform, km 850–908 (Figure 9).

The platform environment is characterized by thick sequences of deposits which pinch out locally on topographic highs (cf. symbol on Figure 3, km 160, km 908) and less frequently on the platform proper (Figure 7, a, km 305; km 780). Thinning of strata is the result of simultaneous deposition and vertical fault offset, which may also result in the development of an offlap sequence (Figure 8, a, km 325) or truncation. Growth-faults (Figure 7) with thickening of sediment layers on the down-thrown block are observed; similar phenomena are described by Hardin and Hardin (1961) in the Gulf of Mexico.

The fault offsets observed in seismic records are associated with tilted blocks, small grabens and horsts (Figure 7), and small mounts (Figure 9, km 880). The ratio of height to width of these tectonically displaced blocks is approximately 1 to 100; the maximum throw of these faults observed in our records is about 200 m (Figure 7); and the maximum topographic relief is about 170 m. Displaced (slumped) Quaternary deposits (Figure 8, b, km 365; Figure 9, a, km 870), and gentle anticlinal (km 220) and synclinal (km 180, km 200) struc-
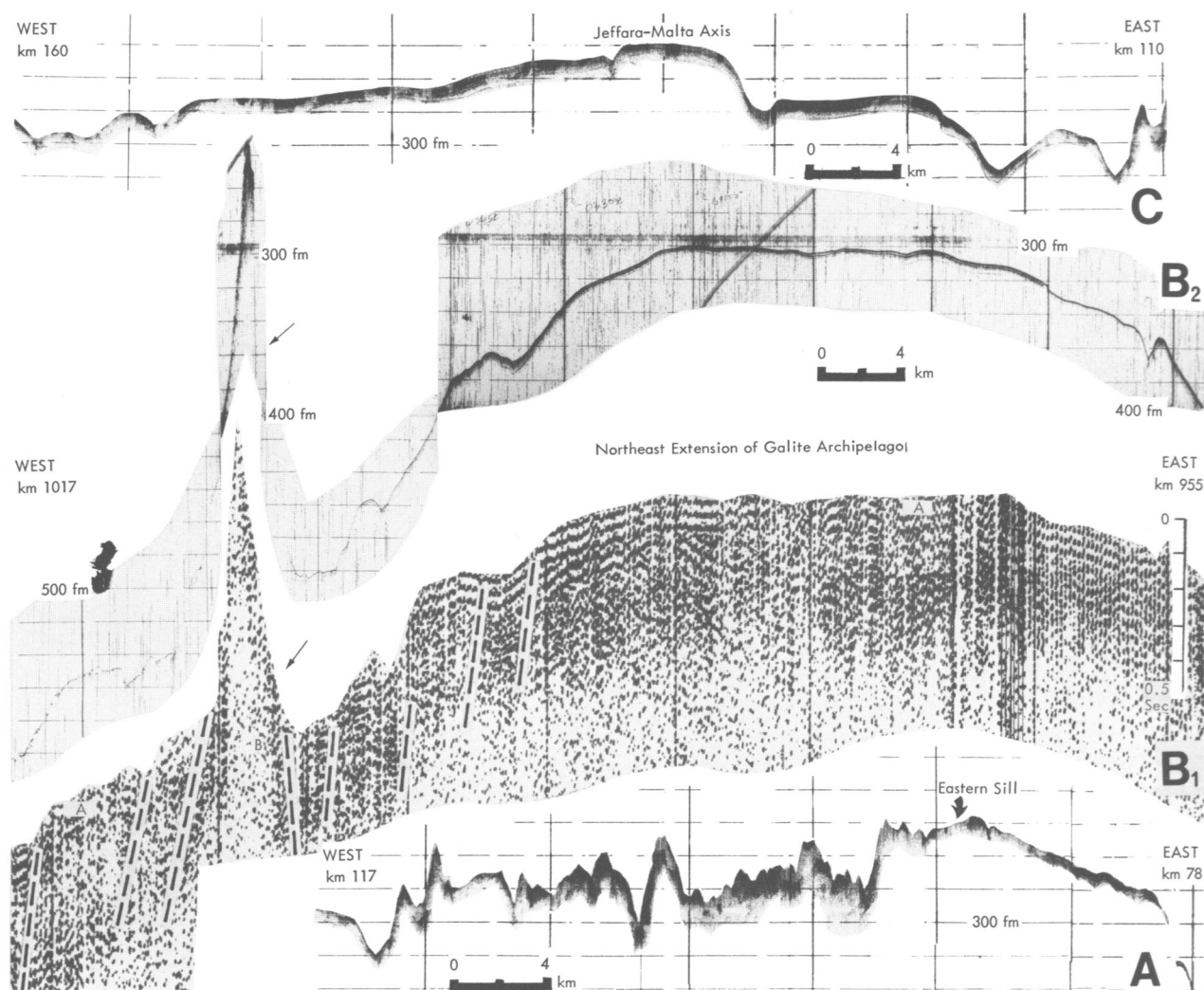
FIGURE 6.—Selected 3.5 kHz and sparker records of neritic-bathyal environments: A, Outer margin, faulted at eastern end of the Strait; note reduced sediment cover on the 3.5 kHz record. B_1 (sparker) and B_2 (3.5 kHz), Across the northeast extension of Galite archipelago (arrows denote marked topographic high (? volcano, B); note reduced sediment cover). c, South Sicily Medina Uplift, Jeffara-Malta axis, showing some sediment in contrast to A; steps and other topographic breaks are almost certainly fault-controlled.

tures are also observed in this environment (cf. Figure 3).

The thickness of the Pliocene-Quaternary sediment section recorded on sparker profiles is highly variable. An average of 0.4 seconds (or 360 m, two-way travel time) is generally present throughout the area; it thickens to 0.7 seconds (630 m) in the axis of the depressions (Figure 7, arrow b) and is reduced or absent on mounts. If a velocity of about

1800 m per second is assigned to these unconsolidated Pliocene-Quaternary sequences (Finetti and Morelli, 1972a, b), we estimate a sediment thickness which ranges from 0 to about 650 m.

Cores collected in this neritic-bathyal platform environment (LY II–4, KS 105) and those from the zone of transition to the next environment ("Neritic-Bathyal Depression" environment discussed in the following section) (LY II–64, KS 78,
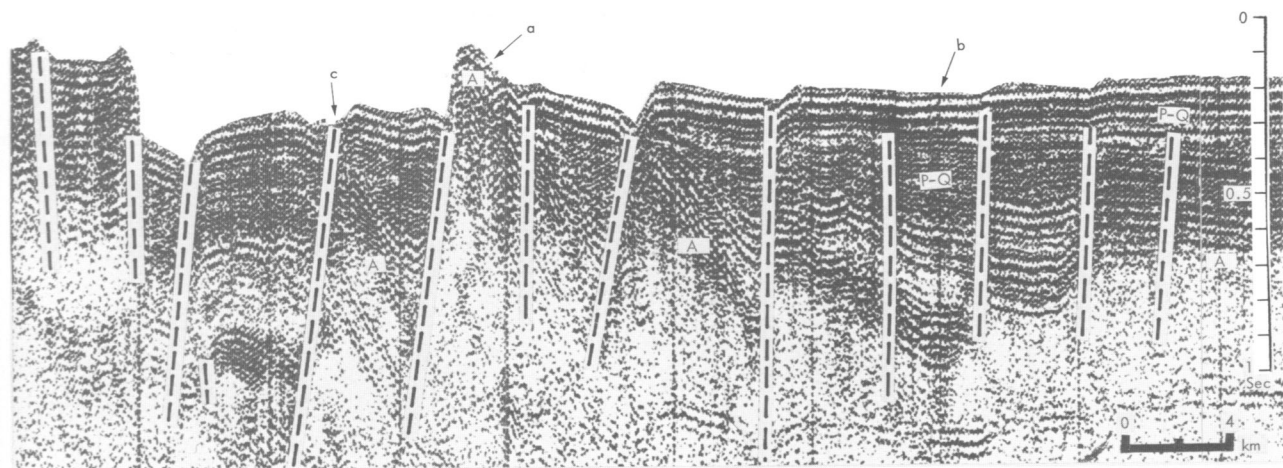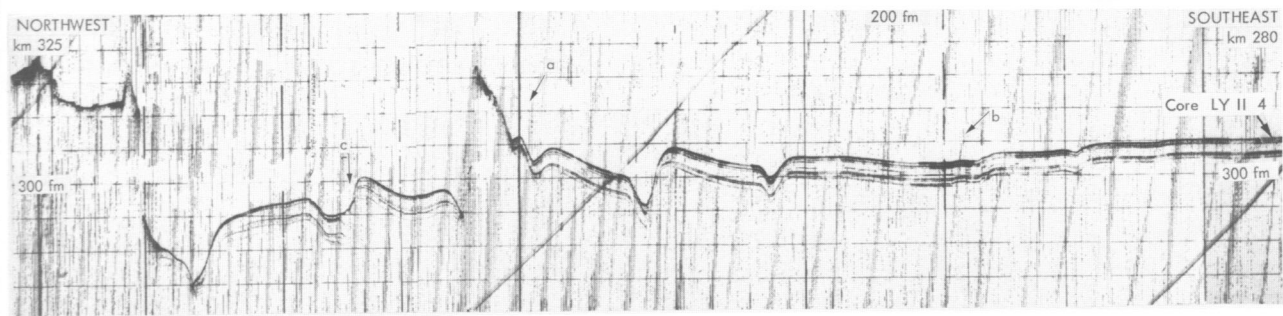
FIGURE 7.—Example of neritic-bathyal platform environment, showing marked topographic irregularities and displacement of the Pliocene and Quaternary (P–Q) and pre-Pliocene (A) sediment sequences by fault offset (*a* = pinchout of surficial sediment cover, *b* = thickening of sediment on a downthrown block, *c* = recent fault scarp exposing uppermost sedimentary sequences).
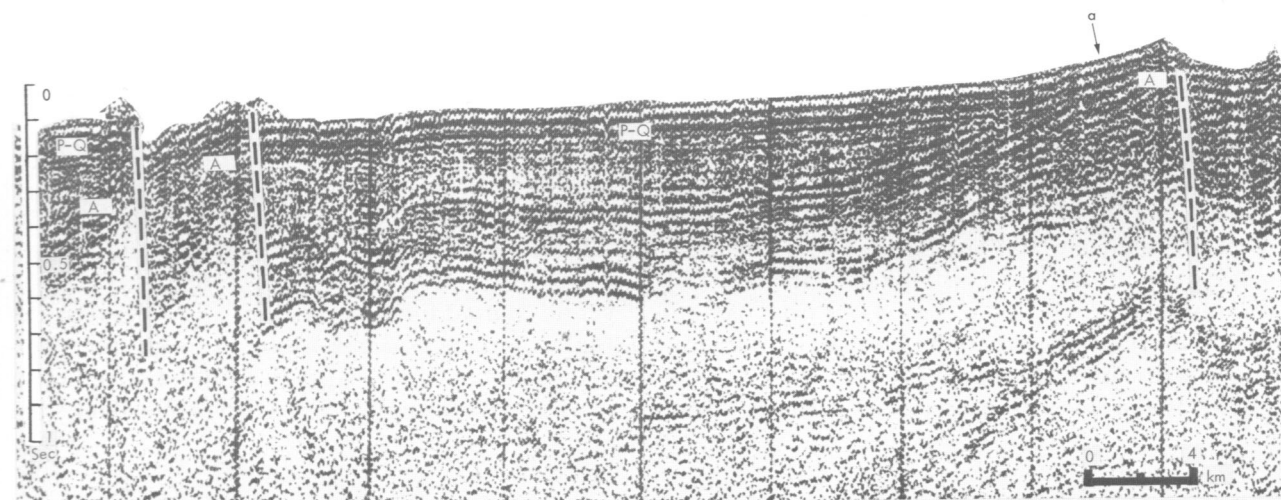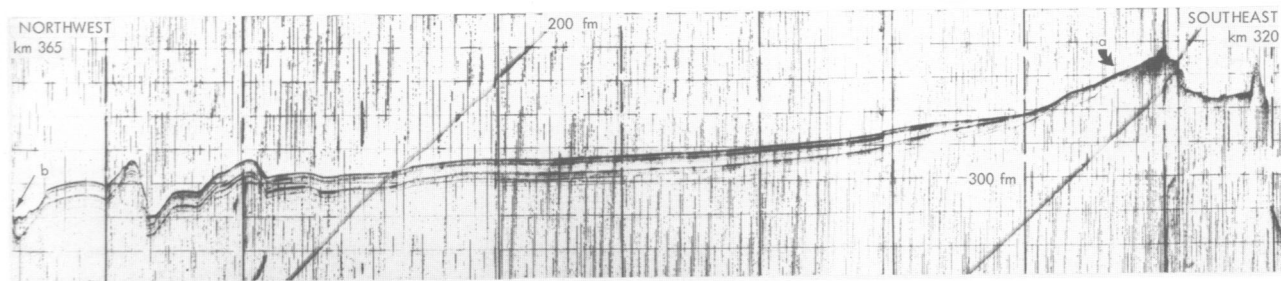
FIGURE 8.—Neritic-bathyal platform (Pelagian Shelf) showing the offlapping of the Pliocene-Quaternary (P–Q) cover off an actively uplifted block (arrows *a*). Note also slumping of recent sediment in a small fault-produced depression (arrow *b*).
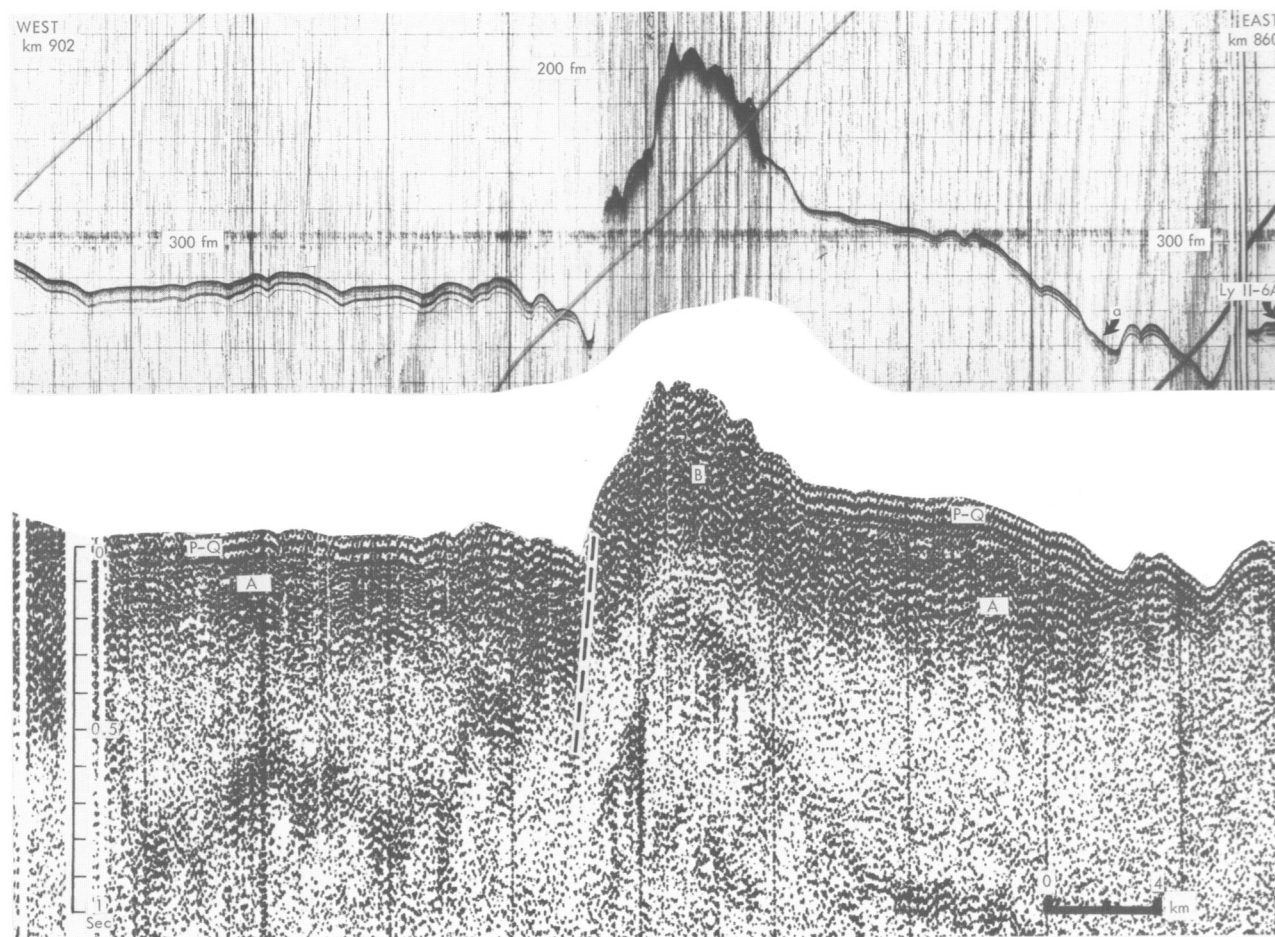
ғɪɢᴜʀᴇ 9.—Neritic-bathyal platform (near Skerki Bank) showing topographic high (horst) underlain by basement (B) and reduced, deformed Pliocene-Quaternary (P–Q) cover. Accumulation of recent sediment is noted in small depression (arrow a).

KS 125) display a characteristic lithological uniformity. No prominent sand layers are recovered and only subtle structures are revealed in the core X-radiographs. Bioturbation structures are present throughout the cored sedimentary sequences.

Although the cores are generally structureless it should be noted that some laterally continuous reflectors can be traced on the 3.5 kHz records; these reflectors are locally displaced vertically by faults. The limited length of the cores has not allowed recovery of sediment sections forming some of these major subbottom reflectors. However, their lateral continuity suggests some process which has resulted in their regional distribution; this mechanism is discussed later.

The importance of neotectonics affecting these

reflectors is readily apparent. The high-resolution 3.5 kHz profiles show that faulting has occurred after deposition (Figure 7, arrow c). In some localities tectonic displacement and sedimentation rates have occurred simultaneously, resulting in the development of pinch-out (Figure 7, arrow a) and offlap sequences (Figure 8, arrow a). The youngest faults reveal a vertical throw of as much as 50 meters (Figure 7, arrow c).

Neritic-Bathyal Depression (Environment 5): There are numerous depressions on the borderland, and four of these have been traversed: the gentle Malta-Linosa depression, a low between the Malta Trough and the Linosa Trough (km 365–470, Figures 10, 11), and three smaller, more marked depressions, north of Adventure Bank (km
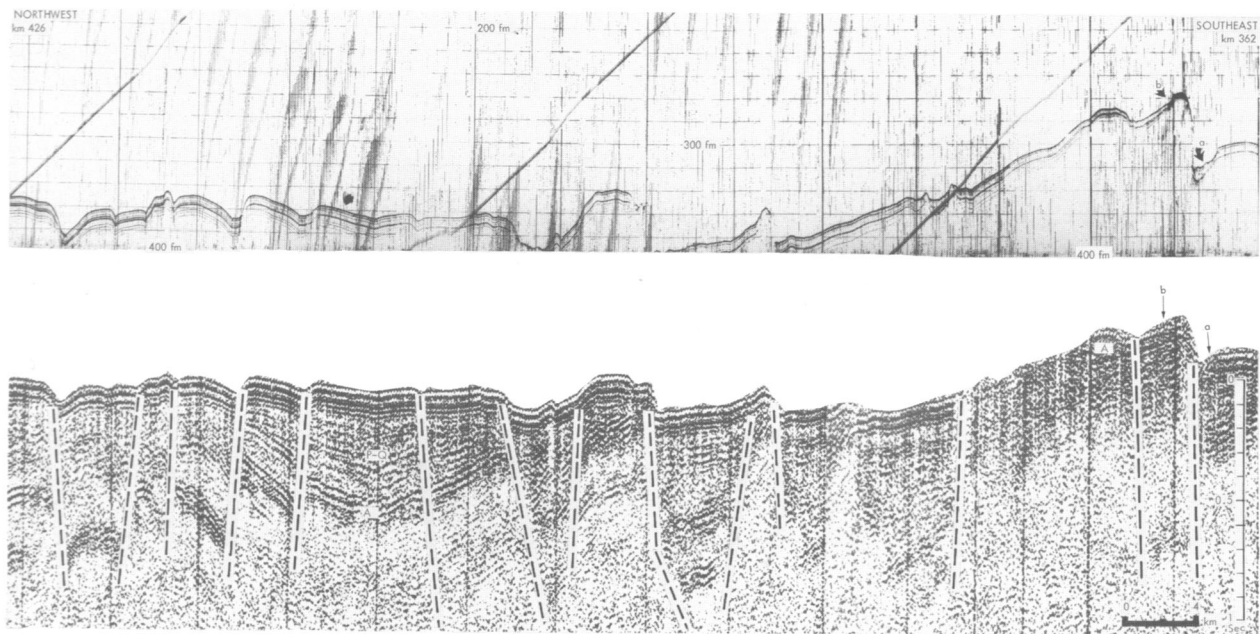
FIGURE 10.—Neritic-bathyal depression, between Malta and Linosa troughs, showing vertically displaced (locally thickened) section of Pliocene and Quaternary (P–Q) sequences. Fault displacement at *a* is over 100 m. (See Figure 11 for continuation of profiles.)
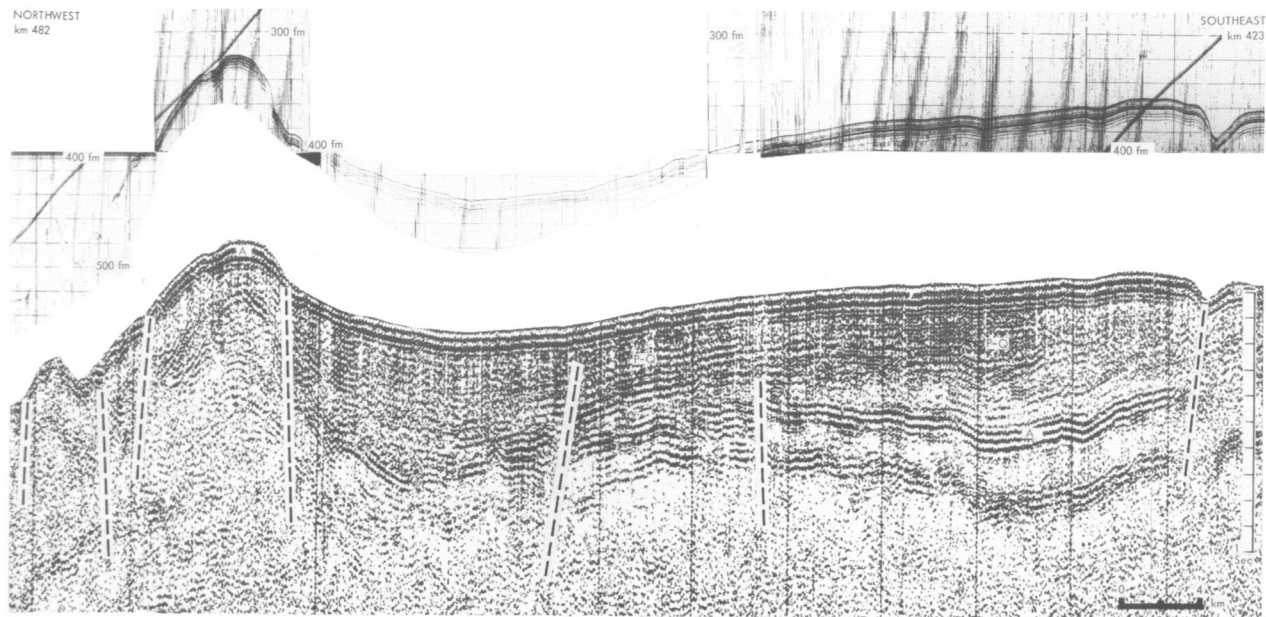
FIGURE 11.—Neritic-bathyal depression between Malta and Linosa troughs (continuation of profiles on Figure 10) showing truncation by fault offset of the Pliocene and Quaternary (P–Q) cover at the edge of the depression.

725–735, km 750–762 in Figure 12, and km 770–780 in Figure 13B$_1$, B$_2$). The transition between some of these depressions and the Neritic-Bathyal platform is subtle. These depressions are differentiated from the adjacent platform surfaces on the basis of a thicker sedimentary cover (range from 0.5–0.8 seconds, 450–720 m), broad basinal morphology, and a marked tectonic pinching out of the sedimentary sequences against the depression margins.

The Malta-Linosa depression is wide (105 km) and displays vertical tectonic structures analogous to those described on the platform (Figures 3, 10, 11). Structurally, this depression is a gentle syncline without major sea mounts or knolls; seismic profiles show the faulted margin of the depression. The fault which has affected the most surficial reflectors displays a downthrow of over 100 m (Fig-

ure 10). This depression extends north of Linosa Island and forms the northwest end of the Pantelleria Trough (Zarudzki, 1972:20). The Pliocene-Quaternary strata are truncated by faults at the edge of the depression.

The small northwestern basin (km 770–780, Figure 13B$_1$, B$_2$) is characterized by intense folding and distortion of the sediment within the depression, suggesting compression (cf. Zarudzki, 1972). This zone provides evidence of recent tectonic movement as indicated by the tilting and folding of the surficial reflectors visible in the 3.5 kHz records (Figure 13B$_2$).

The Gela Basin (Zarudzki, 1972), also called the South Sicily Basin (Finetti and Morelli, 1972), is located between the Malta Trough and Sicily and may be assigned to this environment.

Sediments in cores are characterized by their ap-
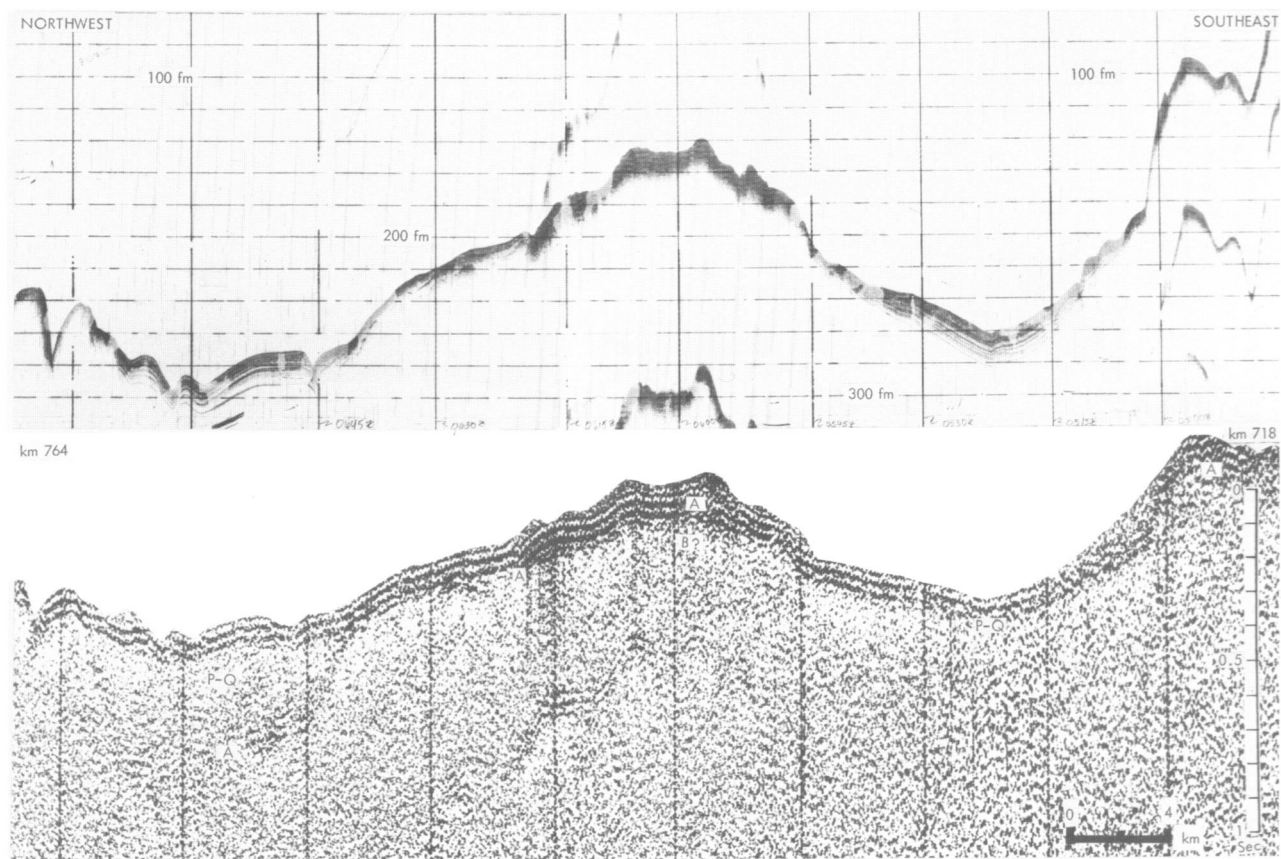
FIGURE 12.—Profiles north of Adventure Bank showing two distinct, small depressions on the neritic-bathyal borderland. Note topographic high devoid of Pliocene-Quaternary sediment cover between the depressions.
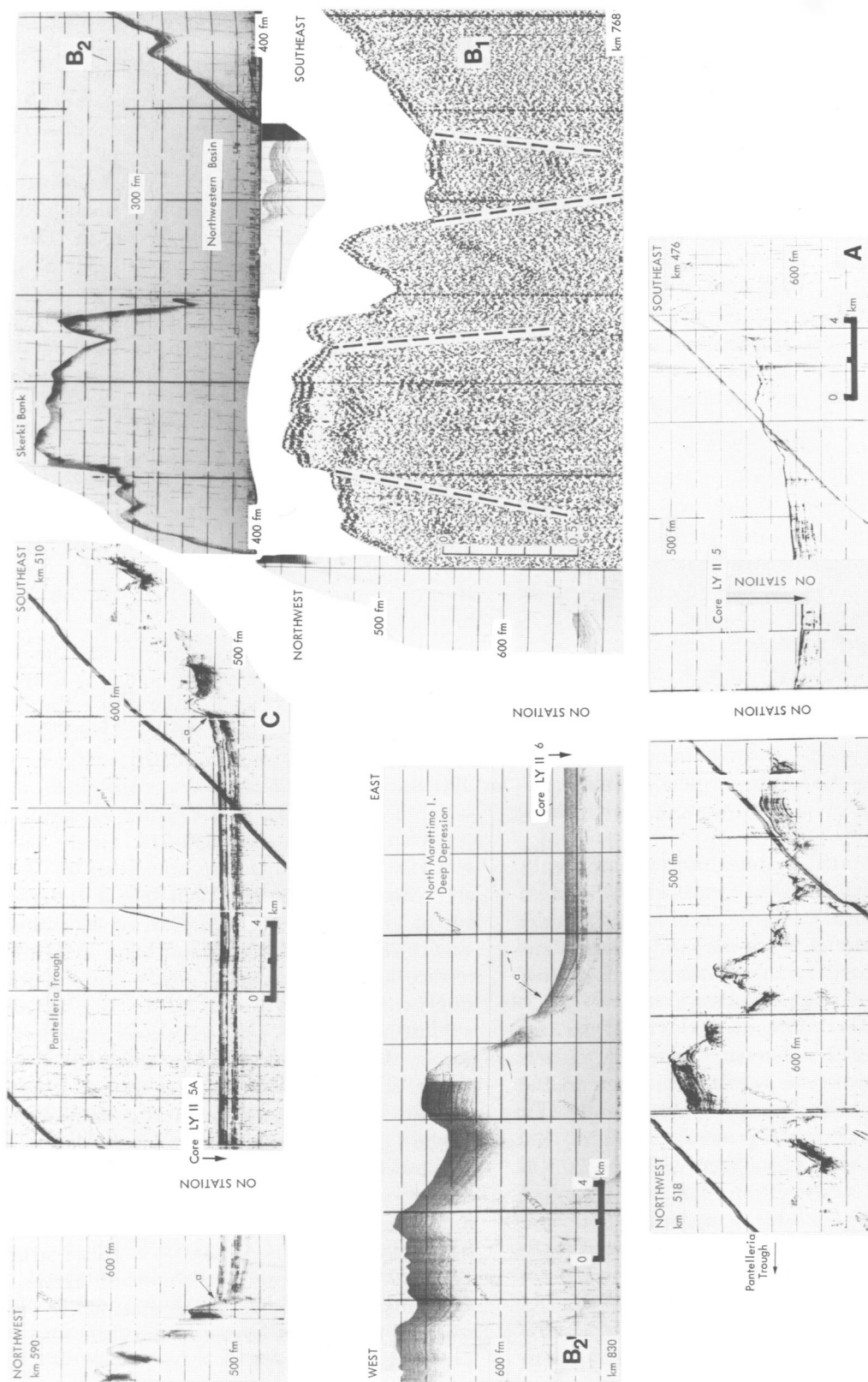
FIGURE 13.—Selected 3.5 kHz and sparker (B₁) profiles showing examples of neritic-bathyal depression (B₁ and B₂) and basins (A = intermediate; B₂′ and C = deep). 3.5 kHz profiles reveal the horizontal strata in North Marettimo deep depression (B₂′) and in the Pantelleria Trough (C). These sequences are truncated (arrow a) by basin-margin faults at edge of the basin plain.

parent uniformity and lack of stratification (i.e., core KS 53). However, it is possible to individualize some vertically graded mud turbidite sequences on the basis of X-radiography. The reflectors on the 3.5 kHz records are more apparent in this environment than on the flatter platform. As in the case of environment 4 these reflectors do not appear to correlate with prominent layers in the cores.

BASIN (Environments 6, 7).—This zone includes the major elongate, troughlike basins of Malta, Pantelleria, and Linosa, as well as small basins occurring either as deep depressions on the continental borderland and on the slopes of the three major deep troughs. Two subdivisions are made, based on the depth and aerial importance of these basins.

Intermediate Depth Basin (Environment 6): The intermediate depth basins are small depressions, partially enclosed and characterized by a considerable thickness of sediment. Figure 13 (A, km 480–495) shows one of these basins located on the slope of the Pantelleria Trough.

Visual examination of split cores collected in this environment (i.e., cores LY II–5, KS 100, KS 104) reveals sedimentary sequences almost as uniform as those in environments 4 and 5. X-radiographs, however, show enhanced stratification attributed to turbidite sequences and a decrease in the degree of bioturbation, particularly in the deeper basins.

Core KS 12, located in one intermediate depth basin in the Strait Narrows, is exceptional because it shows well-marked stratification and includes several coarse layers of bioclastic sand. These characteristics, attributed to the particular geographic position of this core, are discussed later.

Deep Basin (Environment 7): Three narrow, deep, elongate basins, accounting for somewhat less than three percent of the Strait area, occur in the center of the Strait and all three parallel its northwest-southeast trending axis: (1) Malta, 150 km long and 30 km wide; (2) Pantelleria, 90 km long and 30 km wide (Figure 13c); (3) Linosa, 75 km long and 17 km wide. Respective depths are about 1700, 1300, and 1600 m. Other basins, such as the one west of Marettimo Island (Figure 13B₂') also have been sampled (cf. core LY II–6).

The three deep, troughlike basins stand out by their straight, fault-bounded steep walls apparent

in seismic profiles (Figure 5); they have been interpreted as grabens related to postorogenic faulting (Zarudzki, 1972; Finetti and Morelli, 1972a). These deep basins have trapped a thick sequence of unconsolidated sediments; approximately 1000 m of sediments (to about 1.2 seconds penetration) are measured in the Malta Trough (Finetti and Morelli, 1972a). The bottom is a smooth, flat surface resulting from sediment accretion. The strata pinch out sharply against the walls of the depression, and no prominent rise is developed at the foot of the slope (Figure 5, *a;* Figure 13B₂', c).

Cores collected in the deep basins show distinct stratification and the most diverse assemblage of sediment types observed in the Strait. The most characteristic types are turbidite sequences, but terphra (ash) layers are also important locally. Bioclastic sand layers are present, usually at the base of the turbidite sequences. Evidence of slumping is also noted in some basin cores (i.e., core 139, *Vema 14*). Orderly layering and lateral continuity of strata are apparent on the 3.5 kHz records (Figure 13).

SHALLOW PLATFORM (Environment 8).—About 45% of the surface of the Strait is shallower than 200 m. The seismic profiles show that the shallow platform, for the most part, is covered by a considerably reduced unconsolidated sediment cover. The unconsolidated strata are gently tilted, tectonically offset, and truncated (Figure 14, arrow *a*).

Adventure Bank (km 630–718, Figure 14) is essentially a horst structure consisting of Tertiary and Mesozoic deposits. Well-defined terraces are cut at about 107 (± 3) m (arrow *b*) and at 140 (± 10) m (arrow *c*) on some bank margins. The terrace at 140 m forms a gently dipping seaward slope, which may represent a foreshore surface.

Most of the bank surfaces are characterized by a gentle slope, interrupted by small mounts and gentle depressions. This topography is largely the result of alternating erosion and deposition related to the Quaternary oscillations of sea level; recent structural activity, including diapirism and volcanism, also has affected this zone. In this respect, submarine mounts on the northern Adventure Bank have been interpreted as diapiric structures (Zarudzki, 1972), and the southeast extension of this bank is interpreted as the most active volcanic area in the Strait (Finetti and Morelli, 1972a; Zarudzki, 1972).
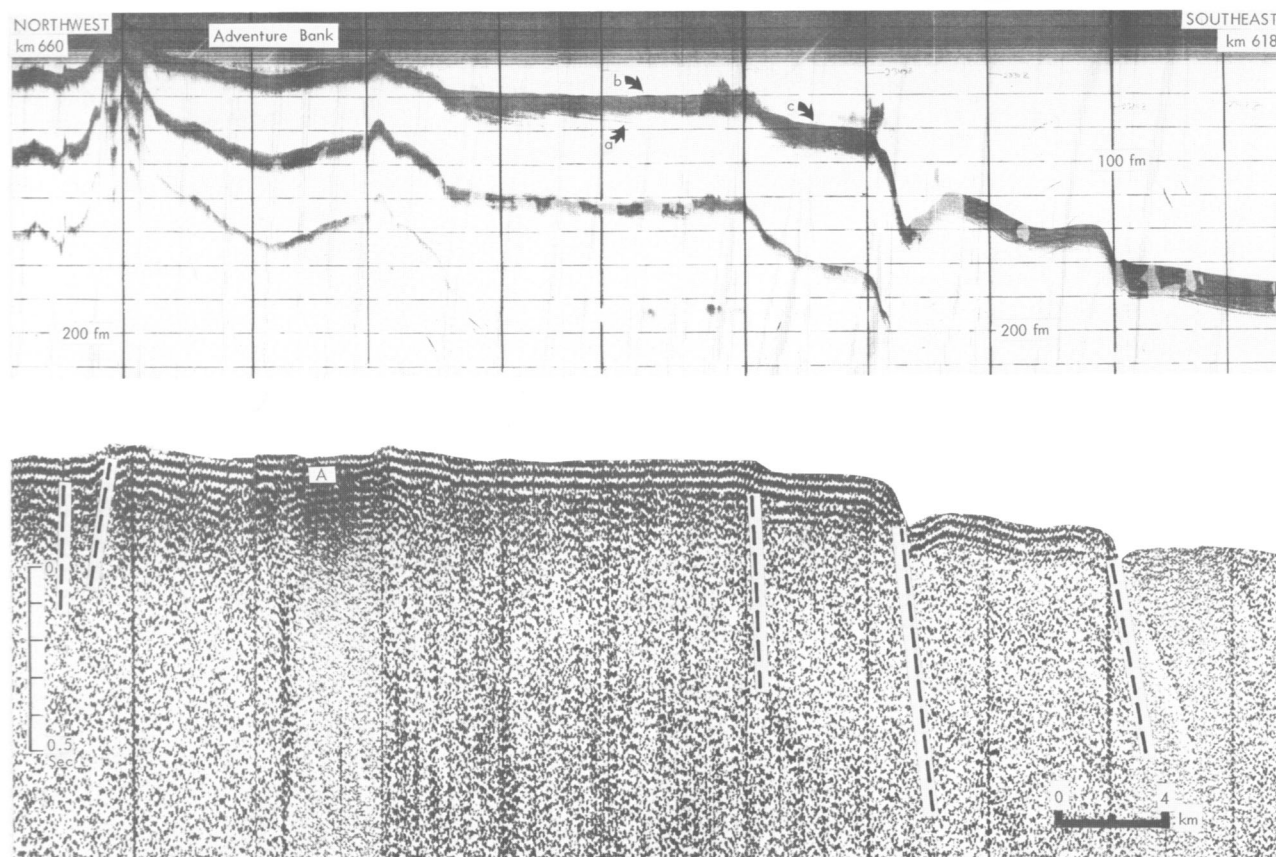
FIGURE 14.—Profiles across part of Adventure Bank off southwest Sicily showing reduced unconsolidated cover above Neogene (A) older units (a = truncated strata, b = terrace at 107 ±3 m, c = terrace at 140 ±10 m).

Maps of the surficial sediment based on bottom photographs, grab samples, and cores (i.e., AS 6–8, AS 6–7, V 14–138, V 14–140) show a mosaic distribution which is not strictly depth controlled. Sediment types include mud to coarse-grained, largely bioclastic and biogenic (calcareous algae, bryozoans, molluscs, foraminifera, etc.) sediment types (cf., Blanc, 1958; Poizat, 1970; Akal, 1972). However, gross texture appears to be broadly related with morphology and depth: coarser sediment types are concentrated on shallow banks and mud in the somewhat deeper and depressed areas.

Layers of cemented crusts and oxidized clasts, mostly biogenic and Pleistocene rock surfaces bare of sediment, are important locally. These horizons can be likened to "hard grounds" recorded in the ancient sedimentary rock record (Blanc, 1958).

MARKED TOPOGRAPHIC HIGH (Environment 9).— The topographic highs are of two major types: (a) those showing a sedimentary cover in the 3.5 kHz records and (b) those without any kind of reflectors or stratification in the records. The first type is in some instances strongly deformed (Figure 13A, km 510), or appears as an anticline (Figure 11, km 470). Some highs without reflectors (an acoustic reflector appears to pierce younger units) can be interpreted as volcanoes (cf., Figure 6B$_1$, B$_2$, km 1010; Figure 9, km 880; Figure 12, km 740), igneous intrusive masses (granite of the Galite Archipelago, Auzende et al., 1974), strongly metamorphosed rock, or diapiric structures (Burollet, 1967; Zarudzki, 1972). The sequence of highs shown in seismic records collected between km 775 and km 790 (Figure 13B$_1$, B$_2$) may represent an extension of the Skerki Bank; this feature displays Quater-
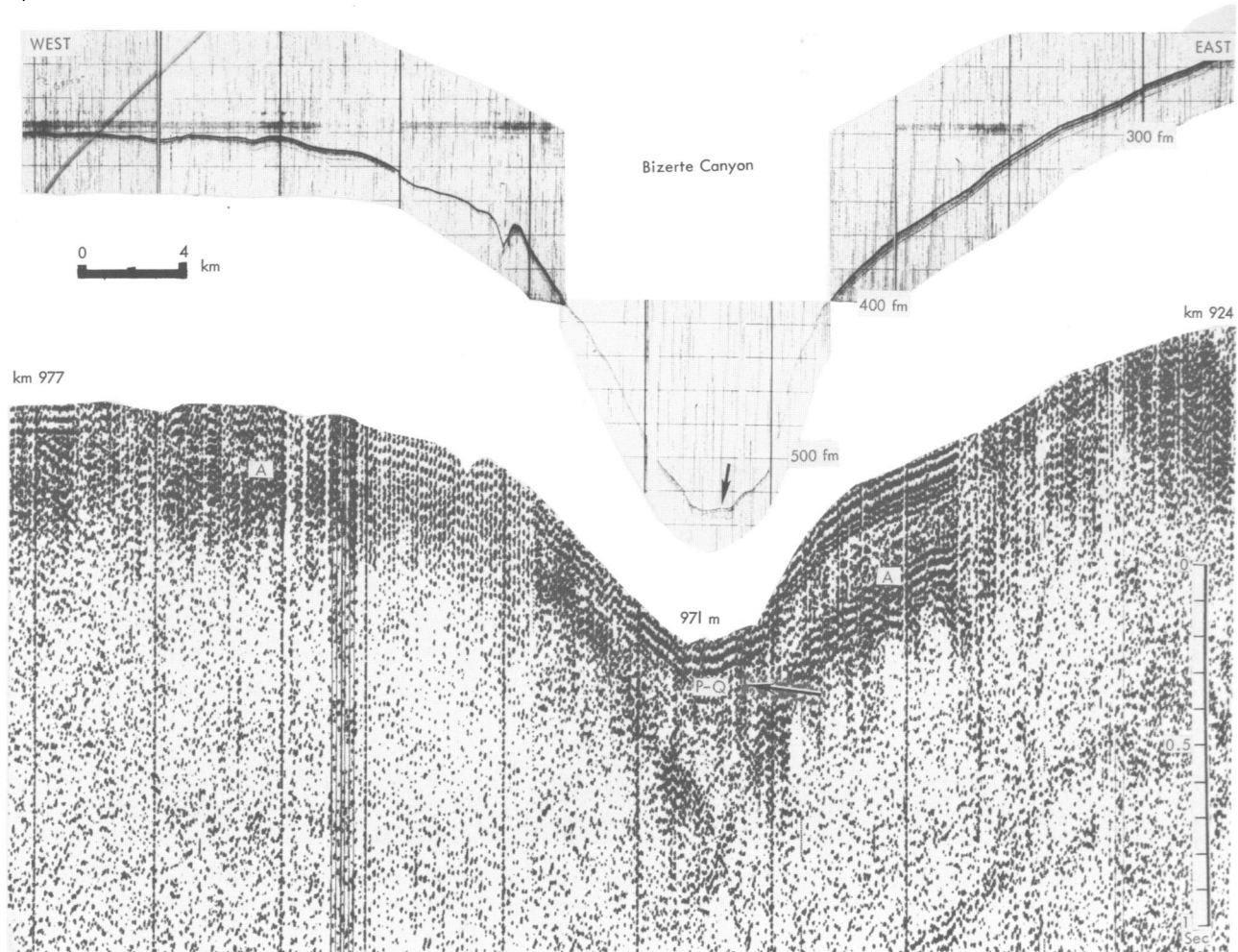
FIGURE 15.—Profiles across the head of Bizerte Canyon showing fault displacement (arrow on sparker record) and unconsolidated sediment in the axis. The irregular configuration of the valley floor (arrow, 3.5 kHz profile) suggests slumping.

nary reef and diapiric structures on its northwest slope (Zarudzki, 1972:18).

CANYON (Environment 10).—One major submarine valley, the Bizerte Canyon, has been recorded in our records on the northern part of the Strait (Figure 15, km 930–970). This canyon extends north-northeast to the Tyrrhenian Basin plain (Carter et al., 1972), and cuts deeply into the northeast extension of the Galite Archipelago (broad uplift environment 3). The eastern wall of this canyon appears somewhat steeper. The sparker profile (see arrow) shows possible fault offset under the canyon axis; this feature may be related with the predominant northeast-southwest structural trend mapped at the western end of the Strait

(Auzende et al., 1974, fig. 3). Unconsolidated Pliocene-Quaternary sequences are recorded in the canyon head; the irregular surface of the axis (arrow on 3.5 kHz record) may be due to displacement of the recent sediment fill.

THE STRAIT NARROWS (Environment 11).—The narrowest portion of the Strait between Sicily and Tunisia presents a diverse topography including shallow banks, intermediate depth basins, and bathyal-neritic environments. Cores in this region are distinctive in that they include a high proportion of coarse bioclastic sand. Core KS 12 (956 meters) in the deeper, small, enclosed basin (environment 6) in the center of the Strait is interesting in this respect. The prominent coarse sand

layers in this core probably were introduced periodically into the depression by turbidity currents and mass flow mechanisms. The organic origin (shells, calcareous algae, and others) of the sediment and the removal of the finest fraction by bottom currents is discussed later.

Sediment Types in the Strait of Sicily

GENERAL DISTRIBUTION OF SEDIMENT TYPES

High-resolution seismic surveys indicate that the unconsolidated section of Pliocene and Quaternary sediments is generally much thinner in the Strait than in the deeper Algéro-Balearic and Ionian basins bounding it. A concentration of distinct reflectors defines the Miocene-Pliocene boundary (contact at top of A in Figures 5–15). Subbottom profiles show that the unconsolidated units are irregularly distributed, i.e., generally thin to absent on topographic highs and thicker accumulations in depressions (Finetti and Morelli, 1972a, b; Zarudzki, 1972). Over 300 m of gently folded, unconsolidated sediment are noted in the northwest sector of the Pantelleria Basin; these may have been transported from the Adventure Bank and Sicily (Zarudzki, 1972). The Malta Basin has trapped a sediment section of about 1000 m (Finetti and Morelli, 1972a), and the Linosa Basin to the south comprises over 1000 m; the latter may be derived from the African craton and adjacent platform (Zarudzki, 1972). A fourth important but shallower (about 700 m) depression, the Gela (or South Sicily) Basin northwest of Malta has ponded over 500 m of unconsolidated sediment according to the above-cited authors. A Flexotir profile trending north northeast–south southwest across this basin (Finetti and Morelli, 1972b, fig. 8a) also shows a thickening of the sediment section toward Sicily and a general southward progradation of the deposits into the Basin.

The grain size distribution of the Strait surficial sediment has been measured by Blanc (1958) and textural maps of this area compiled by the U.S. Naval Oceanographic Office (1965), Fraser et al. (1970), Poizat (1970), Emelyanov (1972), and Akal (1972). Texture appears to be broadly related with morphology: coarser sediment types (silt to sand and coarser) are concentrated on shallow banks, and mud (silt and clay mixtures) in environments deeper than about 200 m (Figure 16). However, detailed mapping of texture, particularly in the shallow environments, indicates that the grain-size pattern is mosaic-like and not strictly depth controlled (Poizat, 1970).

The coarse bioclastic sands are interpreted as current-modified coarse lag deposits resulting from the winnowing of the fine fractions. The bioclastic fragments are reworked as indicated by the local concentrations of oxidized "pralines" (=algal balls, some with volcanic nuclei and cemented crusts; Blanc, 1959, 1972). Oxidized organic fragments include relict Pleistocene faunas, particularly on the shallow banks. These are sometimes entrained into deeper environments by currents or slumping on the margins of shallow banks. Pleistocene rock surfaces bare of sediment are also present. Terrigenous input at river mouths and material provided by erosion along the coast, by wind, and by volcanic eruptions account for only a small fraction of the total sediment cover of the Strait.

Cores collected at shallow to intermediate depths contain alternating mud and coarse bioclastic layers (Akal, 1972; Chassefière and Monaco, 1973). The upper mud and sandy mud layers are oxidized (light yellow coloration) to a depth of 1 m (Blanc, 1958; Chassefière and Monaco, 1973). Neritic-bathyal cores are constituted entirely by mud, while deep basin cores contain alternating sequences of sand, volcanic ash, and mud layers. Fines, presumably winnowed from bank areas, are transported by suspended sediment mechanisms to depths generally in excess of 50 m. Other mechanisms also play an important role in the erosion, transport, and deposition of mud in the deeper environments. Bottom currents flowing across the sills at the margins of the Strait resuspend fine sediments as demonstrated by the increase of suspensate concentrations in near-bottom waters (Pierce and Stanley, 1975). Moreover, mud turbidites are also important constituents of deep cores, as discussed later.

In addition to the characteristically high values of $MgCO_3$, and locally, volcanic ash and lava fragments, the Strait sediment contains high values of montmorillonite (Emelyanov, 1972). The montmorillonite content which appears to increase in the sector near Sicily (Chassefière and Monaco, 1973; Pierce and Stanley, 1975) and the island of Pantelleria (Blanc-Vernet et al., 1975) may be
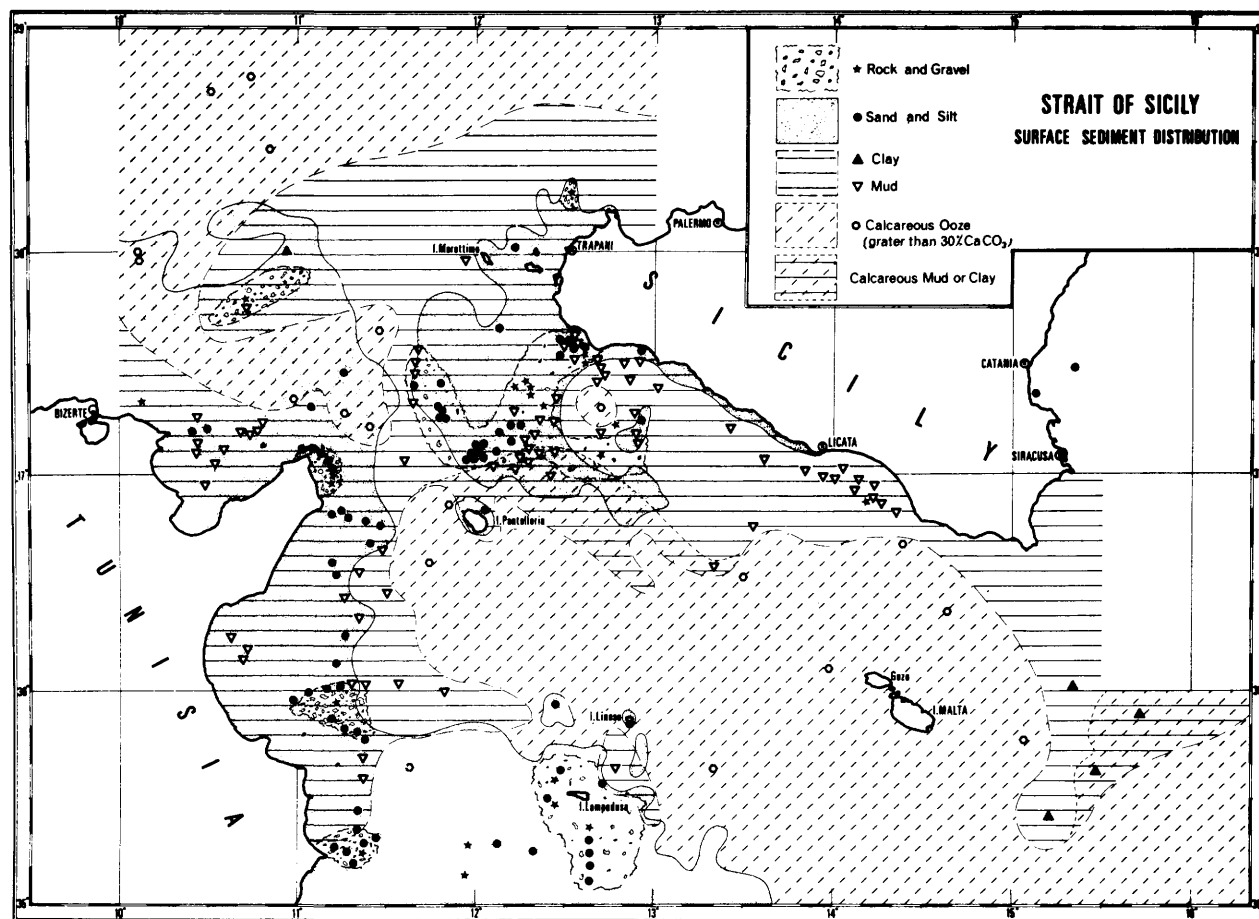
FIGURE 16.—Map showing surficial sediment distribution in the Strait of Sicily.
(From Akal, 1972.)

related to a volcanic source. A survey of the clay minerals in various Strait of Sicily environments is detailed by Blanc-Vernet and others (1975).

DEFINITION OF MAJOR SEDIMENT TYPES IN CORES

Our study emphasizes the vertical and regional distribution of sediment types recovered in cores. Three main assemblages are recognized in Strait of Sicily cores: (1) coarse, calcareous sand layers interbedded with mud and sandy lutite deposits; this association prevails on shallow banks; (2) predominantly homogeneous (nonstratified, bioturbated) light olive gray (5 Y 5/2) to dusty yellow (5 Y 6/4) mud in which the most important structures are biogenic ones; this type occurs most commonly in the neritic-bathyal environments and also

is found in some basins; (3) moderate to well-stratified sand and mud units that include gravity flow deposits (sand and mud turbidites, grain flow units) and/or ash layers interbedded with hemipelagic mud; this assemblage is typical of deep basins and the Strait Narrows. Gradual transition from one lithological assemblage to another is also recorded in the cores.

Cores containing assemblages 2 and 3 generally display an upper 5- to 40-cm thick layer of oxidized light brown (5 YR 6/3) or yellowish brown (10 YR 6/4) mud; olive gray mud lies below this and the vertical color change is usually transitional.

The five major sediment types distinguished in Strait of Sicily cores include: (1) coarse calcareous sand; (2) sand- to silt-size sediment; (3) ash; (4) mud; and (5) sapropel and organic ooze.

COARSE CALCAREOUS SAND.—The sediments included in this group are characterized by a high percentage of calcareous organic fragments,[1] forming generally more than 30% and not less than 15% of the samples. Grain count values as high as 90% are displayed by some samples. The grain size is variable, with a median comprised between 0.5 and 2.5 mm. The content of fines (silt and clay) also is highly variable and ranges from 0.5 to 30%. The calcareous components are largely molluscs (mainly gastropods and pelecypods), coralline algae, echinoderms, bryozoans, and forams.

This sediment type has been observed on various other shelves and banks of the Mediterranean Sea (Dangeard, 1929; Blanc, 1958, 1972; Caulet, 1972a, b; Milliman et al., 1972; and others). On these shelves two main facies are distinguished on the basis of composition: (1) shelly and bryozoan deposits and (2) coralline sands. The first type can be differentiated into several subtypes which appear depth related: (a) "muddy shelly sands" tend to be more important as depth increases (Milliman et al., 1972); (b) "very coarse shelly sands" (cf., *Posidonia* facies as described by Blanc, 1972) also may be represented at shallower depths (about 40 m); and (c) "clean fine-grained shelly sands" are generally found in the nearshore-inner neritic environment.

The second facies, the coralline sands, are dominated by particles of calcareous algae, which constitute as much as 70% of the sediment. Three main subtypes are distinguished on the basis of the calcareous algal type: (a) algal ball facies ("fonds à pralines," cf., Blanc, 1958); (b) encrusting calcareous red algae, commonly developed on rocky substrates; (c) coralline gravel consisting of the accumulations of debris of the red calcareous algae *Lithotamnium calcareum* and *Lithotamnium corallioides*, with a subordinate association of molluscs, bryozoans, and foraminifera (this forms the sediment type termed "maerl" by French authors; cf. Caulet, 1972).

All of the calcareous deposits described above also may be classified into modern, relict, and resid-

ual sediment types where age is taken into consideration (Emery, 1952, 1968). In many parts of the Mediterranean maerl appears to accumulate at present between the intracoastal complex and the inner-outer shelf transition zone. Relict maerl, originating in outcrops on the middle to outer shelf, developed during the last glacial and the subsequent rise of sea level (Caulet, 1972a, b). Since this rise in sea level, a fine fraction has been added, thus modifying the aspect of the original carbonate sediment (cf. discussion in Swift, 1974; Kulm et al., 1975). As an example, Milliman et al. (1972:254) have shown that calcareous sediments on banks in the Alboran Sea are relict and originally formed at depths of 70 to 100 m during lower stands of early Holocene sea level. Residual deposits are well differentiated in these calcareous sediments: they display mixed thanatocoenoses from different environments, and the various components show different states of preservation.

The coarse calcareous sands are present in all shallow platform cores of the Strait, and also are well represented in Strait Narrows cores. Typical shelly coarse sand, abundant in the shallower platform cores, is also found in cores collected in deeper environments (e.g., core SP 8–7, 350 m). Moreover, some cores in deep basins (e.g., KS–12) also display this facies; here the sands have been transported from shallower environments and deposited downslope by gravity flow mechanisms. Coralline sands were not recovered in our cores, but have been reported from the Strait (Blanc, 1958); they also appear in some bottom photographs (Figure 21; Akal, 1972).

SAND-SILT SIZE SEDIMENTS.—The sand-silt sediment type is distinguished on the basis of structure, texture and, to a lesser extent, composition. This type includes sediments which range in size from sand to fine silt, and includes a host of intermediate sizes.

Sand-silt varieties are encountered in the shallow platform environment and in the deep basins, but are uncommon to rare in the neritic-bathyal cores. This sediment type is generally structureless in the shallow platform environment. It is genetically related to the coarse calcareous sand type, and usually shows a gradational transition with these coarser deposits both laterally and vertically. The coarser sediment (median to coarse sand) observed in deep basin cores displays distinct and

---

[1] In this study we call "bioclastic" grains those clasts of organic origin which display evidence of transport and reworking (rounding and shape or other indirect evidence); grains of organic origin which do not show clear evidence of reworking by transport processes are referred to by the more general term, "biogenic."

well-defined sedimentary structures including cross-lamination and oblique lamination, graded bedding, and diverse types of parallel or ripple lamination. The base of this type of layer usually is sharp and erosional, and locally displays scour and fill structures.

The fine silt deposits of this sediment type show structural and lithologic continuity with some coarser deposits, i.e., they usually fine upward texturally (graded bedding) from silt to mud. The most common structures of the silts are parallel and low-angle oblique lamination. Their sand content is low, usually less than 5% and frequently only about 1%.

The composition of this type is variable. There are bioclastic and foraminiferal sands, where the coarse fraction is dominated by biogenic carbonates and/or planktonic foraminifera; in other instances the sand consists almost entirely of volcanic ash. Volcanic ash layers also could be included in this group, but their characteristic composition and origin warrant their assignment in another facies category. Sand composed in part of detrital feldspathic grains is less common.

VOLCANIC ASH.—Volcanic tephra layers are observed in the deep basin cores, especially those from Linosa Trough. Although texturally analogous to the former type, they stand out by their characteristic composition. These deposits do not represent a major sediment type in Strait cores in terms of total thickness.

Two different types of layers containing volcanic ash and dust are distinguished: (1) air-borne tephra layers, derived directly from ash flows, mud flows, or base surges consisting predominantly of volcanic vitric ash and variable amounts of mud; and (2) layers of volcanic ash particles or turbidite layers, which include a significant benthonic and planktonic calcareous bioclastic sand-size fraction. These two types can be differentiated on the basis of petrographic characteristics and primary sedimentary structures (compare the ash layers in cores KS 69, KS 118, KS 120; cf. Figures 27, 31). The carbonate-free tephra layers display a vertical grain-size gradation (fining or coarsening upward), parallel lamination, or in some instances they are structureless. The mixed volcanic-bioclastic layers show well-developed structures and may be similar to the sand-silt type sediments described in the previous section.

MUDS.—The mud type is by far the most abundant deposit in the cores studied. Neritic-bathyal environment cores consist almost exclusively of mud. Genetically there are three main types of mud which can be recognized on the basis of sedimentary structures and composition. These are: shallow water mud, hemipelagic mud, and turbiditic mud. In many cases these are transitional, and not clearly distinguishable.

Shallow water muds collected at neritic depths are structurally homogeneous and the only types of sedimentary structures commonly recognized are biogenic ones. This mud type may contain a relatively high (to 10%–15%) percentage of sand fraction, including either biogenic (mostly well-preserved neritic molluscs and benthic and planktonic foraminifera) or clastic grains. The hemipelagic muds are homogeneous calcareous oozes which also lack well-defined primary sedimentary structures, including lamination, and generally are characterized by vertical bioturbation. The sand fraction content, lower than in the shallow water mud, consists largely of calcareous planktonic components. The turbiditic muds are characterized by a delicate basal lamination or small-scale bioturbation visible in X-radiographs, and a smooth uniform aspect in split cores. They occasionally show continuity and gradation with the sand-silt sediment type in terms of structure and gross lithology (Rupke and Stanley, 1974).

SAPROPEL AND ORGANIC OOZE.—Sapropels are distinctive dark gray to black deposits which have been extensively studied in the eastern Mediterranean (Olausson, 1961; Ryan, 1972; van Straaten, 1972; Nesteroff, 1973; Maldonado and Stanley, 1975; and others). Recently described sequences from the Black Sea appear similar to Mediterranean sapropels (Ross and Degens, 1974, unit 2). This sediment type is commonly encountered in the eastern Mediterranean basin from cores collected at depths exceeding 700 to 1000 m. Sapropels are retrieved on the slope east of the Strait (LY II–3, 2432 m). However, cores in the Strait of Sicily proper (including the deep Pantelleria, Malta, or Linosa troughs) and in the western Mediterranean have not recovered this type of deposit.

The typical sapropel is formed by an alternating sequence of delicate horizontal laminae of white (coccolith rich) and black (largely mud) layers. The sand-size fraction content is about 10%, most of

which includes planktonic foraminifera.

Organic ooze layers are usually associated with sapropel. These two sediment types are compositionally transitional. However, in the split cores the contact between the two is very well marked by a sharp color change: organic oozes are pale olive (10 Y 6/2–5 Y 5/2), while sapropels are dark gray-olive (5 Y 3/2–5 Y 2/1). This contact is also noted on X-radiographs. A type of sediment that resembles organic ooze is present in the Linosa Trough and perhaps also in the Malta and Pantelleria troughs; this type also displays some petrological affinities with the hemipelagic mud type.

A third type of sediment, protosapropel, is associated with this group. While genetically and lithologically related, the protosapropel is not considered a true sapropel because it does not display the typical lamination of the sapropel and may be bioturbated to some extent (Maldonado and Stanley, 1975).

Sand Fraction Composition

GENERAL

The fraction larger than 63 microns was collected from all samples by wet sieving after removal of the organic matter with hydrogen peroxide. The identification of grains was made using a binocular microscope, and relative frequencies were determined by counting 300 to 400 grains per sample. The grain counts were made by unit area measurements as opposed to point counting. The following parameters were determined: pteropods (1); molluscs (2) consisting largely of gastropods and pelecypods; shell fragments (3); planktonic foraminiferida (4); benthonic foraminifera (5); ostracoda (6); bryozoa (7); other invertebrates (8); plant debris (9); heavy minerals (10), including opaque and some characteristic nonopaque minerals; mica (11); pyrite[2] and strongly pyritized tests and burrows (12); light minerals (13), including carbonates and gypsum; and ash (14). The components 1 to 9 represent the biogenic fraction while 10 to 14 are grouped as inorganic fraction.

The results of these counts are listed in Table 3, and the different components have been grouped

---

[2] "Pyrite" as used here is applied to various possible ferrous sulfide types.

in triangular plots shown in Figure 17. In one triangle (Figure 17A$_2$), the end points represent the inorganic fraction (components 10 to 14), planktonic foraminifera (component 4) and the remainder of the biogenic fraction (components 1 to 9, except component 4).

The end members of the other triangle (Figure 17A$_1$) represent the percent of total sand fraction in the bulk sample, the total biogenic fraction in the sand fraction, and the total planktonic foraminifera fraction in the sand fraction; all of these are recalculated to 100%. In this representation any component could actually be as high as 100%; however, the total planktonic foraminifera is equal to, or lower than, the total biogenic fraction. In this type of representation all of the samples plotted are concentrated on the left half of the triangle. The different lines on the triangle mark the boundaries of different components.

Core samples have been assigned a letter symbol on Table 3 and in Figure 17; the numbers associated with the letter key (Table 3) identify their depth (in centimeters) from the top of the core.

COARSE CALCAREOUS SAND TYPE

The samples selected for this study are of the shelly bioclastic sand type as defined in the previous section. The modern, relict, or residual fractions generally can be distinguished on the basis of abrasion and preservation of the skeletal material. Modern biogenic components do not show significant evidence of transport, although tests may be broken. Relict and residual calcareous components are composed of organic remains deposited during the Pleistocene and early Holocene (see core AS 6–8, Figure 34), or reworked from older deposits; these bioclastic particles are characterized by an iron oxide stain and the rounded, worn shape of the grain edges. In the Strait of Sicily the sand fraction of relict sediments also is characterized by a relatively high feldspathic content (Blanc, 1958); the modern biogenic sediment is generally associated with a low feldspar content.

Other organic components of the calcareous sand type are bryozoa, echinoderma, calcareous algae, crustacean fragments, and plant debris. Pyrite is not very common, and where present is usually oxidized, particularly in relict and residual sands. Glauconite is more abundant. Gypsum frag-

TABLE 3.—Percentage of sand fraction (>63 μm) and major components in selected

CORE	SAMPLE DEPTH IN CORE (cm)	BIOGENIC FRACTION								
		PTEROPODS	MOLLUSKS	TEST FRAGMENTS	PLANKTONIC FORAMS	BENTHONIC FORAMS	OSTRACODS	BRYOZOANS	OTHERS	PLANT DEBRIS
LY II-3	5(a)	9.3	-	14.9	68.0	-	-	-	1.5	6.3
LY II-3	210-255(b)	0.6	0.6	8.5	66.4	0.6	2.7	-	2.4	0.3
LY II-3	338(c)	-	-	13.7	73.5	8.4	-	-	0.9	-
LY II-3	408(d)	-	-	5.7	84.5	-	-	-	3.4	2.0
LY II-3	412(e)	10.5	0.8	10.0	65.3	0.5	-	-	-	0.8
LY II-3	415(f)	7.2	-	16.1	57.3	1.8	0.6	-	-	0.9
LY II-3	418(g)	-	-	-	-	-	-	-	-	-
LY II-3	428(h)	0.3	-	0.9	0.3	-	-	-	-	-
LY II-3	465(i)	-	-	0.8	85.3	-	-	-	6.7	3.2
LY II-3	467-512(j)	2.6	-	14.4	54.7	2.3	-	-	1.5	-
LY II-3	557(k)	-	-	1.2	92.8	-	-	-	3.1	1.2
LY II-4	70-115(a)	0.3	0.6	16.9	29.4	4.6	1.5	-	5.2	-
LY II-4	298-351(b)	-	0.6	5.8	55.3	2.6	0.3	-	1.6	-
LY II-5	60-100(a)	0.9	0.9	28.1	60.8	0.6	0.9	-	6.9	-
LY II-5	270-310(b)	1.9	-	24.3	39.6	8.6	1.3	-	3.8	-
LY II-5A	15(a)	1.1	0.8	12.9	30.7	8.4	0.8	-	0.5	-
LY II-5A	20-60(b)	1.8	0.6	18.2	65.3	1.2	2.2	-	2.2	0.6
LY II-5A	61(c)	5.5	-	7.3	38.4	0.9	-	-	-	-
LY II-5A	105(d)	0.6	0.9	6.4	35.7	4.3	0.6	-	0.6	-
LY II-5A	125(e)	-	-	2.5	2.7	3.8	-	-	4.6	-
LY II-5A	133(f)	-	1.2	5.9	9.6	4.2	0.7	-	4.2	0.5
LY II-5A	270(g)	2.1	0.3	15.5	24.2	19.1	4.2	-	13.9	1.5
LY II-5A	270-310(h)	1.2	-	11.1	57.5	9.2	2.2	0.6	2.2	-
LY II-5A	318(i)	5.4	-	19.6	24.7	8.1	1.8	-	2.7	0.3
LY II-5A	550-590(j)	0.3	-	13.9	49.9	7.3	1.9	-	2.2	1.2
LY II-6	5(a)	3.8	0.6	31.3	38.4	7.5	1.4	-	10.4	3.5
LY II-6	45-85(b)	1.2	-	6.9	82.5	0.3	1.8	-	3.9	0.3
LY II-6	90(c)	0.5	-	1.0	96.5	0.5	-	-	-	-
LY II-6	263(d)	0.8	0.3	5.0	62.7	2.2	0.6	-	23.1	-
LY II-6	273(e)	1.3	-	7.7	69.9	3.5	1.3	-	2.6	0.3
LY II-6	285(f)	2.5	0.3	19.4	49.5	11.5	1.6	-	3.2	-
LY II-6	450-490(g)	1.2	-	9.7	66.1	5.3	0.9	-	2.9	0.6
LY II-6A	10-50(a)	-	0.6	11.8	77.0	5.0	2.2	-	1.9	-
LY II-6A	230-270(b)	0.5	-	9.0	72.1	6.2	1.9	-	6.0	-
LY II-6A	530-570(c)	1.9	0.6	9.9	66.8	4.5	1.0	-	3.2	-
LY II-7	260(a)	10.5	-	1.0	72.3	1.2	0.8	-	1.2	-
LY II-7	270(b)	1.2	-	0.8	62.1	3.5	0.5	-	-	-
LY II-7	275(c)	2.1	0.8	11.3	43.4	4.2	1.2	-	4.3	-
AS 6-8	33-65 (>200μm)	-	3.6	8.6	2.8	30.1	13.1	0.9	17.9	9.7
AS 6-8	33-65 (200-63μm)	-	-	3.2	2.9	7.8	1.5	-	-	4.1
AS 6-8	33-65(a)	-	1.8	5.9	2.8	18.9	7.3	0.4	9.0	6.9
AS 6-8	510-550(b)	-	1.3	9.4	2.2	11.8	5.3	-	5.0	0.9
AS 6-7	0-45(a)	0.8	1.0	12.1	14.4	36.8	3.8	0.4	10.8	0.5
AS 6-7	185-200(b)	-	26.5	13.4	0.6	19.7	1.0	-	4.7	0.3
AS 6-7	685-728(c)	0.3	-	5.5	4.0	15.3	3.2	-	4.3	1.7
KS 63	200-250(a)	-	1.6	10.0	5.6	4.7	0.9	-	10.0	1.9
KS 63	500-550(b)	3.3	3.9	11.5	27.9	15.4	7.1	-	11.2	3.3
KS 63	800-850(c)	-	2.6	8.8	5.2	5.9	1.6	-	4.9	0.3

Note:

Sand-Silt
Sand ●   Volcanic Ash △   Coarse Calcareous Sand ◉
Fine Silt ◑   Organic Ooze ☐   Sapropel ■

samples from different Strait of Sicily sedimentary environments

INORGANIC FRACTION								
HEAVY MINERALS	MICA	PYRITE	LIGHT MINERALS	VOLCANIC ASH	TOTAL GRAINS COUNTED	%BIOGENIC/ %INORGANIC	%SAND FRACTION (>63µ)	SEDIMENT SYMBOL ON FIGURES
-	-	-	-	-	335	100/0	7.4	■
3.9	11.9	-	1.2	0.9	329	82.1/17.9	4.6	⊘
0.7	1.9	-	0.9	-	321	96.5/3.5	6.4	⊘
-	0.7	3.7	-	-	349	95.6/4.4	4.8	■
1.0	3.6	5.9	1.0	0.6	389	87.9/12.1	8.0	□
4.8	5.7	-	1.8	3.9	335	83.8/16.2	1.4	⊗
5.9	0.3	-	5.9	87.9	322	0/100	34.5	△
1.5	-	-	0.9	96.1	334	1.5/98.5	64.2	△
-	-	4.0	-	-	375	96.0/4.0	6.9	■
8.1	2.3	4.4	4.7	5.0	339	75.5/24.5	5.2	⊘/□
-	-	1.5	0.2	-	326	98.3/1.7	10.9	■
23.3	4.0	1.2	8.1	4.9	326	58.5/41.5	9.5	⊗/○
12.8	4.8	-	14.6	1.6	311	66.2/33.8	3.1	⊘/○
0.6	-	-	0.3	-	332	99.1/0.9	4.2	⊘
7.7	2.9	5.5	2.2	2.2	312	79.5/20.5	3.5	⊘
9.7	1.3	0.5	18.3	15.1	371	55.2/44.8	29.3	●/△
0.6	3.1	0.3	3.9	-	319	92.1/7.9	4.2	⊘
3.5	-	-	1.7	42.7	344	52.1/47.9	5.8	△
9.1	-	0.6	11.3	29.9	328	49.1/50.9	41.4	/△
5.2	3.1	-	2.1	76.0	480	13.6/86.4	10.7	△
1.2	0.7	-	4.0	67.8	426	26.3/73.7	8.6	△
6.4	0.9	1.5	8.2	2.2	330	80.8/19.2	4.6	◐
7.5	0.6	4.4	2.5	0.9	315	84.1/15.9	2.8	⊘/⊗
10.5	0.6	7.8	18.5	-	332	62.6/37.4	1.3	◐
2.8	2.2	8.2	10.1	-	317	76.7/23.3	2.8	/⊘
1.7	0.8	-	0.6	-	345	96.9/3.1	4.9	⊘
0.3	-	2.8	-	-	332	96.9/3.1	0.1	⊗/⊘
-	0.3	1.2	-	-	120	98.5/1.5	0.1	⊗
1.7	2.2	0.6	0.8	-	360	94.7/5.3	5.7	◐
2.3	1.3	1.3	8.5	-	309	86.6/13.4	24.8	●
4.1	0.9	1.9	5.1	-	313	88/12	32.5	●
3.5	3.2	4.4	2.2	-	340	86.7/13.3	5.3	⊘/⊗
0.6	0.3	0.6	-	-	321	98.5/1.5	5.9	⊘
1.9	0.3	1.1	1.0	- -	370	95.7/4.3	6.2	⊘
2.2	1.2	2.5	6.2	-	314	87.9/12.1	5.4	⊘/⊗
1.1	3.1	3.8	5.0	-	289	87.0/13.0	5.8	⊘
6.8	8.9	1.0	15.2	-	305	68.1/31.9	1.3	⊗
5.7	6.3	0.5	20.2	-	316	67.3/32.7	3.2	◐
1.2	-	-	12.1	-	420	86.7/13.3	-	⊙
18.4	0.6	-	61.5	-	338	19.5/80.5	-	⊙
9.8	0.3	-	36.8	-	-	53.1/46.9	90.2	⊙
20.0	0.6	0.9	42.6	-	320	35.9/64.1	21.9	◐
3.0	0.7	5.1	10.6	-	450	80.6/19.4	3.2	○
14.8	0.6	2.0	16.4	-	305	66.2/33.8	25.0	⊙
7.8	1.2	1.1	55.6	-	347	34.3/65.7	8.0	○
8.8	3.7	10.1	42.7	-	319	34.7/65.3	2.5	⊘/⊗
2.2	1.7	2.6	9.9	-	353	83.6/16.4	6.0	⊘
12.4	1.9	3.1	53.3	-	306	29.3/70.7	3.5	⊘/⊗

Shallow-Water Mud ○   Turbiditic Mud ⊗
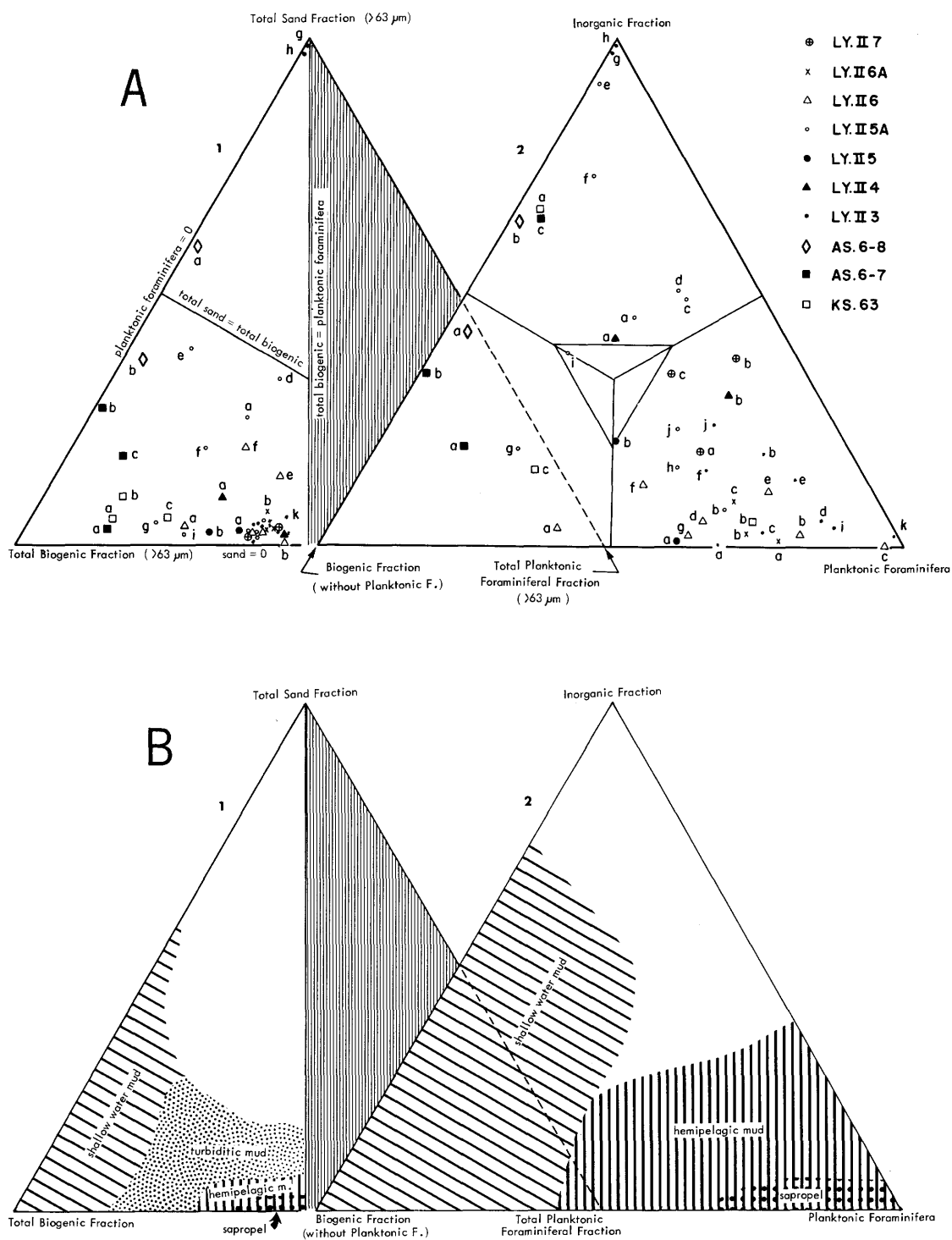
Hemipelagic Mud ⊘

FIGURE 17.—Mineralogical analysis of selected samples from 10 cores collected in different environments: A, plots of the actual sand fraction from samples analyzed (letter code given in Table 3); B, interpretation of data plotted in (A) showing the distribution of some major sediment types based on several components of the sand fraction. (Explanation in text.)

ments are also present in some samples, probably resulting from the erosion of outcrops on the shelf during the eustatic low stands of sea level.

SAND-SILT SEDIMENT TYPE

In the sand-silt type we consider all textural types ranging from sand to silty sand to sandy silt to silt. In the coarse sand-silt type, the sand content is above 20% of the entire fraction, and the sand fraction generally comprises more than 50% calcareous biogenic components. However, in shallow platform samples (i.e., AS 6–8b) the calcareous content is lower due to a masking effect produced by the addition of detrital material.

The sand-silt sediments collected in the shallow environments have a biogenic content usually well represented by shells, shell fragments, benthonic foraminifera, and other calcareous biogenic components similar to those of the coarse and bioclastic sands. Planktonic components are also present.

The composition of the organic fraction in the majority of the sand-silt samples collected in the deep environments is more varied: planktonic and benthonic foraminifera, echinoderm spicules and fragments, bryozoa, calcareous algae, sponge spicules, mollusc shell and shell fragments, plants, etc. Radiolarian fragments, pteropods, and diatoms also occur. In general, this type of "mixed" bioclastic assemblage is interpreted as a thanatocoenosis containing biogenic remains derived from various environments (Parker, 1958). Thus, it is interpreted as a resedimented deposit.

Quartz and feldspar account for much of the inorganic fraction except in volcanic ash layers. Heavy minerals, glauconite, and mica also occur.

The composition of the sand fraction of this sediment type provides some information as to (1) sediment provenance and depositional environment, and (2) hydrodynamic processes. The first factor is interpreted mainly on the basis of the biogenic components and, to a lesser extent, the inorganic (mostly authigenic minerals) fraction; insight as to the processes is provided by the physical character of the grains, particularly density and particle shape. As an example, the mica and flaky particles, including shell fragments, tend to be concentrated in parallel laminae, i.e., either as part of the d-division of the Bouma turbidite sequence or as horizontal laminations produced by bottom currents. These concentrations can be interpreted in terms of hydraulic equivalents inasmuch as the large flaky grains are more easily maintained in suspension than the smaller round ones. The relatively denser and more spherical particles, such as heavy minerals, tend to be concentrated in the lower turbidite divisions although they are smaller in size than the majority of grains with which they are associated (Rupke and Stanley, 1974).

VOLCANIC ASH TYPE

The volcanic ash layers, as in the above-described sediment type, also comprise a textural mix of sand- and silt-size grades. However, compositionally this type is quite characteristic and is thus discussed as a separate entity. Ash layers usually contain a high sand fraction (above 30%), much of which is constituted by fragments of volcanic origin; there are many textural varieties ranging from sand to mud. Two distinct types are recognized. The first is characterized by its calcareous biogenic content in the sand fraction, which is composed mostly of foraminifera, pteropods, and minor subordinate amounts of other biogenic components. The composition of this calcareous fraction is similar to the one displayed in the hemipelagic mud type, defined later. The second type of volcanic ash layer presents a more variable calcareous fraction, represented by mixed biogenic assemblage from different environments (i.e., similar to that of the sand-silt sediment type). The first type results from pelagic settling of volcanic air-borne ash, which may eventually be winnowed and modified by bottom currents (cf. tephra layers described by Ninkovich and Heezen, 1965; Keller et al., 1974). The second type of volcanic ash layer is related with turbiditic sedimentation (Sarnthein and Bartolini, 1973).

SHALLOW WATER MUD TYPE

The shallow water mud type is highly variable in both sand-size content (4%–20%) and biogenic content (30%–90%). There is a gradual transition between this type and the sand-silt type from shallow water environments described earlier. The sand fraction in the mud includes benthonic foraminifera and a relatively low (< 30%) planktonic

foraminiferal content. In these samples the relation of planktonic to benthonic tests can be used as an indication of depth (Boltouskoy, 1965). However, use of this ratio is valid only if the sediment accumulates in situ; interpretation of these ratios is difficult when sediments are transported to deeper environments (for example in the case of turbiditic muds). Some samples (cf., LY II–4a), located in intermediate to deep water, are interpreted as a sediment type transitional between shallow water mud and turbiditic mud. Such samples have a relatively high benthonic foraminifera and shell fragment content and the degree of abrasion observed indicates that they have been reworked to some extent prior to final deposition.

Compositional plots of samples from this type of mud are shown in Figure 17A. Here the samples tend to be distributed on the left side of the triangular diagrams. Figure 17B reveals a relatively high biogenic fraction but a low planktonic foraminifera content in the sand fraction.

Hemipelagic Mud Type

The hemipelagic muds have a sand content of 2.5% to 6.5%. This sand fraction is 80% to 99% biogenic and usually comprises more than 40% of planktonic foraminifera [3] (Figure 17, Table 3). Other components of the biogenic fraction include pteropods, mollusks, radiolaria, diatoms, sponge spicules, ostracoda, fecal pellets, and benthonic foraminifera. The inorganic clastic fraction consists of quartz, mica, pyrite, heavy minerals, glauconite, and volcanic ash. Fragments of pyritized burrow tubes also are common in some samples.

The compositional plots of this type of mud tend to be distributed in the lower right sector of the triangular representation (Figure 17B). The position occupied by this type of mud is distinct from that of the shallow water mud type in triangular diagrams A_1 and B_1 in Figure 17.

Turbiditic Mud Type

The two end members of the turbiditic mud type

[3] A list of planktonic foraminifera identified in cores KS 33, 78, and 105 and an evaluation of their vertical distribution are presented by Blanc-Vernet et al. (1975).

are contrasted as follows: one has a very low sand fraction ($\cong 1\%$) which is mostly bioclastic ($\geqslant 70\%$), and the other is a more sandy terrigenous turbiditic mud ($\simeq 5\%$ sand fraction of which 50 to 80% is bioclastic). In the first type the calcareous fraction includes mostly planktonic foraminifera, while the second type has a higher content of benthonic foraminifera and shell fragments. The terrigenous components are analogous to those of hemipelagic muds, although the burrows and tubes are rare.

The composition of the sand fraction in the turbiditic and hemipelagic muds differs from that in the Algéro-Balearic Basin described by Rupke and Stanley (1972). This difference reflects (1) a higher terrigenous influx in the Strait of Sicily, as a result of proximity to land (i.e., important clastic influence) and (2) more extensive vertical bioturbation of the sediments. In some cases, it is difficult to distinguish between hemipelagic and turbiditic mud on the basis of composition because of reworking by currents (see Table 3).

The turbiditic mud samples occupy a random distribution and are not distinctly concentrated on the triangular representation in Figure 17A$_2$. However, this sediment type is better delineated in the triangular diagrams A$_1$ and B$_1$ in Figure 17; here turbiditic mud occupies an intermediate position between hemipelagic and the shallow water mud. The three types of mud appear transitional on the basis of composition.

Sapropel Type

The sand content in the sapropel type ranges from 5% to 10%, and is mostly biogenic (95%–100%). The inorganic fraction consists of authigenic minerals (pyrite and gypsum) and, to a lesser extent, mica. The calcareous sand fraction is dominated by planktonic foraminifera (generally $\geqslant 70\%$) and also includes plant fragments, pteropods, radiolaria, and diatoms. A high proportion of foraminiferal tests are pyritized. All these components indicate a low detrital input during deposition, although normal turbidites can be intercalated in the sapropel deposits (van Straaten, 1972; Nesteroff, 1973).

The characteristic composition of sapropel samples is shown in triangular representations B$_1$ and B$_2$ in Figure 17. Sapropel deposits are concentrated in the lower right corner of both types of triangle.

Organic Ooze Type

The organic ooze and protosapropel types are transitional between the hemipelagic mud and the sapropel types in terms of sand-fraction composition, texture, and structure. Thus, a small amount of clastic sand fraction is present as well as a less uniform biogenic fraction in contrast to the sapropel type. Organic ooze is characterized by the frequent occurrence of pyritized worm tubes; these are concentrated at the top of the organic ooze layer and are well displayed in the core X-radiographs (Figure 28).

Bryozoan Content

The sand fraction of 44 samples from different environments (cores LY II and AS) were examined for bryozoan content (Salvador Reguant, University of Barcelona, Spain, pers. comm.). The bryozoan content is low except in shallow platform cores. Bryozoan fragments may be transported in the various environments in the same fashion as are the planktonic foraminiferal tests associated with them; fragments of cellariiform zooarial tubes and, locally, of catenicelliform species (in LY II–6, g) disintegrate when animals die and can be transported in suspension prior to deposition. Rapid burial in fine sediment is necessary for the preservation of these delicate fragments.

Sample AS 6–8, a, is of interest because it contains an assemblage of species indicative of a somewhat low energy environment although the core was collected at a depth of 93 m. An examination of 97 fragments reveals the following zoaria: membraniporiform (3); celleporiform (2); adeoniform (12); vinculariiform (30); reteporiform (8); cellariiform (42). This zoarial assemblage is closely related to that reported from slope environment (cf., Caulet, 1972:239, 243). It is difficult to explain in terms of the sea-floor depth where this core was collected and the age of this sample (17,000 to 20,000 years BP, Table 5). One possible interpretation is that this sample consists of residual material (i.e., a thanatocoenosis) from a different environment. The possibility of reworking of older material appears corroborated by the abundance of gypsum grains in the same sample, also believed to have been eroded from outcrops of the shelf.

SEM Analysis of the Lutite Fraction

A scanning electron microscopic analysis serves to determine the composition of the lutite fraction and provides a rough quantitative approximation of the different components. In order to prepare the samples for electron microscopy, the organic matter is first destroyed with 30% hydrogen peroxide. Then the sample is wet sieved to separate the fraction coarser than 63 microns. The residue is then placed in suspension. A drop of this suspension is pippeted immediately after mixing and placed on a standard metal specimen plug. The sample is then dried at room temperature and coated with gold. No sticking tape was used. In the case of some coarser grained samples, grains were glued (Elmer's glue) to the plug to avoid discharge.

The plug was examined with a Cambridge Instrument Stereoscan. Photographs were made of each sample using SEM low magnification (100–500 magnification), which reveals details of sediment texture and a rapid inventory of the fossil, authigenic, and detrital assemblages in the silt fraction. Individual grains and the fine silt and clay fraction have been examined systematically using high ($\times$ 2000) magnification.

The identification of the different particles is based on a comparison with previous works and, in particular, those of Stieglitz (1972) and Milliman (1974) for the calcareous fraction. The distinction between the calcareous biogenic and the inorganic clastic particles is often subtle, especially in the finest fractions.

The common components of the lutite fraction are clay-size particles and aggregates, calcareous fragments of tests, siliceous grains, aggregate grains, calcareous inorganic grains, calcareous nannoplankton, spicules, foraminifera, and volcanic ash fragments. Pollen, dinoflagellate cysts, pyrite framboids, diatoms, plant fragments, and silicoflagellates are abundant in some samples.

The composition of the lutite fraction of the sand-silt sediment type (Figures 18, 19A–C) is the most variable of all the sediment types studied. Calcareous biogenic and bioclastic particles and terrigenous feldspathic grains are predominant in the coarse silt fraction (c and f in Figure 18A,B). The biogenic calcareous grains, mostly calcareous algae and foraminiferal test fragments (c), are the dominant components (Figure 18B). Well-
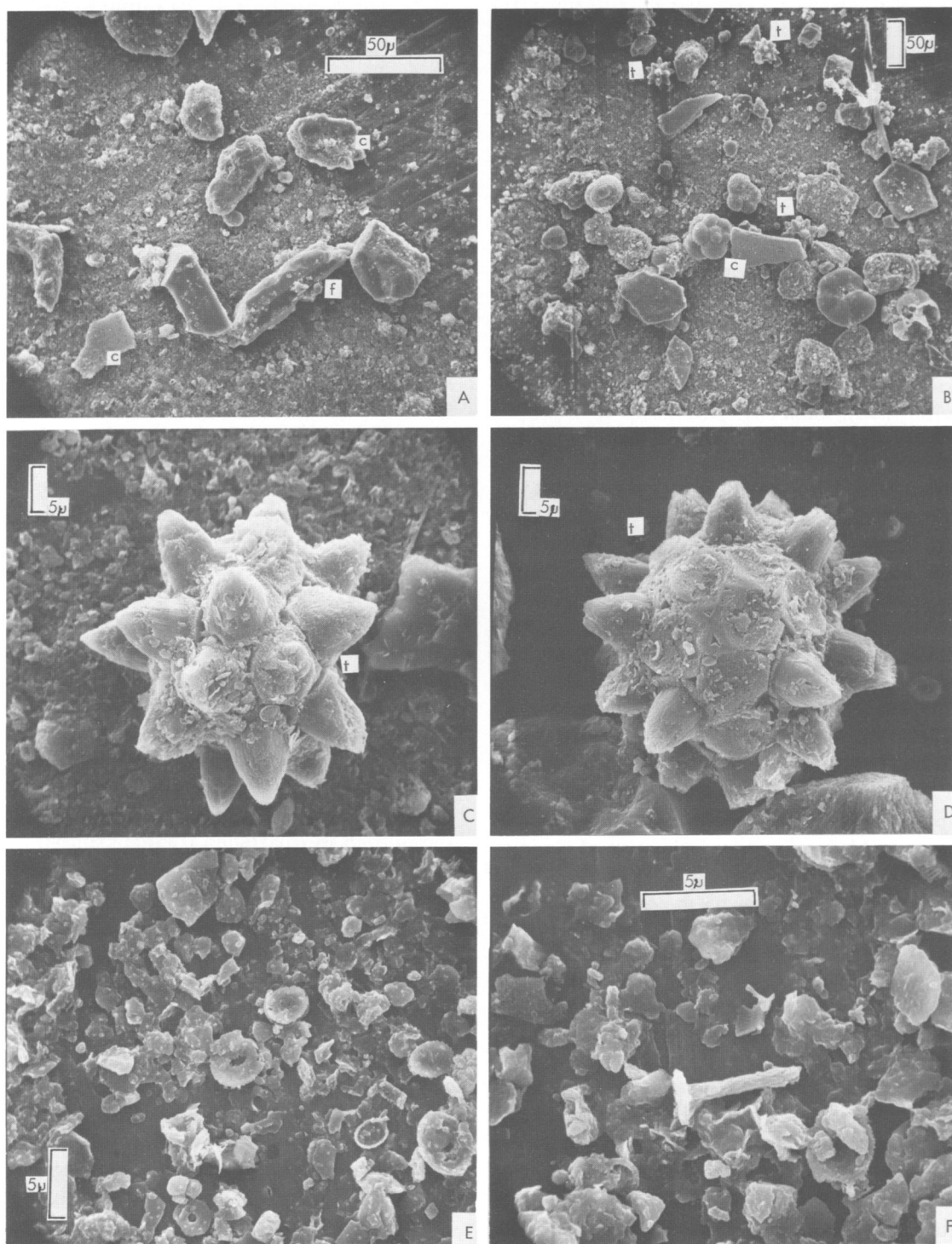
FIGURE 18.—SEM photographs showing silt and clay fraction of the sand-silt sediment type: A–D, sample LY–II–6, d; E–F, LY II–5A, g (c = calcareous biogenic grain, f = feldspathic clastic grain, t = tunicate ascidian spicule). (Poorly defined clay and silt-sized crystals, needles, aggregates, and coccoliths shown in E and F; explanation in text.)
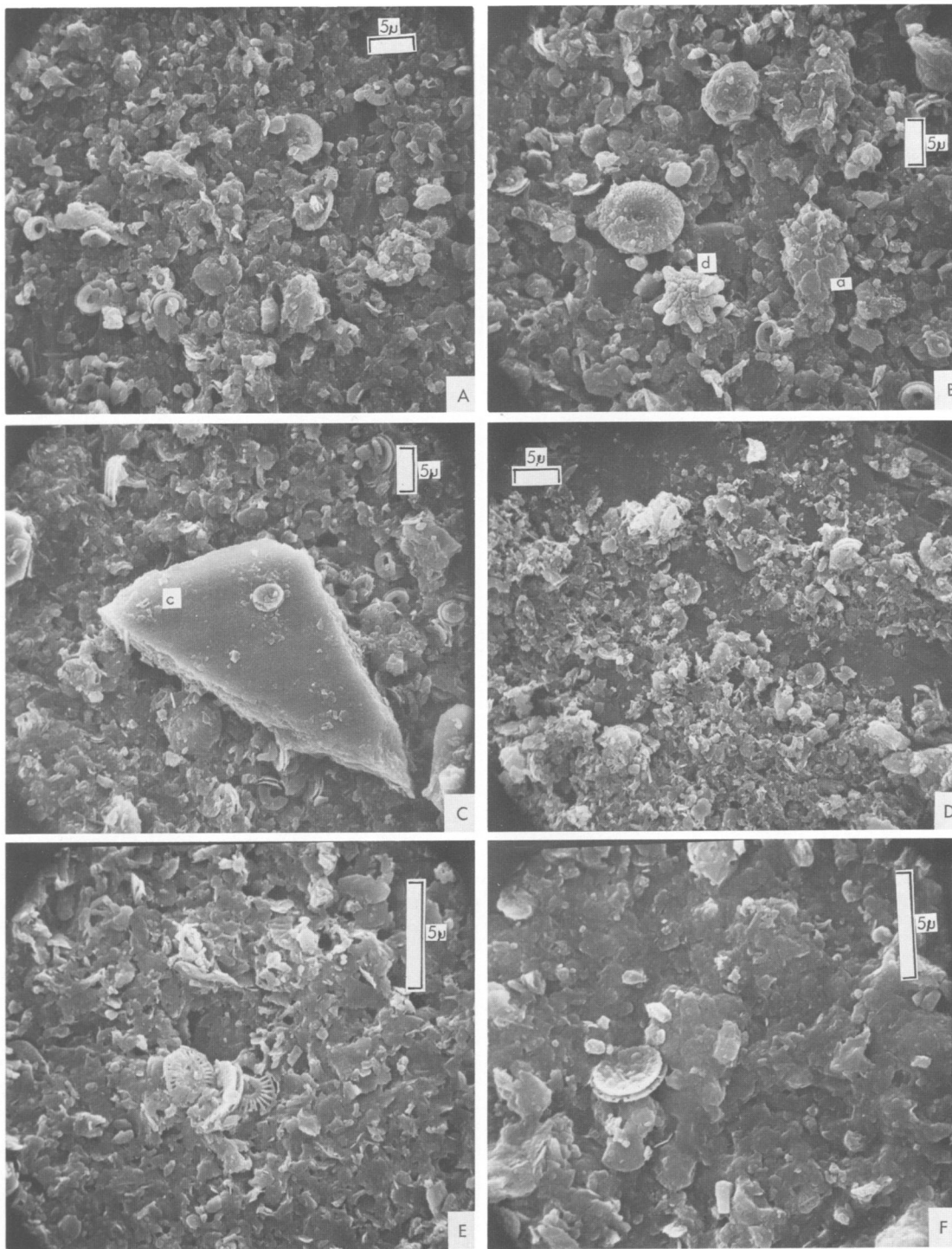
FIGURE 19.—SEM photographs showing silt and clay fraction of the sand-silt sediment type (A–C), turbidite mud (D), hemipelagic mud (E), and shallow water mud (F): A, B, sample LY II–5A, i; C, LY II–6, f; D, LY II–6, c; E, LY II–6, a; F, AS 6–7, a (a = aggregate grain, c = calcareous bioclastic grain, d = discoaster). (High concentration of irregular plates, needles; aggregate grains and poorly defined crystals are shown in E and F; explanation in text.)

preserved and broken tests of foraminifera and calcareous tunicate spicules are also commonly associated with this sediment type (Figure 18B). The presence of calcareous ascidian (tunicates, *t*) spicules (Figure 18B–D) are of primary interest because they characterize the turbidite sand-silt sediment type. Factors controlling the distribution of living ascidians are the bathymetric range and the nature of the substrate. The didemnids, a common type of ascidian, extend from the intertidal zone (very abundant) to about 500 m; they prefer a hard substrate on which to build their colonies (P. Mather, pers. comm.; Hekel, 1973:10). Thus, the presence of a high concentration of ascidian spicules in samples collected in deep water may indicate an original shallow water origin and subsequent transport downslope.

In the fine silt and clay fraction of the sand-silt sediment type (Figures 18E,F, 19A–C) the more common components are calcareous nannoplankton, especially coccoliths, aggregate grains (Figure 19B, *a*), terrigenous clay-size particles, and nonidentified calcareous grains of biogenic origin. Coccoliths may represent up to 50% of this fraction. Their characteristic is a poor preservation and a mixed thanatocoenosis, which may include reworked Tertiary species (e.g., discoaster, Figure 19B, *d*). However, all the samples studied belong to the *Emiliania huxleyi* zone of Upper Quaternary age.

The terrigenous grains usually show an angular to round outline and well-developed facets (Figure 18A, *f*). In general, the surface texture characteristics of the siliceous grains (regardless of their mineralogy) in this very fine fraction cannot be correlated with similar structures observed on coarser grains (Krinsley and Doormkamp, 1973; Krinsley et al., 1973; Margolis and Krinsley, 1974; Whalley and Krinsley, 1974). For instance most of the fine silt-size grains investigated show very high relief conchoidal breakage pattern, imbricated breakage blocks, and other grain surface features which have been related to glacial action by these authors. This interpretation is probably not applicable to these Mediterranean sediments.

Turbiditic mud (Figure 19D) displays many of the same characteristics as the sand-silt sediment type. However, fine turbidites are better sorted toward the fine fraction and there is a noticeable scarcity of intact fossil remains. *Emiliania huxleyi*

and *Cyclococcolithus leptoporus* account for most of the nannoplankton remains, but a detailed analysis of the coccoliths has not been made.

The coarse silt fraction of the hemipelagic mud type is dominated by biogenic calcareous and aggregate grains (Figure 19E). In the fine fraction two subtypes are distinguished: (1) sediments rich in coccoliths, and (2) sediments rich in poorly defined fine silt- to clay-size crystals, needles, plates, and irregularly shaped grains, with a relatively low coccolith content (Figure 19E). The general aspect of this second type resembles the magnesian calcite sediments of the eastern Mediterranean (Milliman and Müller, 1973).

The silt fraction of the shallow water mud shows a high percent of needles, plates, and irregularly shaped grains, and, in general, a lower nannoplankton content (Figure 19F) than in the other mud types sampled. However, coccolith-rich mud has been reported elsewhere from shallow water environments (Scholle and Kling, 1972).

The coarse fraction of the shallow water mud is dominated by calcareous biogenic grains. The better state of preservation of these grains facilitates their identification on the basis of grain surface texture (cf., Stieglitz, 1972). Calcareous algae, foraminiferal, and molluscan fragments are among the most characteristic calcareous components.

Volcanic ash is well distinguished with the aid of the SEM (Heiken, 1974). Two main types of ash particles have been identified: (a) broken droplets with abundant vesicles, and (b) angular glass shard, where inclusions are rare (Figure 20A). Furthermore, the carbonate-poor tephra air-borne layers are characterized by a decrease in calcareous (usually nannoplankton) components, while ash layers reworked by turbidity currents, slumps and other subaqueous gravity mechanisms contain a significant calcareous fraction derived from several shallow to deepwater environments. The first type represents an essentially primary ash layer deposit, while the second type is identified as a downslope reworked unit.

The organic oozes are characterized by a great abundance and variety of nannoplankton species (Figure 20C,D). *Coccolithus pelagicus* (Wallich) Schiller, and *Scyphosphaera apsteini* Lohmann are among the abundant species in these oozes; they are reported from cold water (McIntyre and Bé, 1956; Müller, 1973). The other major com-
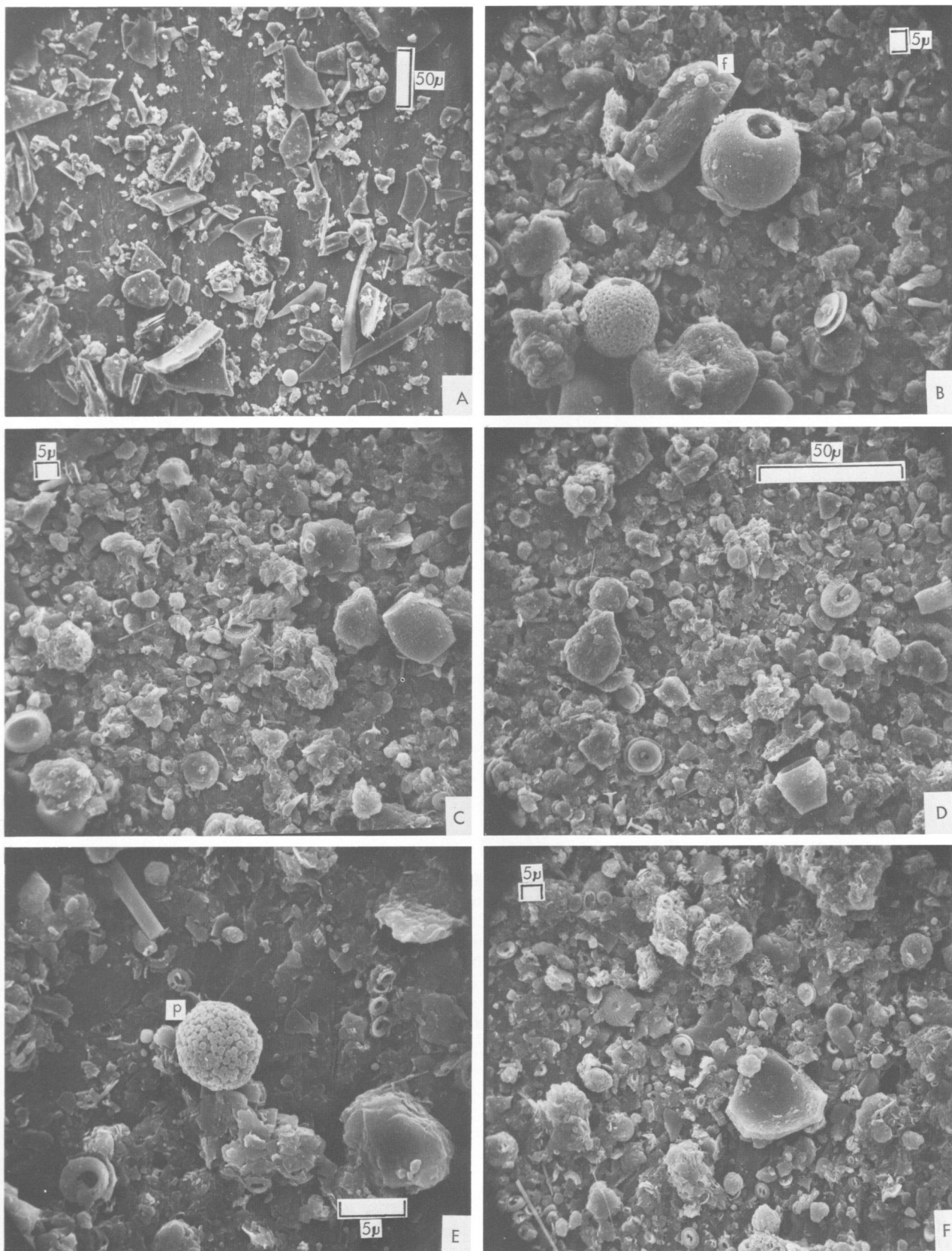
FIGURE 20.—SEM photographs showing silt and clay fraction of the volcanic ash type (A), organic ooze (B–D), and sapropel (E and F): A, sample LY II–3, h; B–D, LY II–3, e; E–F, LY II–3, i (*f* = feldspathic grain, *p* = pyrite framboid). (Volcanic glass shards in A; explanation in text.)

ponents of these oozes are aggregate grains, needles, and irregularly shaped grains, many of which are attributed to terrigenous clay particles.

The fine fraction of sapropel (Figure 20E,F) is characterized by an impoverishment in the number of species and the amount of nannoplancton in the black clayey laminae and a high coccolith content, represented by only a few species, in the white lamine. *Helicopostosphaera kamptneri* Hay and Mohler and/or *Emiliani huxleyi* may be the only species present in these white lamine and constitute as much as 100% of the bulk sediment.

An association of nannoplankton interpreted as a warm water assemblage is reported from sapropel layers in the eastern Mediterranean (Müller, 1973). Thin laminae of diatoms, radiolarians, and silicoflagellates may also be associated with sapropel or organic oozes. Pyrite framboids (p) are also characteristic of sapropel (Figure 20E). The spheroidal form of the framboids is an inherited characteristic provided by a preexisting template (Rickard, 1970; Sweeney and Kaplan, 1973). They are attributed to the pseudomorphism processes of pyrite formation (Rickard, 1970) during early diagenesis of the sediment or in the water column (Ross and Degens, 1974:187). Twin-gypsum crystals also are common in the sapropel; they are attributed to neogenesis processes (Nesteroff, 1973: 719).

Sea-Floor Photography

Sea-floor photographs collected in the different Strait of Sicily environments illustrate some surficial sediment types described in the previous sections. These photos are of some assistance in the interpretation of biogenic structures recorded in the cores.

The shallow platform and banks are characterized by a generally flat bottom with many small irregularities resulting from biological activity. The most typical surface type is one covered by coarse sediment with little or total absence of relief (Figure 21). Calcareous algae is a common biogenic component. Three of the photographs illustrated in Figure 21 (A,B,D) show sand and calcareous algae (algal balls) of the type described in the shallow platform environment by Blanc (1958); this sediment type has been termed "maerl" (Caulet, 1972). A coarse calcareous shelly sand is

shown in Figure 21c.

The importance of bioturbation which predominates on such well-oxygenated shallow platforms is well documented (Sarnthein, 1972; Reineck, 1973), but burrowing of the sediment is not clearly apparent on the Strait of Sicily photographs. The absence of biogenic and current-produced structures such as ripples, scour shadows, and grooves is not necessarily an indication of lack of vigorous bottom current activity. Strong bottom currents have been measured in this part of the Strait (Molcard, 1972). Some photographs, for instance, show crinoids heeling over (Akal, 1972, fig. 8); this and the absence of fines together reflect the effect of strong flow capable of modifying the sea floor. An analogous set of observations has been made on the banks of the Alboran Sea by Milliman and others (1972), who record the heeling over of organisms but find little evidence of current-produced structures in the coarse-textured sea floor. It appears that coarse, poorly sorted sediment of the type observed on the shallow banks does not preserve such features well.

The sea floor of neritic-bathyal environments (Figure 22) is characterized by strongly pitted and trailed muddy sediments. Most of the sediment surface has been intensely disturbed and burrowed, reflecting significantly high activity by benthic organisms. Broad depressions, small holes, and plow marks or grooves are also common. The biogenic bottom structures in these environments are well preserved, while evidence of bottom current activity is not well displayed by the sediment.

Photographs of the deep basin environment (cf. Malta Trough, Figure 23) show a mud floor almost entirely reworked by benthic organisms, although burrowing appears to be less extensive and less varied than in the former environment. The most characteristic feature is the high density of granular mud rods identified as large fecal pellets. Holothurians, the most common of the mud-eating benthic organisms (Ewing and Davis, 1967; Heezen and Hollister, 1971), are probably the producers of these pellets. Biogenic structures include small to medium-size mounds with apical holes (holothurian) and depressions, and sinuous trails left by wandering gastropods or echinoderms. One large rim crater (Figure 23D) resembles fish-produced structures described elsewhere (Stanley, 1970; Heezen and Hollister, 1971).
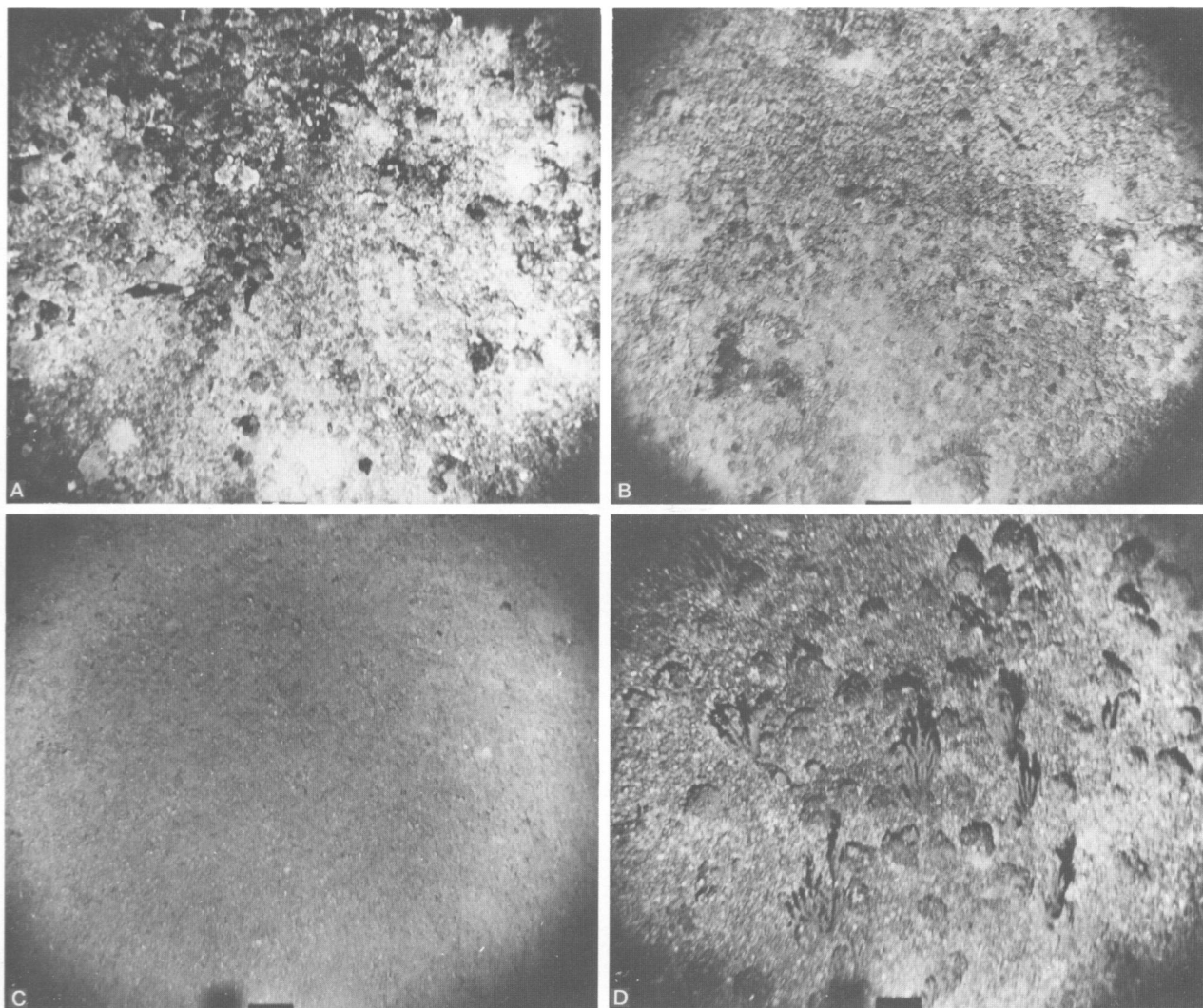
FIGURE 21.—Bottom photographs collected in shallow environments in the Strait of Sicily: A, Patches of sand and gravel showing coarse, calcareous sediment, including calcareous algae, algal balls and shells; station 151–59, 88 m, a shallow bank in the Strait Narrows. B, Calcareous sand and gravel, including shell and algae, on a bank south of Pantelleria Island; station 151–56, 119 m. C, Shelly sand on a shallow bank north of Cape Bon in the Strait Narrows; station 151–60, 106 m. D, Crinoids on a coarse calcareous sand and gravel, including calcareous algae and shell (example of *maerl*) on a bank northwest of Marettimo Island, north of the Strait Narrows; station 151–62, 133 m. (Photos courtesy of the Woods Hole Oceanographic Institution.)

One photograph (Figure 23A) shows the close relation between sedimentation and bioturbation: the fecal pellet-covered sea floor in the Malta Trough is partially veneered by a thin, smooth layer of fine-grained sediment. The lack of tracks on this smooth coating suggests that the mud layer has been recently deposited, although the transport process involved (gravity assisted bottom or turbidity current?) is unknown.

Structures Observed in X-Radiographs and Split Cores

Core radiography is a valuable technique for the definition of the different Strait of Sicily sediment types which in earlier sections were identified on the basis of texture and composition. X-radiographs are of particular importance for the recognition of the different mud types, and this technique also
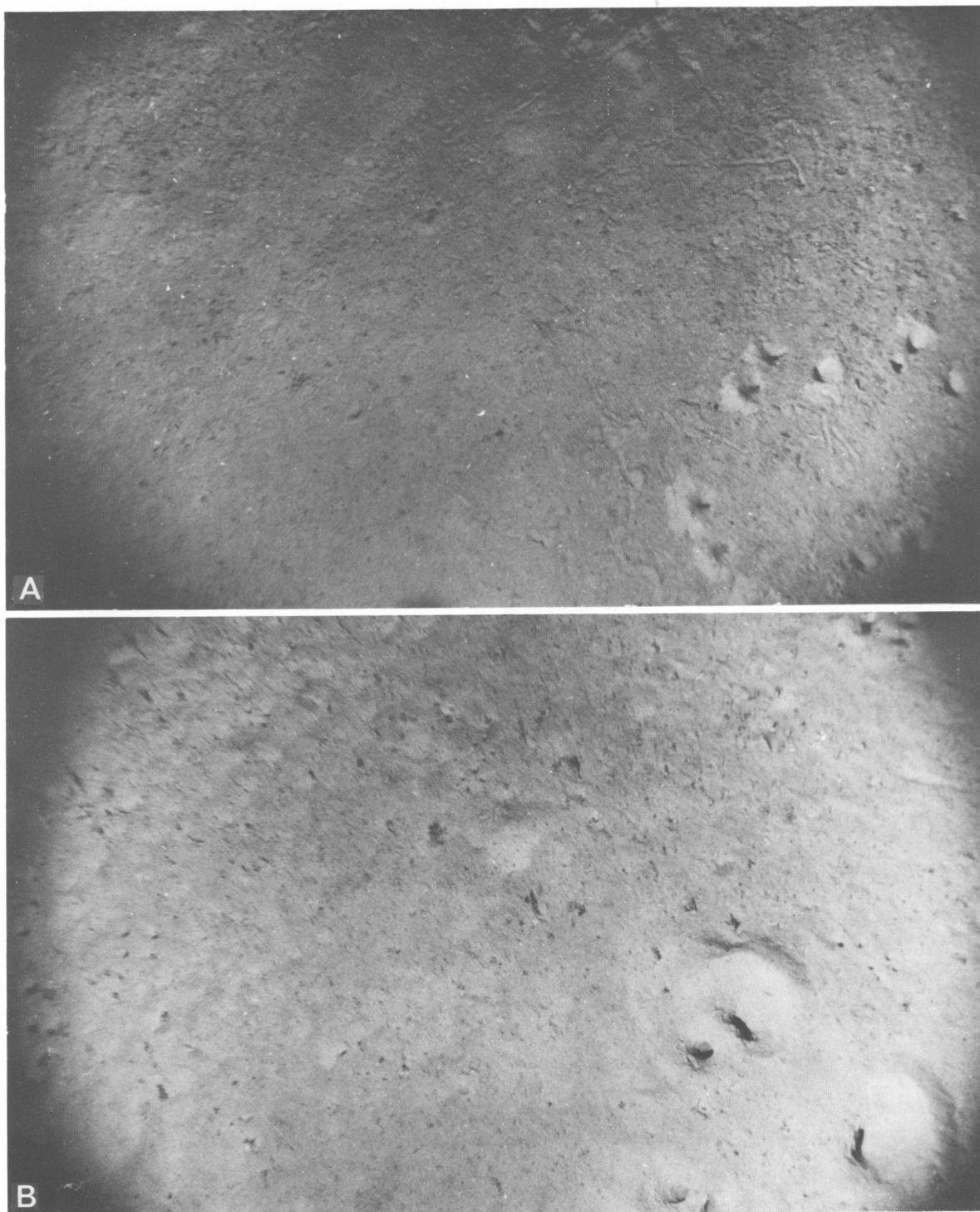
FIGURE 22.—Bottom photographs collected at intermediate depths in the neritic-bathyal platform showing bioturbated, oxidized hemipelagic mud surface: A, northwest of Marettimo Island; station 151–61, 380 m; B, Strait Narrows; station 151–58, 567 m. (Worm tubes—see shadows— are noted in lower photograph; photos courtesy of the Woods Hole Oceanographic Institution.)
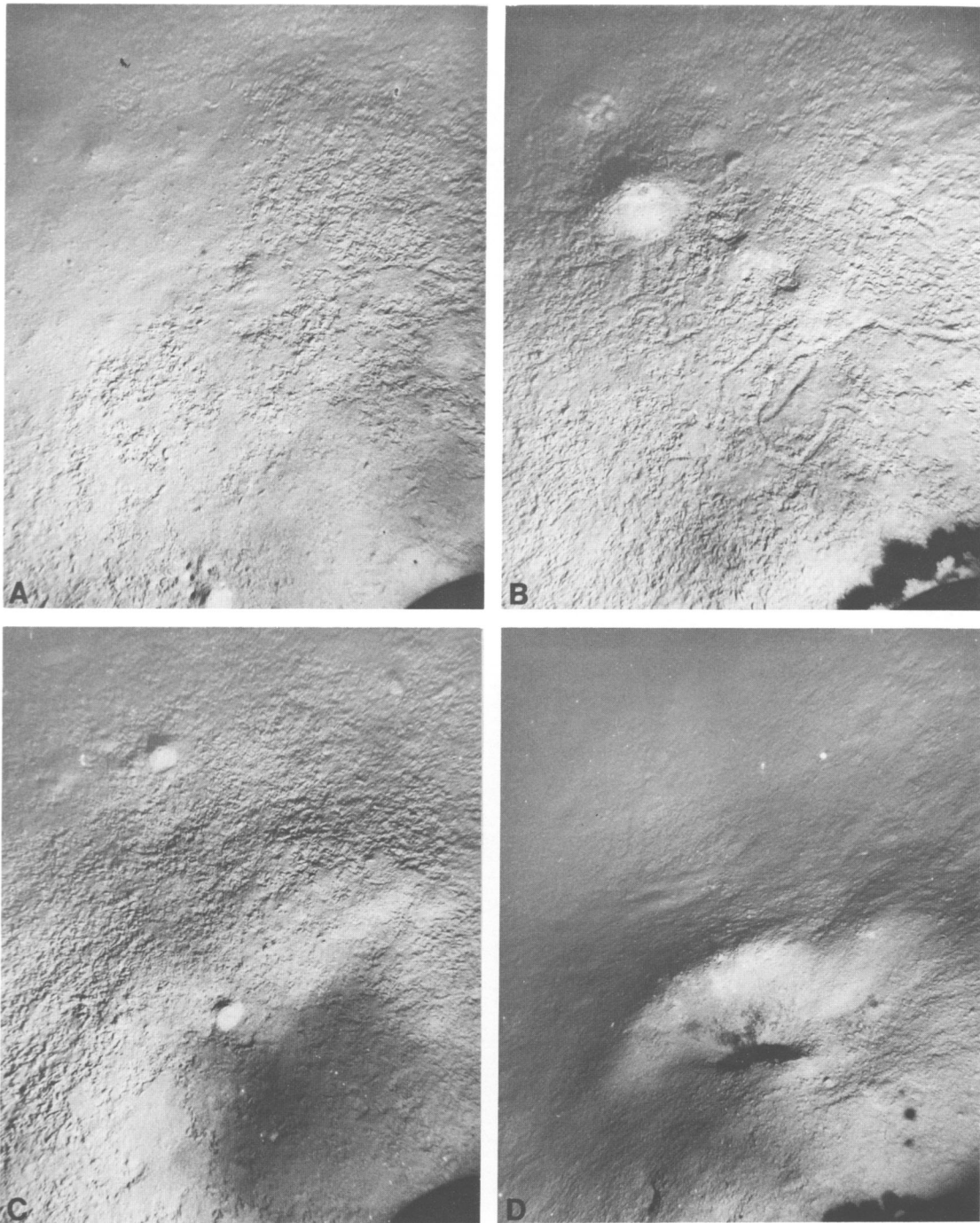
FIGURE 23.—Bottom photographs collected in Malta Trough (station V 14–K53, 1587 m) showing typical deep basin surficial sediment cover consisting of bioturbated structures and fecal pellets: A, partially buried biogenic structures and pellets by fine-grained sediment; B, meandering plow marks (holothurian or echinoid trails) and small volcano-like mound with apical vents; C, conical mounds and locally partially buried fecal pellets; D, large depression, possibly fish produced structure. (Photos courtesy of the Lamont-Doherty Geological Observatory of Columbia University.)
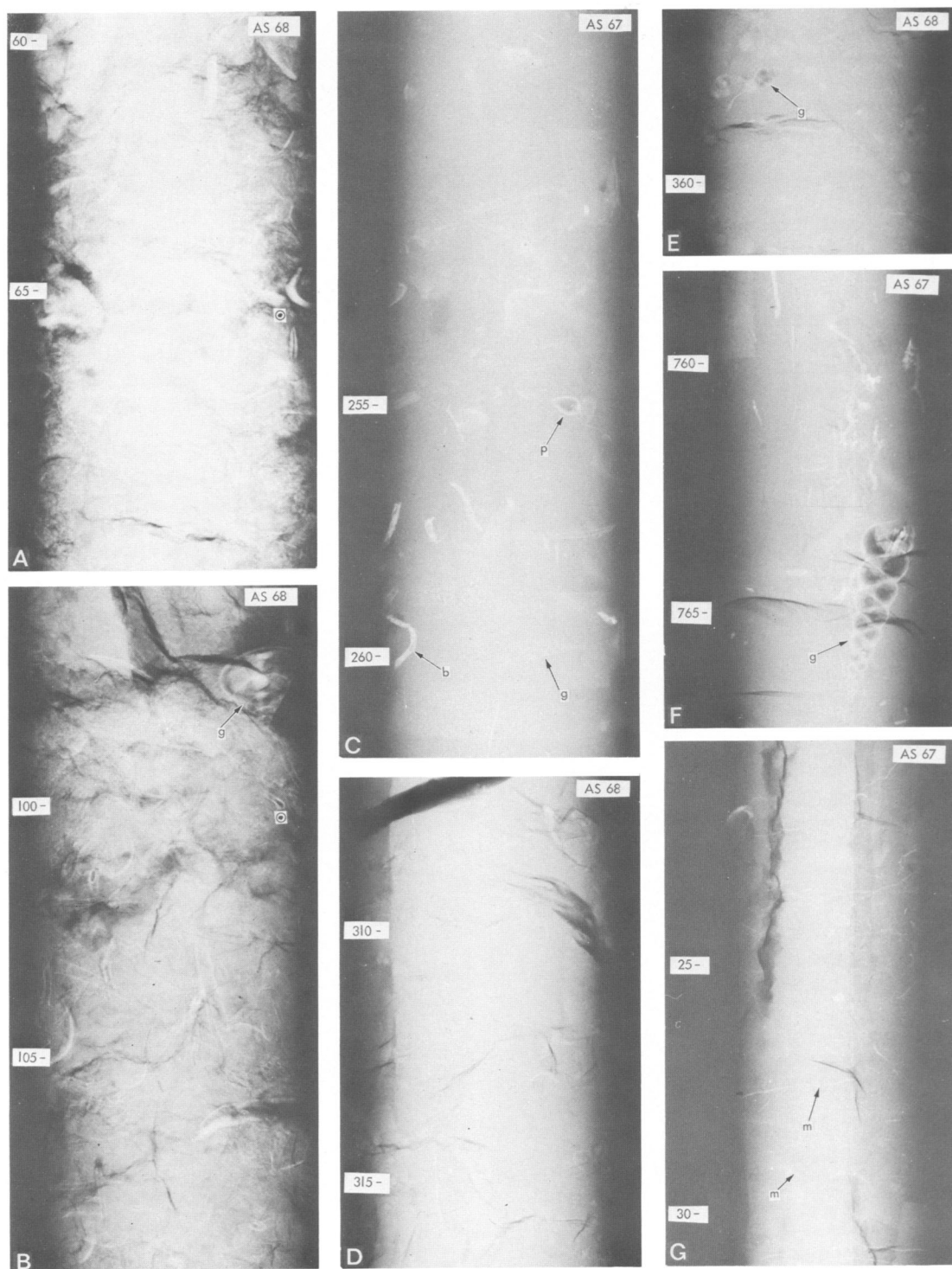
FIGURE 24.—Selected X-radiographs (negative prints) of cores collected in the shallow platform environment: A, B, coarse calcareous sand type; C, D, sand-silt shallow water sediment type; E–G, shallow water mud type (b = burrow, g = gastropod, p = pelecypod, m = *mycellia*). (Vertical scale given in centimeters from top of core; see also Figure 34 for core logs.
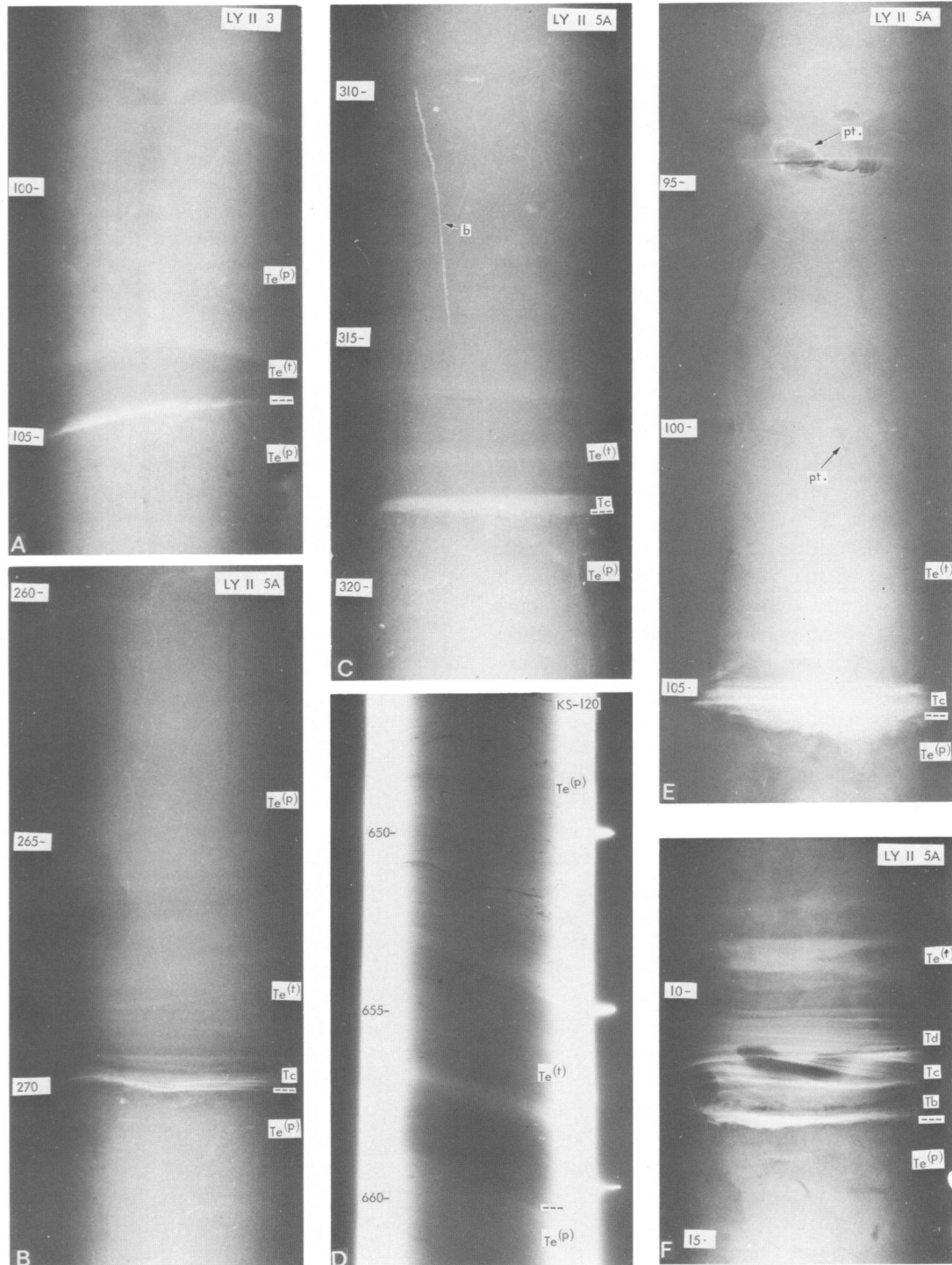
FIGURE 25.—Selected X-radiographs (negatives, except D) of cores showing turbibite sequences collected on the Ionian slope (LY II–3) east of the Strait and in deep basins (LY II–5A, Pantelleria; KS–120, Linosa). Sand and silt laminae appear light in negative prints (Tb–Td = Bouma turbidite sequence; $T_e^{(t)}$ = turbidite mud; $T_e^{(p)}$ = hemipelagic mud; b = burrow; pt = pteropod). (See also Figures 34 and 35 for core logs.)

serves to define sediment sequences. The X-radiographs illustrated in this study (Figures 24–32) in most cases are negatives (identical to the original radiograph, where silt and sand layers appear as light-toned bands); in a few cases we have used positives (Gesite cores in Figures 27, 31, 32).

The coarse calcareous sand type can easily be recognized in both split cores and X-radiographs. It does not show any primary stratification or grading (Figure 24A,B), and well-preserved shell, small shell fragments, and detrital grains are well mixed texturally. Different degrees of abrasion are displayed by the coarse calcareous debris of relict and residual origin. These characteristics are the result of intense vertical bioturbation (cf., Sarnthein, 1972; Reineck, 1973; Kulm et al., 1975). Burrowing activity revealed in cores includes thick burrows and pods filled with coarse calcareous materials.

The sand-silt sediment type generally presents an excellent set of structures: parallel, ripple, and cross lamination are the most common. Sets of 1 mm or less in thickness prevail, while the cosets range from a few millimeters to several centimeters (Figures 25B,E,F, 32B). The basal contact of the sand and·silt layers records erosion, as indicated by scour-and-fill structures (Figure 25E). However, some of the finest grained silt deposits do not display an erosional basal contact (cf., Balearic Basin plain deposits discussed by Rupke and Stanley, 1974). Vertical graded bedding is usually visible in the lower member of the layers; a general upward decrease in grain size within the sand to silt grades is also present. Parallel lamination of fine silt and mud (darker zones in the X-radiograph negative prints) are in continuity with the basal silt or sandy layer (Figure 25F). Biogenic structures are rare in these deposits, except for some so-called "escape" traces.

The two basic types of ash layers differentiated earlier are also well marked in the X-radiographs. The pelagic settling type of volcanic air-borne ash is in most cases nonlaminated (Figure 27A,B); however, an upward coarsening or fining (i.e., an increase or a decrease in the amount and size of ash particles in the mud) is often apparent (Figure 27A,B). This gradual vertical change in the amount of ash particles in the mud is reflected in X-radiographs by a gradual change in tonality, from gray to black. Individual coarse grains of ash

in the mud are represented by black spots disseminated in a light matrix (Figure 27B).

Tephra layers also may display horizontal lamination (Figure 27C). However, the other types of structures recorded in the sand-silt sediments, particularly cross and ripple lamination, are uncommon in these deposits. The type of tephra layer structures are related to some degree with the distance from the volcano and the type of explosive activity.

Turbiditic ash layers, on the contrary, show the same type of structures as reported from the sand-silt type sediment (Figure 32B) and are difficult to differentiate from typical terrigenous turbidites on the basis of structures alone.

The shallow water, hemipelagic, and turbiditic mud types are differentiated in X-radiographs on the basis of the degree of bioturbation and the calcareous biogenic fraction disseminated in the mud matrix. Shallow water mud is highly bioturbated and contains abundant mollusc shells (gastropods, pelecypods) floating in the mud matrix (Figure 24E–F, arrows g, p). This mud types does not show any kind of lamination or other type of primary sedimentary structure. Biogenic structures are abundant and include various types of burrows (mycellia in Figure 24G, arrow m; coils and spiral-shaped burrows; single cylindrical burrows; etc.). Shallow water mud is usually gradually transitional with the sand-silt type of shallow water deposits (Figure 24C,D); both types display similar features in the X-radiographs.

The hemipelagic mud type is characterized by diverse types of biogenic structures (see Uniform Sequences, next section), light specks dispersed in the mud matrix and pteropod shells "floating" in the fine matrix (Figures 25, 26.) The speckled aspect is produced by large numbers of foraminiferal tests and small fragments of pteropods (cf., Rupke and Stanley, 1974).

The turbiditic mud type displays a generally smooth, uniform aspect in the X-radiographs; its basal part, however, may be finely laminated (Figure 25B,D). This mud type is generally not bioturbated, but may show threadlike vertical tubes (Figure 25C). Mycellia, although uncommon in this type of mud, is sometimes observed (Figure 25B).

Sapropel layers are characterized by fine, horizontal laminae and no biogenic structures (Figure
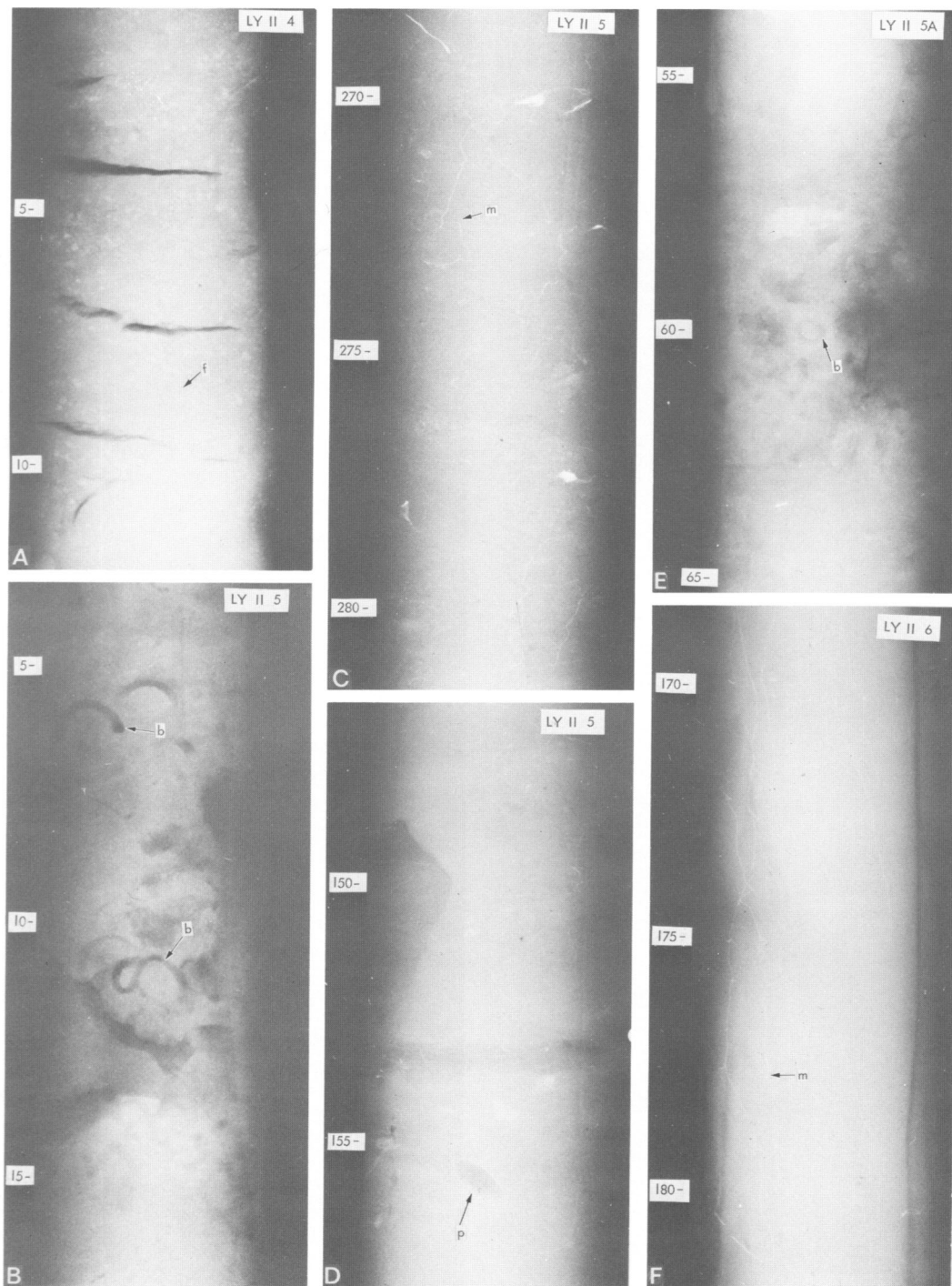
FIGURE 26.—Selected X-radiographs (negatives) showing hemipelagic mud and biogenic structures: A, Neritic-bathyal environment; speckling produced by foraminifera (*f*). B, Intermediate depth basin environment; core section shows intense bioturbation and coiled burrow (*b*). C, D, *Mycellia* small fucoid-like tubes (*m*) and pelecypod (*p*) (dark laminae may be a reworked turbidite mud layer). E, Intensely mottled mud in Pantelleria Basin. F, Uniform hemipelagic mud with *mycellia* in the North Marettimo Basin. (See also Figure 34 for core logs.)
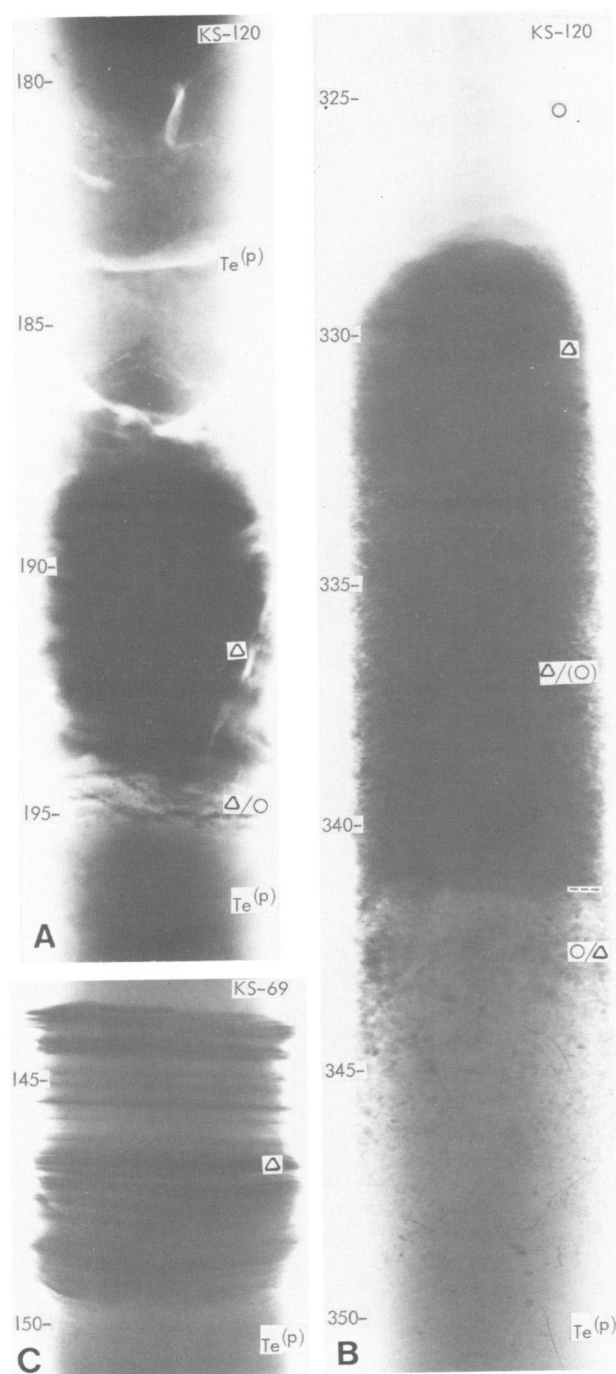
FIGURE 27.—Selected X-radiographs (positives) showing examples of volcanic ash interbedded in mud from cores in Linosa Trough: A, vertically graded ash layer (194–185 cm); B, coarsening-upward ash layer; C, laminated type (open triangle = ash; open circle and $T_e^{(p)}$ = hemipelagic mud). (See also Figure 35 for core logs; explanation in text.)

28, black square symbol). In contrast, the organic ooze displays evidence of burrowing activity (Figure 28, open square). A layer of concentrated pyritized tubes (b) is commonly associated with this type of deposit. The organic ooze extends vertically to the base of protosapropel deposits (partially blackened square symbol). The burrowing activity decreases sharply in the protosapropel sediment proper and phases out in the overlying sapropel.

Definition of Sequences

GENERAL

The late Quaternary Strait of Sicily lithofacies can be distinguished from those in the adjacent deep basins (Balearic, Ionian) by a high degree of bioturbation and mixing of sediment by organisms, which results in textural uniformity, and by the presence of relatively large amounts of coarse bioclastic sediment. Cores east of the Strait on the Ionian Basin slope (cf. core LY II–3) are more highly variable both in terms of facies and sequences; cores on the western slope into the Algéro-Balearic Basin comprise a large proportion of turbiditic sequences (sand and mud turbidites). Cores collected in the Strait proper are distinct and generally not transitional with those of the contiguous slopes and adjacent deep basins. We can demonstrate that regional sedimentation patterns and petrology in the Strait are closely related with geographic setting and specific depositional environment, including proximity to the Strait Narrows.

The different types of sediment present in each Strait of Sicily core can be grouped into major assemblages. The sediment types grouped within each of these assemblages are termed sequences, and these are defined on petrologic characteristics which present distinct natural lateral and vertical trending lithological transitions. Each sequence is defined on the basis of a succession of sediment types that reflect deposition resulting from either a specific sedimentary process (turbidity current, mass flow, etc.) or a regionally important, large-scale environmental event (cf., climatic changes significant enough to alter water mass stratification and flow, eustatic oscillatory sea level patterns, and/or biogenic production).
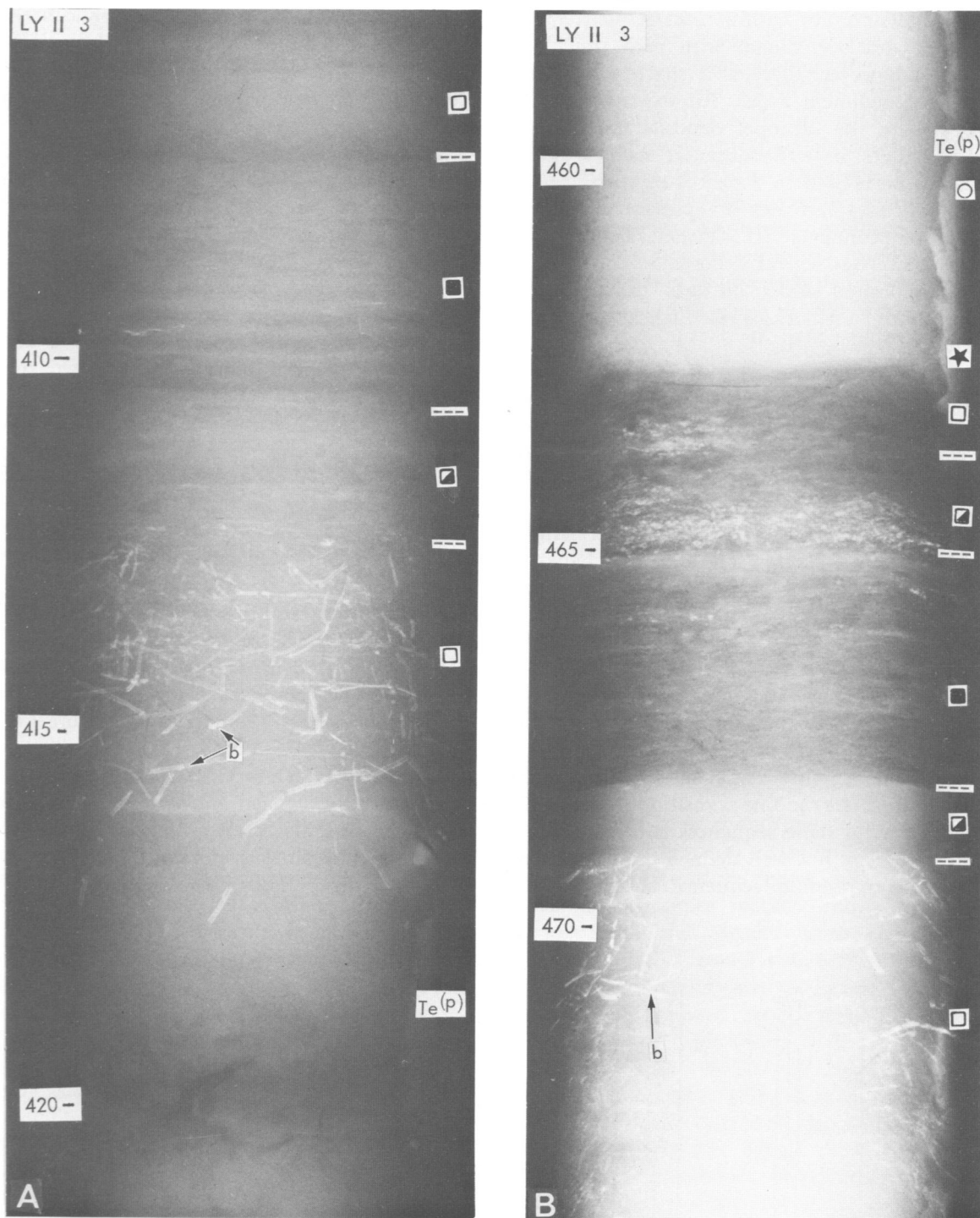
FIGURE 28.—Selected X-radiographs (negatives) from core LY II–3 collected on the Ionian slope east of the Strait of Sicily (see Figure 34): A, B, illustrate the sapropel sequence which includes, from the base up, organic ooze, protosapropel, and sapropel. (Symbols explained in Figure 29; note high concentration of pyritized burrows (b) in the organic ooze layer; see Figure 34 for core log.)

The sediment types within most sequences are gradational and transitional with each other; in some cases, however, there is a sharp distinction between the sediment types. An example of the latter case are the sapropel deposits that record marked changes in environmental factors. A sequence can be related to a plexus of specific sedimentary processes and thus it represents a natural grouping of sediments (cf., Visher, 1965). Each sequence comprises several lithosomes ("a body of sediment deposited under uniform physicochemical conditions," American Geological Institute, 1972:413).

Four major sequences are distinguished (Figure 29): (1) upward-coarsening or upward-fining sequence; (2) uniform sequence; (3) turbiditic sequence; (4) sapropel sequence. Probably the most characteristic of these in the Strait of Sicily is the uniform sequence. The upward-fining and upward-coarsening sequences are also well represented, particularly on the shallow platform and banks.

Upward-Fining and Upward-Coarsening Sequences

The upward-fining and upward-coarsening sequences (Figure 29A) are best developed in the shallow platform environment (8); they comprise bioclastic sands (Figure 24A,B) and shallow water muds (Figure 24E,F,G). The transition between the different terms of these sequences is often gradual and the limits are not well defined (Figure 24C,D). The upward-coarsening sequence shows an up-

ward increase in sand and coarser fractions (largely bioclastic), including shells (largely molluscan). The basal mud of this sequence (Figure 24E,F,G) contains a neritic faunal assemblage, including benthic foraminifera. The transitional facies show a gradual change between the extreme textural types. The total thickness of the sequence can exceed 5m (Figure 34, cores AS 6–7, 6–8). The upward-fining sequence shows an inverse development of texture and sedimentary structures (cf., Figure 34, upper part of core AS 6–7).

Of the four major sequences, these show the most gradational transition between the different sediment types. In some cases, however, the bioclastic sand layer displays an irregular basal contact as a result of erosion or nondeposition. Where the base is sharply defined, evidence of biogenic activity is preserved in the form of sand burrows in the underlying mud just below the coarse calcareous sand layer.

Cores in the Strait Narrows are interesting in that, although recovered from greater depths, they display sequences similar to those described as typical of shallow platform sedimentation. Core 140, *Vema 14*, at 166 m (Figure 33), shows a marked upward-fining sequence, like those in other shallow depth bank environments, while core KS 12 at 956 m (Figure 35) shows distinct alternations of thick (to 90 m) coarse sands and bioturbated muds. The sands have been introduced periodically by turbidity currents (graded sand to mud units) and mass flow mechanisms (texturally clean grain flow to muddy debris flow units). One core, 7, *San Pablo*
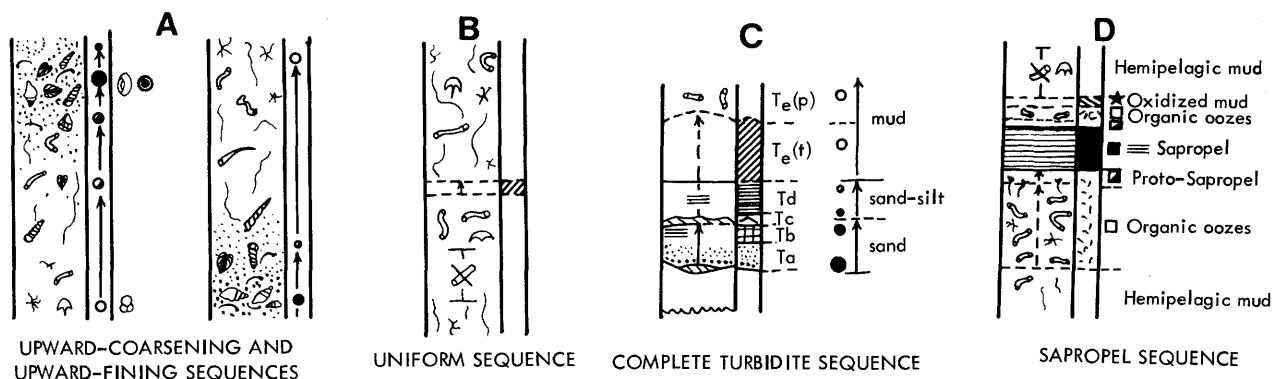

FIGURE 29.—Schematic representation of the major sediment sequences discussed in text. (Symbols here are used in core logs (Figures 33–35) and on X-radiographs (Figure 24–32); explanation in text.)

8, at 166 m (Figure 33), collected near the center of the Strait at intermediate depths (350 m), shows a lithology transitional with the types described above: i.e., a vague upward-fining sequence with intercalations of coarse bioclastic sand layers and muds toward the upper portion of the sequence.

The coarsening- and fining-upward sequences are similar to those cored in deltaic environments (Oomkens, 1970; Maldonado, 1975). The upward-fining type may be analogous to transgressive deltaic sequences while the upward-coarsening sequences correspond to deltaic offlap sequences. However, the assemblage of sedimentary structures present in the Strait cores are not closely similar to those of deltaic origin, and the source and composition of detrital material is also different. The upward-fining sequences in the Strait and deltas in general essentially are produced by the same type of sedimentary event, i.e., the postglacial eustatic rise of sea level. On the other hand, the upward-coarsening sequences in deltas are the result of progradation as reflected by a high detrital influx; in the Strait this vertical progression is related to eustatic changes of the sea level across the Strait surface. These oscillations altered productivity and current activity and thus controlled the subsequent deposition of coarse biogenic deposits.

On some banks, fine grained sediments have accumulated since the last rise of sea level, thus developing an upward-fining sequence. On others, truncation and continued nondeposition have prevailed since the last eustatic low stand.

Radiocarbon dating (Milliman et al., 1972, discussion in later section) substantiates the theory that the coarse calcareous sand is best developed during the rising stages of sea level rather than during the lowering or lowest sea level stage. In any case, there can be little doubt that these sequences are closely associated with dynamic sea level changes. During periods of stabilized sea level (such as at present) the rate of sedimentation has been notably reduced, at least in the deeper sectors of the shelf.

Uniform Sequence

The most diagnostic features of cores from the neritic-bathyal environments are (1) their extremely uniform, homogeneous aspect, even in X-radiographs, and (2) the abundance of bioturbation structures. Poorly stratified mud layers are noted in a few cases. Typical examples of such uniform cores include, among others, LY II–4 and 6A (Figure 34), and KS 78 and 105 (Figure 35). Another distinction is the low sand content (2%–7%) in the mud; this fraction consists mostly of planktonic foraminifera, pteropods, and a minor but diverse assemblage of faunal remains.

The uniform sequence includes hemipelagic and, less frequently, turbiditic muds which have been intensively homogenized by biogenic sedimentary structures (Figure 26). These sequences are most prominent in neritic-bathyal platform and depression environments (4, 5). The most common structure is subtle mottling visible in X-radiographs (Figure 26E). Bioturbation is vertically developed and not of the "layer-by-layer" type characteristic in some areas of the Mediterranean such as the Strait of Otranto (cf. Hesse and von Rad, 1972). There are various types of distinct burrows in addition to mottled structures. The finest deposits display tiny light-colored threadlike shafts (Frey, 1973); these are straight or slightly curved, sometimes sharply bent, and are usually less than 0.5 mm thick and several decimeters in length (Figure 26F). This structure is similar to the fine stringlike feature called *mycellia* (Bouma, 1964; Reineck and Singh, 1973:406), also noted elsewhere in the Mediterranean (Huang and Stanley, 1972). Burrow systems of small fucoid-like or chondrite-like tubes are similar to the above; these are a few millimeters long and branch dendritically (Figure 26c). The burrow casts of both types include either carbonate or pyritized material. According to Hesse and von Rad (1972), the chondrite-like burrows and burrow casts are possibly the hyphae of marine fungi. Nevertheless, Howard and Frey (1973) describe the burrows of capitellid polychaetes in estuarine muds, which are similar to both *mycellia* and chondrite-like types. The laterally stopping structures (Hesse and von Rad, 1972), or press structures of Reineck and Singh (1973:141), are also abundant, and these are interpreted as sea-urchin tracks (Howard et al., 1974). Other burrows include tunnels, shafts, and spiral-shaped coils that are between 2 to 20 mm wide and a few centimeters or decimeters long (Figure 26B). These burrows are attributed to acorn worms. The simple, bifurcated burrow perpendicular, or inclined, to bed-

ding can be ascribed to dwelling structures; the single cylindrical type may be feeding and/or dwelling structures, while the spiral pattern burrow may represent travel traces (Seilacher, 1953; Frey, 1973).

The processes that result in homogeneous sequences are either of primary or secondary origin. Homogeneous sediments result from regular, uniform deposition or very high sedimentation rates (= primary type, cf. Moore and Scruton, 1957). Homogeneity of deposits can also result by a total destruction of minor internal structures by burrowing organisms (= secondary origin); this process has been described in the Gulf of Mexico (Moore and Scruton, 1957). The presence of poorly preserved turbiditic layers intercalated with uniform sequences and a rate of sedimentation which is not particularly high suggest that the latter origin is of greater importance in the Strait of Sicily.

TURBIDITIC SEQUENCE

The most distinctive sediment types in basin cores (environments 6 and 7) are the turbiditic units alternating with hemipelagic mud. The turbidites include classic sand and silt turbidites (Figures 30, 31) displaying various terms defined by Bouma (1962) and others, as well as mud turbidites, $T_e^{(t)}$, as described in detail by Rupke and Stanley (1974). Only rarely is the complete Bouma sequence (Figure 29c) observed; one example of a sequence of Ta-b-c-d units is shown in Figure 30. Most of the turbidites in Strait basins are base-cut units of the Bouma division, i.e., Tb-c-d, Td (Figure 25).

The mud turbidite sequences are important in this area. These display all of the characteristics of sand turbidites including fine lamination (analogous to the d-division of sand-silt turbidites), vertical sorting of the components, and graded bedding. Evidence for this type of fine-grained turbidite has been provided during the past few years by several authors (van Straaten, 1970; Piper, 1973; Rupke and Stanley, 1974; etc.). Nevertheless, it should be noted that other depositional mechanisms have been proposed for vertically graded pelitic sediments, in addition to pelagic settling and turbidity currents. For instance, normal bottom currents, and in particular geostrophic currents (Heezen et al., 1966; Flood and Hollister,

1974), have been suggested as a major factor in deepsea sediment deposition although it is questionable that they would result in graded deposits. Other proposed mechanisms are low-density and gravity-assisted flows carrying fine-grained sediments to deep marine environments (Moore, 1969; Stanley et al., 1970, 1971; Huang and Stanley, 1972; van Straaten, 1972).

The base of turbidites in Strait basins sometimes includes calcareous sand, but more often the turbidites consist almost completely of silt and clay. Compositionally, the bioclastic sand fraction in turbidites is comparable to sands on the shallow and neritic-bathyal platform above the basins but contains a higher percentage of planktonic foraminifera.

In some cores, particularly those in the Linosa Trough, tephra (ash) layers are important (Figure 27, 31); a number of these sand-size deposits also present typical turbidite structures including graded bedding (Figure 31A). Although some volcanic sands have been transported into the basins by turbidity currents, we suggest that graded volcanic layers also can form by lateral wind and water transport of ash and subsequent settling of these particles through the water column.

Some layers composed largely of ash particles show the typical sequence of turbidite structures (Figure 31A, 108–30 cm; 31B, 530–508 cm; Figure 35). Sarnthein and Bartolini (1973) discussed this type of sedimentation in the Tyrrhenian Sea. In contrast, air-borne tephra layers lack the vertical sequence of primary sedimentary structures associated with the typical turbidites although they may display reversed or normal grading (either coarsening upward, Figure 27B, 345–328 cm or fining upward, Figure 27A, 194–187 cm and Figure 31A, 115–111 cm) or horizontal lamination (Figure 27C, 150–143 cm). These two structures reflect different types of explosive activity.

The adjacent islands of Linosa (di Paola, 1973) and Pantelleria (Villari, 1969) shed some information on this matter. Pantelleria, for example, is composed of a large number of interbedded ignimbrites, and both welded and unwelded pumice fall deposits and some well-stratified fine ash (R.S.J. Sparks, pers. comm.). Gas-blast eruptions of the Plinian or sub-Plinian type are known to generally produce poorly stratified and often reversely graded deposits (Sparks et al., 1973; Walker, 1973). Well-
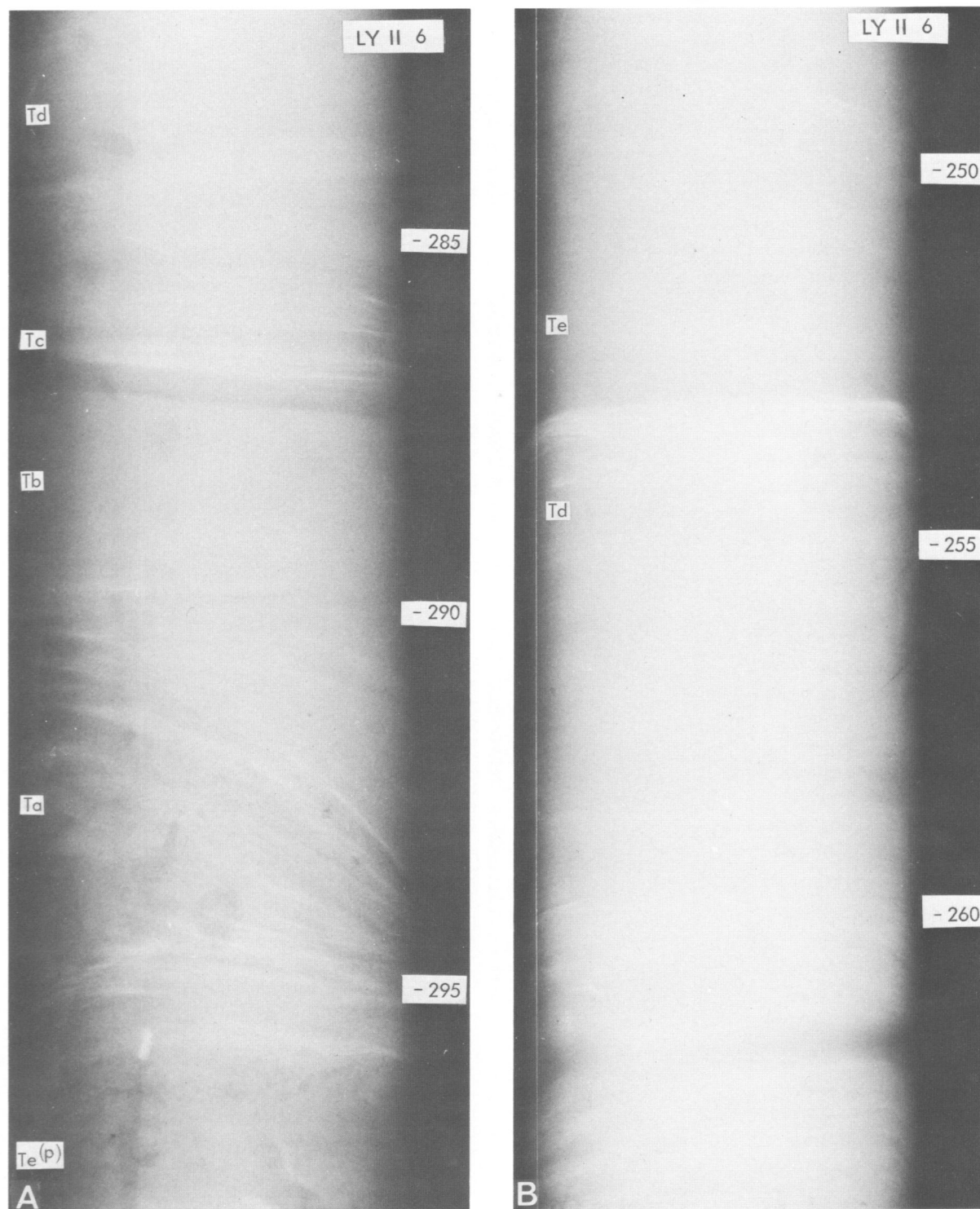
FIGURE 30.—Selected X-radiographs (negatives) from core LY II-6 collected in the North Marettimo depression showing one complete vertically graded sand to mud turbidite sequence. (See Figure 34 for core log.)
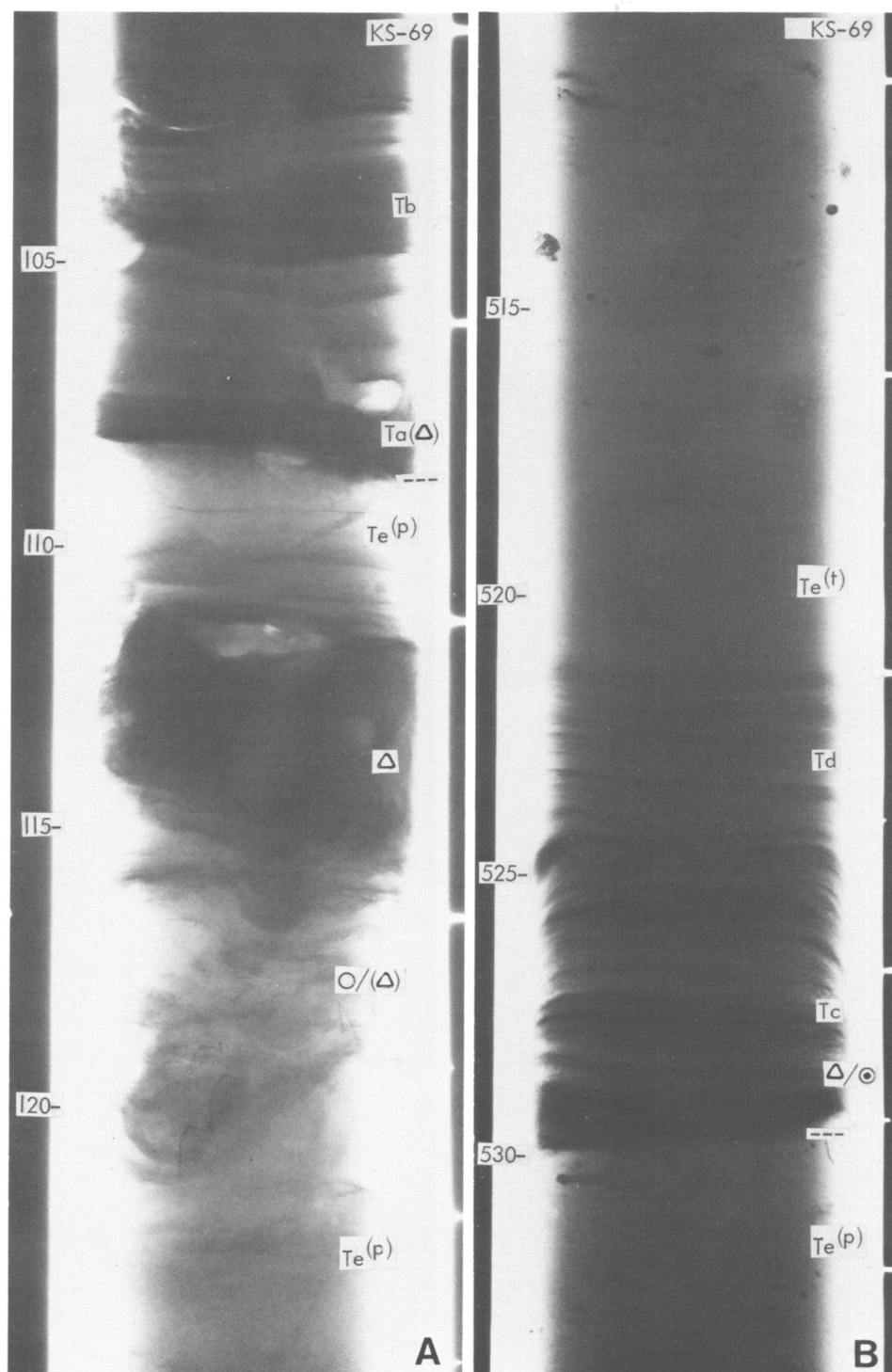
FIGURE 31.—Selected X-radiographs (positives) of core KS 69 from Linosa Trough showing turbidite sequence and ash layer between mud units. (Open triangle = volcanic ash; open circle and $t_e^{(p)}$ = hemipelagic mud; circle with dot = calcareous bioclastic sand; other symbols on Figure 29; see Figure 35 for core log.)

stratified deposits on land are associated with phreatomagmatic eruptions or vulcanian pulse eruptions. The structures observed in the Strait may be analogous. Each graded ash layer probably records a single eruption. Base surge density flows (Moore, 1967) as well as ash flows may be of some importance in the formation of the volcanic deposits cored in the Strait.

Another type of gravity flow deposit is illustrated in Figure 32. Core KS 12 collected in a small basin in the Strait Narrows displays thick layers of sand and sandy mud interbedded with mud (Figure 35). These layers consist of calcareous sand, in some instances clean and in some instances muddy, without grading or sharp contact in some cases. Mechanisms other than turbidity currents are postulated: in the case of clean sand, grain flow transport is envisioned; debris flow or slumping may explain the sandy mud and muddy sand mixtures (Hampton, 1972; Middleton and Hampton, 1973). Further evidence of slumping is recorded in basins, such as a 70-cm thick contorted unit in core 139, *Vema 14*, at 1703 m in the Malta Trough (Figure 33).

SAPROPEL SEQUENCE

The sapropel sequence is found only in cores on the eastern margin of the Strait (i.e., on the slope extending into the Ionian Basin) but not in the Strait proper. The idealized complete sapropel sequence (Figure 29) based on an analysis of core LY II–3 (Figure 34) comprises a basal organic ooze layer (Figure 28) usually in continuity over gray hemipelagic mud. The organic ooze is intensively bioturbated (presence of burrows, etc.) and frequently includes a zone of pyritized worm tubes (Figure 28, *b*) toward the top. Organic ooze grades upward into a protosapropel sediment type distinguished by a low degree of bioturbation. The black, organic rich sapropel layer proper is usually well defined, particularly in X-radiographs, where it appears as a bundle of thin parallel laminae (Figure 28A) consisting of alternating calcareous coccolith-rich muds and somewhat thicker layers of calcareous-poor terrigenous mud. The sapropel is capped by a thin protosapropel layer, which grades upward into an organic ooze (Figure 28B). The sequence is covered by a layer of light brown to dark yellowish orange (5 YR 5/6–10 YR 6/6) oxi-

dized mud. In core LY II–3 the sequence is about 20 m thick and is usually complete.

Sapropels in the eastern and central Mediterranean are believed to have accumulated during stagnant phases associated with stratification of water masses and formation of H_2S-rich anaerobic bottom waters (Olausson, 1961; Ryan, 1972; van Straaten, 1972). The vertical sequence appears to closely reflect large-scale oceanographic fluctuations. The organic ooze indicates that, initially, conditions (including vertical mixing and oxygenation of water masses) fostered a high degree of benthic activity as attested by the importance of bioturbation. Evidence that the water mass above the sea floor became progressively anaerobic and rich in H_2S is provided by an increase of pyritized burrows and eventual absence of any bottom organic activity in the protosapropel and sapropel. The sapropel proper records a major anaerobic phase (van Straaten, 1972). The varvelike sapropel laminations, unlike those of the protosapropel, are attributed to periodic high coccolith productivity possibly resulting from seasonal upwelling and subsequent sinking of the coccoliths (cf., Gulf of California, van Andel, 1964; Black Sea, Degens and Ross, 1974). A progression to more normal open ocean conditions and vertical mixing is indicated by the subsequent deposition of protosapropel and organic ooze. The upper orange oxidized layer represents a return to oxygen-rich bottom water conditions. It is concluded that sapropel sequences observed east of the Strait are comparable to those in the Herodotus Abyssal Plain and Nile Cone areas detailed by Maldonado and Stanley (1975).

Sedimentation and Stratigraphy in the Strait Environments

REGIONAL DISTRIBUTION OF SEQUENCES

Our regional survey of sediment types and sequences reveals the close correlation between the Strait of Sicily depositional environments and the resulting Quaternary sedimentary facies. This relation is illustrated in Figures 33, 34, and 35. The shallow platform environment is characterized by coarsening- and fining-upward sequences, which result from the association of two major sediment types: coarse calcareous sand and shallow water
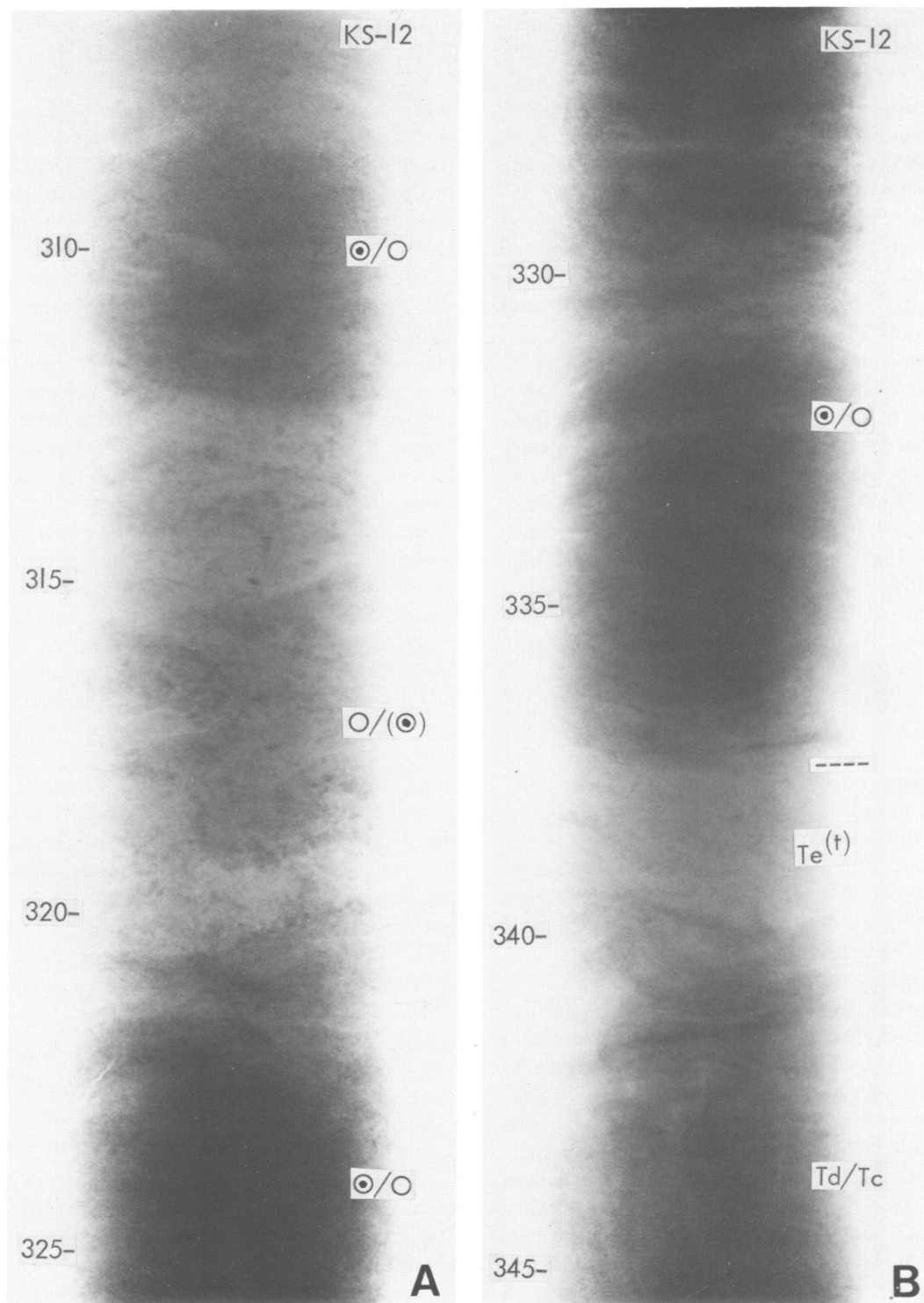
FIGURE 32.—Selected X-radiographs: positives of core KS 12 from small basin in the Strait Narrows showing sandy mud and muddy sand layers interpreted as gravity flow deposits. (Open circle = hemipelagic mud; circle with dot = calcareous bioclastic sand; other symbols on Figure 29; see also Figure 35 for core log.)

FIGURE 33.—Lithologic core logs along a transect crossing the Strait Narrows, shallow platform, and basin environments in the Strait of Sicily. (Isochron position is tentative; correlation is based on comparison with cores in Figures 34 and 35 where carbon-14 dates are available. Symbol legend also in Figure 29.)

FIGURE 34.—Lithologic core logs along a transect crossing slopes east and west of the Strait, shallow platform, neritic-bathyal platform, and basin environments in the Strait of Sicily. (Isochrons based on carbon-14 data (see Figure 38). Symbol legend in Figures 29 and 33.)

mud. The uniform sequence prevails in the neritic-bathyal environments; here sedimentation of hemipelagic muds is dominant. The muds are subsequently bioturbated; intercalations of mud turbidite sequences are also present in these environments. Sedimentation in the basin environments is similar in some respects to that in the neritic-bathyal environments. However, deep basin deposits are recognized on the basis of well-stratified units including alternating layers of turbiditic sequences, hemipelagic mud, and volcanic ash layers. Gravity flow deposits such as slump and grain flow units also occur in the basin environment. Environments in or close to the Strait Narrows are generally typified by a relatively higher proportion of coarse calcareous sand deposits.

Certain coarse calcareous sand layers encountered in all of the shallow platform environments may be lithostratigraphically correlatable. However, the age of this lithosome need not be strictly isochronous since such deposits are closely related to depth, and thus in turn to the rise or lowering of sea level and productivity as explained earlier. It is conceivable that the calcareous sand recovered in different cores collected at the same depth may be of the same age. However, it has not been ascertained that the beds are continuous laterally and they may in fact be related to several different Pleistocene eustatic oscillations.

We were unable to correlate individual layers or sequences between the cores collected in other environments, even within the small deep basins. One of the difficulties in the case of the neritic-bathyal cores is their uniformity and lack of distinct correlatable horizons. Furthermore, sapropel sequences which are useful for correlation purposes, particularly in the eastern Mediterranean (Ryan, 1972; Maldonado and Stanley, 1975), do not occur in the Strait proper. Even well-stratified basin cores in specific basins could not be correlated on the basis of individual turbiditic sequences and tephra ash layers. Cores KS 120, KS 69, and KS 118 (Figure 35), and CH 61–19 (Figure 33) from the Linosa Trough are particularly interesting in this respect, for all were collected at about the same depth (within less than 40-m depth difference) along a transect about 20 km in length across the basin plain. Although these cores are similar in general appearance, the radiocarbon dates (Figure 35) indicate that correlation either

by individual layers or by sequences is not reliable. This does not rule out the possibility that some techniques, such as detailed chemistry and petrologic analysis of tephra layers (Keller et al., 1974; F. W. McCoy, pers. comm.), may be used in this respect. It should be recalled, however, that turbiditic ash layers tend to have a more limited aerial distribution than that of air-borne volcanic ash layers.

A discussion of correlation of Strait of Sicily cores by carbon-14 techniques will be treated in a later section.

ENVIRONMENTAL FACTORS CONTROLLING THE STRAIT SEDIMENTATION

In the following discussion we shall consider several aspects of the Strait of Sicily sedimentation in terms of environmental factors. In particular the following will be considered: (1) the role of Quaternary dynamics, including the factors related to the changes of climate and eustatic sea level oscillations; (2) the importance of depth; and (3) the biological factors. Although lateral correlation of specific units has not been accomplished, it is nevertheless possible to distinguish dominant patterns of sedimentation in each of the major environments. As will be recalled, three main parameters control sedimentation in any given environment: physical, chemical, and biological. Within the first group are included such factors as climate, depth, temperature, salinity, current systems, and boundary conditions of the environment (geometry, bathymetry, and geology, among others).

The Quaternary sea level oscillations related to major climatic changes are the most important factors that have determined the sedimentary processes in the shallow water platform environment. As demonstrated, the different sediment types and sequences developed here are to a large extent related directly to depth. As a consequence of depth changes, there have been alterations in current patterns and intensity, salinity and temperatures which inevitably affected the vertical evolution of the sediment sequences in this environment. It is apparent that the shallow platform lithofacies would be considerably more uniform had there been no Quaternary oscillations.
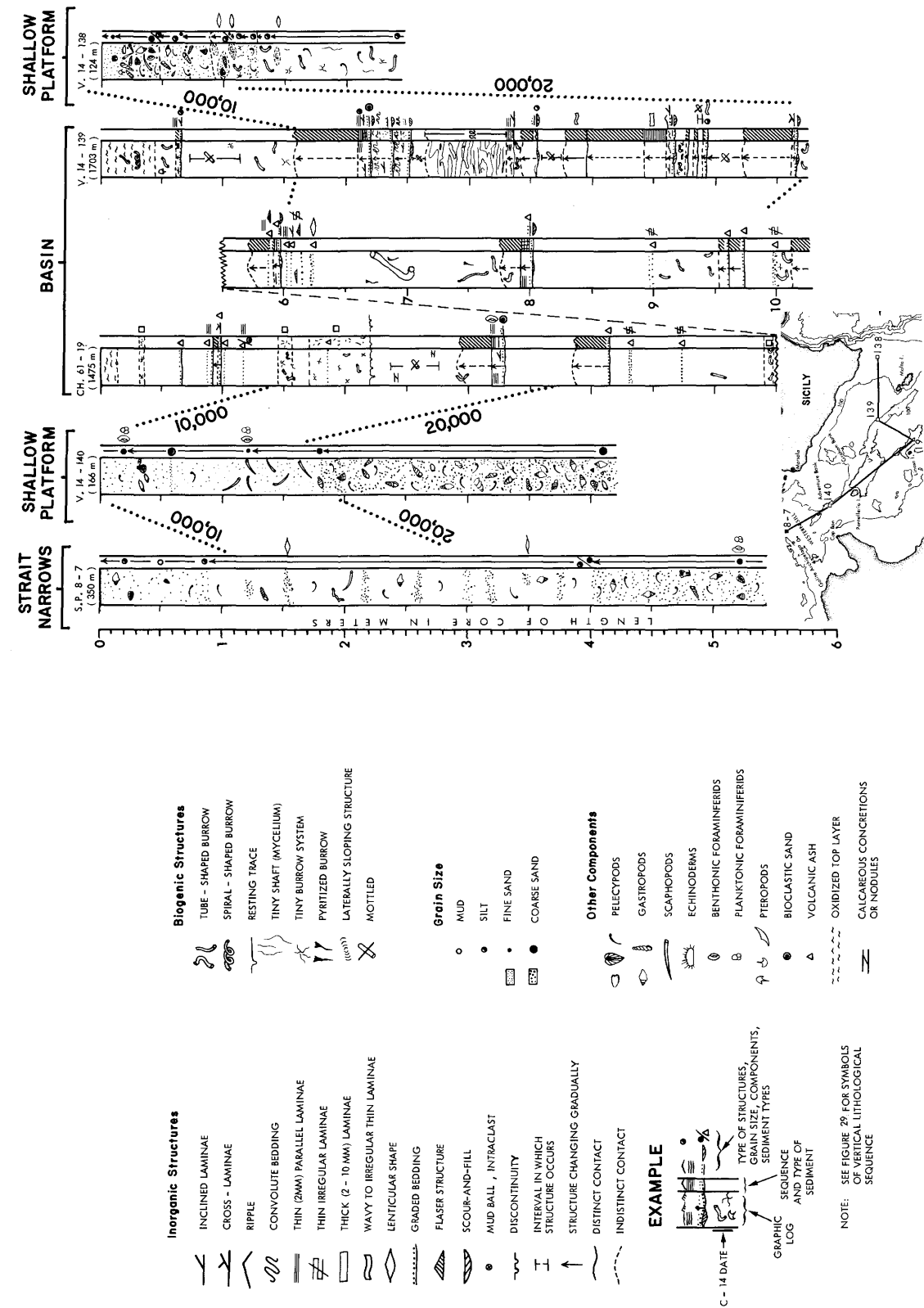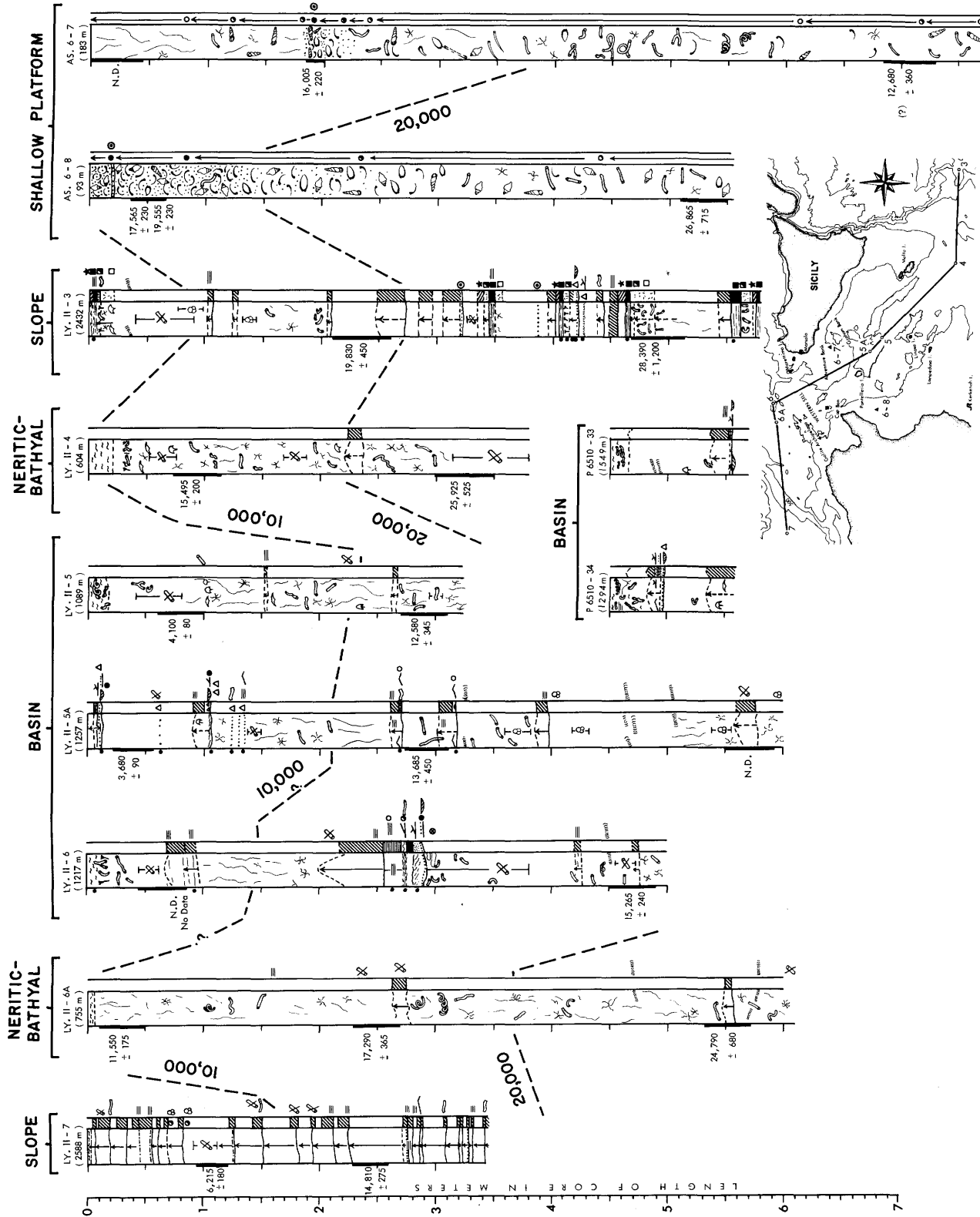
Moreover, the sediment types in the neritic-

FIGURE 35.—Lithologic core logs along a transect crossing Strait Narrows, neritic-bathyal, and basin environments in the Strait of Sicily. (Isochrons based on carbon-14 data (dashed line) and lithologic correlation (dotted line). Symbol legend in Figures 29 and 33.)
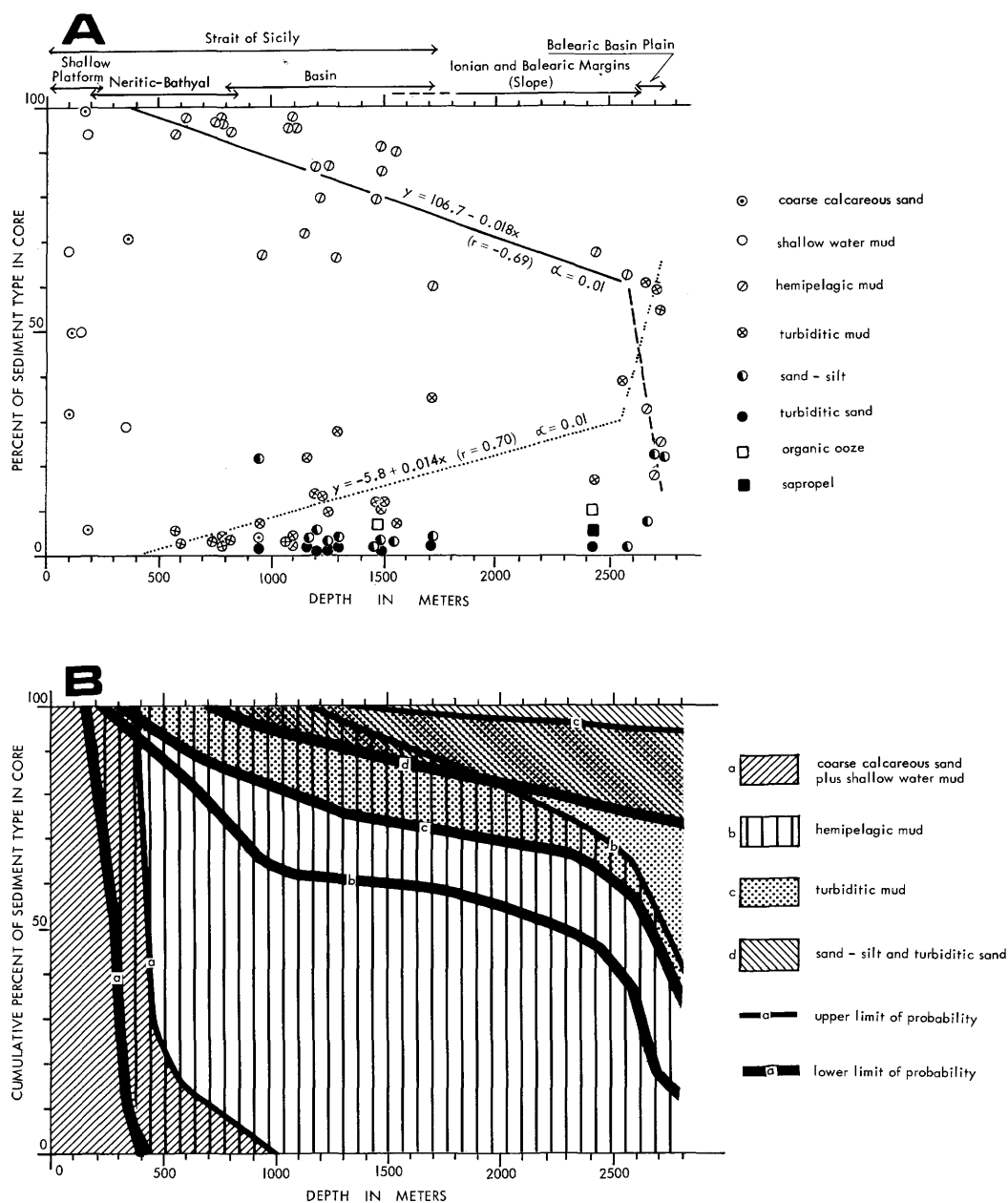
FIGURE 36.—Plots showing relation between sediment types in the different Strait of Sicily environments and depth: A, Percent of sediment type in core versus depth (solid line = regression line for hemipelagic mud type in Strait environments; dotted line = regression line for turbiditic mud in Strait environments; dashed line (for hemipelagic mud) and triple dotted line (turbiditic mud) = regression lines for Balearic Basin plain (includes data from Rupke and Stanley, 1974); this figure shows the inverse relation between depth and the percent of hemipelagic mud and the direct relation between depth and turbiditic mud). B, Cumulative percent of sediment types versus depth (cumulative percent of each group of sediment is calculated as follows: a, a + b, a + b + c, a + b + c + d; thin line = upper cumulative limit of probability for a given sediment group; heavy line = lower cumulative limit of probability for same sediment group; this diagram serves to predict the relative amounts of sediment types at given depths: at 1000 m, for example, 0% of type a, 65–100% of b, 0–18% of c, and 0–5% of d; at 2500 m, 0% of type a, 40–70% of type b, 10–35% of type c, 5–25% of d).

TABLE 4.—Percent and cumulative percent (in parentheses) of different sediment types in Strait of Sicily cores (percent of bioturbated section of total core thickness also shown; only two main types of sediments differentiated in shallow platform cores; coarse and bioclastic sand, and shallow water mud; sand-silt fraction of these cores attributed to either one type or another)

CORE	COARSE CALCAREOUS SAND	SHALLOW WATER MUD	HEMIPELAGIC MUD	TURBIDITIC MUD	SAND-SILT	TURBIDITIC SAND	ORGANIC OOZE	SAPROPEL	BIOTURBATION
LY II-3			68/(68)	16/(84)		1/(85)	10/(95)	5/(100)	14
LY II-4			97/(97)	3/(100)					100
LY II-5			98/(98)	2/(100)					97
LY II-5A			87/(87)	10/(97)	2/(99)	1/(100)			36
LY II-6			79/(79)	14/(93)	6/(99)	1/(100)			60
LY II-6A			97/(97)	3/(100)					98
LY II-7			62/(62)	37/(99)	1/(100)				6
P6510-34			66/(66)	28/(94)	4/(98)	2/(100)			18
P6510-33			90/(90)	7/(97)	3/(100)				10
AS 6-8	32/(32)	68/(100)							
AS 6-7	6/(6)	97/(100)							
SP 8-7	71/(71)	29/(100)							
V14 138	50/(50)	50/(100)							
V14 139[1]			60/(60)	35/(95)	3/(98)	2/(100)			7
V14 140	100/(100)								
CH61 19[2]			79/(79)	12/(91)	1/(92)	1/(93)	7/(100)		7
KS 12	4/(4)		67/(71)	7/(78)	21/(99)	1/(100)			67
KS 23[3]			86/(86)	14/(100)					26
KS 33			72/(72)	22/(94)	4/(98)	2/(100)			26
KS 53			96/(96)	4/(100)					75
KS 69[4]			72/(72)	19/(91)	9/(100)				5
KS 78			97/(97)	3/(100)					91
KS 100			96/(96)	4/(100)					92
KS 104			96/(96)	4/(100)					94
KS 105			95/(95)	5/(100)					100
KS 110			91/(91)	9/(100)					(74)
KS 118[5]			86/(86)	11/(97)	2/(99)	1/(100)			43
KS 120[6]			82/(82)	14/(96)	3/(99)	1/(100)			14
KS 125			97/(97)	3/(100)					91

(1) Slump sediment: 76 cm (not computed);   (2) Ash: 22 cm (not computed);   (3) Ash: 1 cm (not computed);

(4) Ash: 39 cm (not computed);   (5) Ash: 4 cm (not computed);   (6) Ash: 28 cm (not computed).

bathyal environments and basin environment show a clear correlation with present depth, particularly the hemipelagic mud and turbiditic mud types which form the major components of cores in these environments. The close correlation between sediment type and depth is illustrated in Figure

36A, where the percent of the different types of deposits in each core are plotted against depth (cf. Table 4).

Shallow water mud and coarse calcareous sand tend to be restricted to depths less than 500 m. Core KS 12 in the Strait Narrows does not follow

this trend because other specific depositional mechanisms particular to this environment are involved (discussed in a later section).

The distribution of turbiditic sand and sand-silt sediments appears independent of depth. Other environmental factors related to the boundary conditions of the environment (such as distribution of channels, natural levees, small basins, etc.) may be of primary importance in their distribution.

Hemipelagic mud is more closely related to depth, showing a decrease with an increase in depth. The turbiditic mud type also shows a correlation with depth, but in contrast to the hemipelagic mud, its importance increases with depth. The correlation coefficients between depth and the percent of sediment type in the cores and the regression lines have been calculated for both types of mud (Figure 35A). The value for hemipelagic mud is r = −0.69, y = 106.7 − 0.018x; for turbiditic mud it is r = 0.70, y = −5.8 + 0.014x. Both correlations are statistically significant at the α = 0.01 level.

The correlation is not very strong in either case, inasmuch as only about half of the variance (47% for the hemipelagic and 49% for the turbiditic mud) in the percent of sediment type in cores can be explained by a change in depth. However, it is interesting that depth, which is only one of several possible environmental factors, apparently controls about half of the variance in the distribution of these sediment types.

Another significant aspect of the relationship between depth and sediment distribution can be inferred from the graphic representation. Core data from the Balearic Basin plain (Rupke and Stanley, 1974) have also been plotted. A sharp change in trend of the regression line is clearly evident when the data from the Balearic plain are compared to the data from the Strait of Sicily cores. The intersection of the regression lines from both sets of data occurs just beyond 2500 m, which corresponds well with the depth of the basin plain-base of slope break.

This type of correlation between sediment sequences and depth may be applicable in other parts of the Mediterranean, but further testing is needed. This model, taking into account the statistical limitations of the technique, also may be of considerable importance for the interpretation of depth of paleoslope and recognition of base-of-

slope environments in ancient sediments.

The cumulative percent of the different sediment types in each core also has been calculated (Table 4). This was accomplished as follows. First, the total percent in each core of four major sediment groups (legend a, b, c, d in Figure 36B) were calculated. Then the cumulative percent of each group of sediment was calculated in the following sequence: a, a + b, a + b + c, and a + b + c + d. The results are shown schematically in the interpretative diagram in Figure 36B, which displays the variance of sediment types in cores as a function of depth. For each sediment type two graphic limits are depicted: one corresponds to the upper cumulative limit of probability of a given sediment group (thin line); the other represents the lower cumulative limit of probability for this sediment group (heavy line). It is apparent from this graph that hemipelagic mud is the most important sediment type in the neritic-bathyal environment. The importance of the turbiditic mud type increases with depth; below 2500 m the percent of turbiditic mud increases sharply and becomes as important as hemipelagic mud. The sand-silt sediment type also increases in cores paralleling an increase in depth. Coarse calcareous sand and shallow water mud are ubiquitous in the shallow water environment and their importance decreases sharply below the 200 to 500 m zone. The distribution of sapropel, organic ooze, and related deposits which do not occur on the Strait proper is not depicted on the graph.

BIOTURBATION AS AN ENVIRONMENTAL INDICATOR

Bioturbation, an indicator of biomass and benthic activity, is considered in this discussion of Strait sedimentation. The preservation of primary structures in marine sediments is the result of a delicate balance between rate of sedimentation and rate of benthic activity on, and just below, the water-sediment interface (Moore and Scruton, 1957). The degree of bioturbation in cores against depth is depicted graphically in Figure 37. The correlation coefficient is r = −0.87 (significant at the α = 0.01 level) and the regression line is y = 169.6−0.101x. Data from core KS 110, a deep basin core, was not used in the calculation; it is too short to provide reliable data. The correlation between depth and degree of bioturbation (about 75% of the variance) is higher than the correlation between
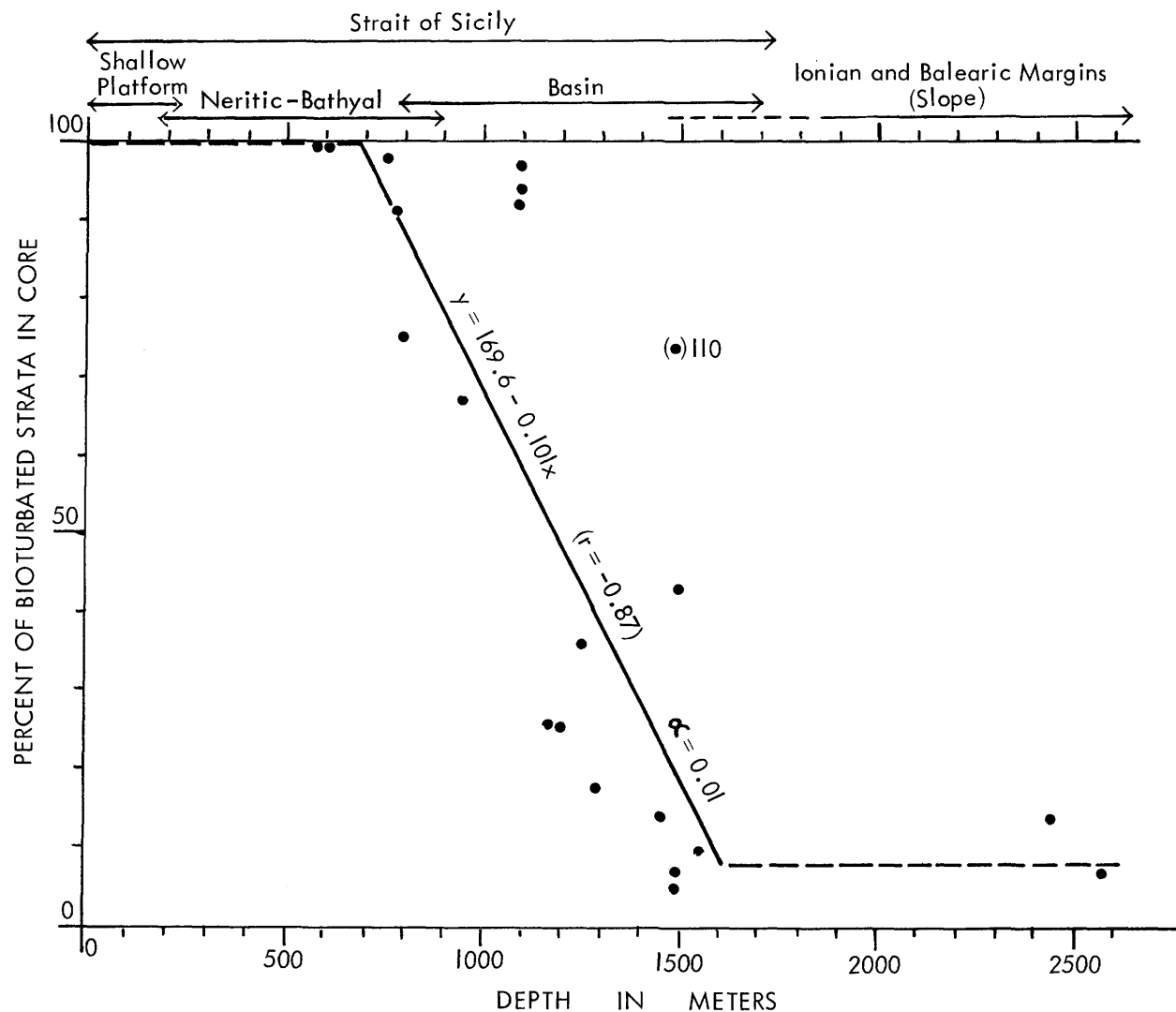
FIGURE 37.—Percent of bioturbated strata in cores versus depth in different Strait of Sicily environments. Regression line and correlation coefficient shows close relation between depth and degree of benthic activity. Data from core KS 110 was not used in the calculation. (Explanation in text.)

sediment type and depth described in the previous section. Benthic organisms are closely depth controlled and the resulting degree of bioturbation should closely correlate with depth. Bioturbation is a function of the number of organisms, type of activity, and rate of sedimentation. Inasmuch as the first two appear so closely related to depth, we suppose that the other factor, less important than the rate of biological activity, is the rate of sedimentation.

The regression line shown on Figure 37 inter-

sects the 100% abscissa at about 700 m. The neritic-bathyal cores shallower than this depth are completely bioturbated (examples: cores LY II-4 in Figure 34 and KS 105 in Figure 35). Even in coarse-grade sediments of the shallow platform, bioturbation is an important factor (Figure 24A, B); in some cases, however, the coarse texture of sediments in shallow water cores masks biogenic structures.

There is a general decrease in the relative amount of bioturbated core section between about

700 and 1600 m, and below a depth of 1600 m the degree of bioturbation is quite low (i.e., about 10% of the core). This low value of reworking by organisms probably reflects a decrease in the amount of biogenic activity concurrent with an increase in the rate of sedimentation.

RATES OF SEDIMENTATION

During the course of this study, 41 radiocarbon dates were obtained (Table 5), and these data have been plotted on the core log diagrams (Figures 34, 35). These diagrams show that the top of the cores are of highly variable age, and some of them are very old. When all age data are plotted against core sample depth no coherent pattern emerges, indicating an absence of uniform trend in the rate of sedimentation from core to core. However, when the core data are grouped in terms of environment more distinct trends appear as to the rate of sedimentation and the age of the sediment at the top of the core (Figure 38).

The shallow platform environment (cores AS 6–7, AS 6–8) is characterized by (1) a high rate of sedimentation (52 cm/100 years for core AS 6–8 in the Gulf of Hammamat) and (2) a truncation (or lack of sedimentation) in some of the cores before the end of the Pleistocene (Figure 34). The sedimentation rate calculated for core AS 6–8 is the highest measured except for sections of two cores in the deep basin environment (Figure 38).

In the neritic-bathyal environments, rates of sedimentation range from 16 to 40 cm/1000 years (average of about 25 cm/1000 years), and the tops of a number of cores in this environment terminate in the early Holocene (Figure 38A). One core (KS 105), unlike the above, shows a lower sedimentation rate (similar to that of the deep basins) and continued deposition through much of the Holocene.

The rates of sedimentation in the basins approximate 20 to 25 cm per 1000 years (Figure 38B). The much higher rates in two core sections (lower half of KS 109 in Malta Basin, and in the upper half of KS 63 in Linosa Basin) are the result of a greater abundance of turbidite and ash incursions at these two localities. It should be noted that in contrast to cores at shallower depths, deep basin deposits accumulated on a more continuous basis until the present (Figure 38 B). Sedimentation

rates in core LY II–6 in the small depression west of Marettimo Island are similar to those in other deep basin cores.

Carbon-14 data of core Ges-12 in the small Strait Narrows basin indicate relatively low (15 cm/1000 years) sedimentation rates, but continuous deposition from the late Pleistocene until recent time (Figure 38B).

The cores examined from the Ionian margin (LY II–3) and Balearic margin (LY II–7) slopes provide an average sedimentation rate of 30 cm and 15 cm per 1000 years, respectively (Figure 38A). On the Balearic Basin plain an average rate of sedimentation of 23 cm/1000 years is reported (Rupke and Stanley, 1974).

Three aspects of the sedimentation pattern in the environments discussed earlier are considered: (1) rate of deposition; (2) uniformity of these rates in time; and (3) the age of the sediments at the top of the cores, or the degree of continuity in sedimentation from the Pleistocene to the present. Sedimentation rates (with some exceptions) generally decrease with increasing bathymetric depth, i.e., from the shallow banks to the neritic-bathyal platform to the deep basins. With the available carbon-14 data, it appears that deposition in all environments, except in the two deep basin cores (KS 63 and KS 109, which have higher ash and turbidite layers), has been relatively uniform in the late Quaternary.

However, there is a significant difference in the age of sediments at the tops of cores in the different environments. On shallow banks, the tops of some cores are truncated in the late Pleistocene to early Holocene; in the neritic-bathyal environments in early Holocene; and in the deep basins, sediments have accumulated on a fairly continuous basis from the Pleistocene until the recent (Figures 34, 35). As discussed in earlier sections, sedimentation in the shallow platform environment is closely related to Quaternary events. It has been emphasized, for example, that the upward-coarsening and upward-fining sequences in shallow environments are a direct response to eustatic oscillations.

We have demonstrated that in the neritic-bathyal environments bioturbation is an important factor and that the rate of reworking by benthic organisms has continued during deposition of the entire core sections. Equally significant are the carbon-14 dates, which indicate that oceanographic

TABLE 5.—Radiocarbon dates based on carbonate sand fraction and bulk sample from cores selected in different Strait of Sicily environments

CORE	AVERAGE DEPTH (cm)	SAMPLE DEPTH	SAMPLE WEIGHT (gm)	CARBONATE MATERIAL	RADIOCARBON DATE (in years B.P.)	NOTATIONS
LY II-3	235	210-255	16.7	Forams (>63μm)	19,830 ± 450	Small sample, diluted
LY II-3	490	467-512	18.8	Forams (>63μm)	28,390 ± 1,200	Small sample, diluted
LY II-4	93	70-115	34.1	Forams (>63μm)	15,495 ± 200	
LY II-4	325	298-351	13.0	Forams (>63μm)	25,925 ± 525	Small sample, diluted
LY II-5	80	60-100	13.5	Forams (>63μm)	4,100 ± 80	Small sample, diluted
LY II-5	290	270-310	11.1	Forams (>63μm)	12,580 ± 345	Small sample, diluted
LY II-5A	40	20- 60	13.3	Forams (>63μm)	3,680 ± 90	Small sample, diluted
LY II-5A	290	270-310	9.0	Forams (>63μm)	13,685 ± 450	Small sample, diluted
LY II-5A	570	550-590	11.0	Forams (>63μm)	No Date	Sample too small
LY II-6	65	45- 85	1.0	Forams (>63μm)	No Date	Sample too small
LY II-6	470	450-490	16.8	Forams (>63μm)	15,265 ± 240	Small sample, diluted
LY II-6A	30	10- 50	19.0	Forams (>63μm)	11,550 ± 175	
LY II-6A	250	230-270	19.8	Forams (>63μm)	17,290 ± 365	
LY II-6A	550	530-570	17.3	Forams (>63μm)	24,790 ± 680	Small sample, diluted
AS 6-7	225	0- 45	5.7	Forams + Shells (>63μm)	No Date	Sample too small
AS 6-7	192	185-200	16.0	Shells (Forams) (>63μm)	16,005 ± 220	
AS 6-7	701	685-728	14.0	Forams (Shells) (>63μm)	12,680 ± 360	Small sample, diluted
AS 6-8	49	33- 65	40.0	Shells (>210μm)	17,565 ± 230	
AS 6-8	49	33- 65	40.0	Forams (>63μm)	19,555 ± 230	
AS 6-8	530	510-550	35.0	Forams + Shells (>63μm)	26,865 ± 715	
KS 63	225	200-250	15.8	Forams + Shells (>63μm)	18,465 ± 240	Small sample, diluted
KS 63	525	500-550	9.5	Forams + Shells (>63μm)	10,795 ± 270	Small sample, diluted
KS 63	825	800-850	23.4	Forams (Shells) (>63μm)	19,980 ± 380	
KS 12	92	85-100	250	Bulk Sample	9,530 ± 140	
KS 12	687	680-695	250	Bulk Sample	48,950 ± 7,370	Apparent age
KS 53	131	124-138	250	Bulk Sample	15,340 ± 145	
KS 53	579	574-585	250	Bulk Sample	35,160 ± 1,970	Age reversed with sample below
KS 53	639	632-646	250	Bulk Sample	34,550 ± 1,870	Age reversed with sample above
KS 100	85	77- 94	250	Bulk Sample	6,310 ± 95	
KS 100	607	599-616	250	Bulk Sample	26,000 ± 375	
KS 105	65	58- 71	250	Bulk Sample	7,245 ± 115	
KS 105	530	524-537	250	Bulk Sample	36,620 ± 1,800	
KS 109	122	113-131	250	Bulk Sample	5,145 ± 55	
KS 109	362	354-370	250	Bulk Sample	16,895 ± 175	
KS 109	695	687-703	250	Bulk Sample	19,950 ± 300	
KS 118	87	79- 95	250	Bulk Sample	7,050 ± 95	
KS 118	423	415-432	250	Bulk Sample	19,500 ± 425	
KS 118	786	778-795	250	Bulk Sample	41,700 ± 4,500	
KS 120	73	66- 81	250	Bulk Sample	8,640 ± 105	
KS 120	359	351-367	250	Bulk Sample	23,940 ± 610	
KS 120	688	681-695	250	Bulk Sample	42,850 ± 6,680	Apparent age

Core LY II-7 radiocarbon dates from Rupke and Stanley (1974, their Table 8, p. 32).

conditions directly affecting the seafloor changed markedly between the late Pleistocene and the early Holocene, and that nondeposition and/or erosion have prevailed since about 10,000 years BP in the neritic-bathyal and shallow platform environments.

In contrast, none of the above patterns are noted in the deep Strait basins. Rates of sedimentation approximate those on the neritic-bathyal environments but lower benthic populations on the basin floors have resulted in less bioturbation and better preservation of stratification. Furthermore, no obvious changes either in lithofacies sequence patterns or sedimentation rates are recorded in this deep environment between the late Pleistocene and the recent, i.e., a period of at least 30,000 years.

However, other studies indicate that rates of sedimentation in deep basins of the Mediterranean (Huang and Stanley, 1972; Rupke and Stanley, 1974; and others) and the Black Sea (Ross and Degens, 1974) have not been constant during the upper Quaternary. A decrease in the rate of sedimentation is reported in most Mediterranean areas during the late Pleistocene to Holocene.

An anomolous reversal in the age of some core samples (cf. cores KS 53 in Figure 35 and AS 6–7 · in Figure 34) may be the result of mixing by organisms. Vertical mixing of 3 to 4 m, for example, has been noted in some Holocene shelf cores in the Persian Gulf (Sarnthein, 1972). Another aspect that should be considered in analyzing radiocarbon dates is that different types of carbonate material within the same sample may give different radiocarbon dates (Milliman et al., 1972). An example of this is shown by two samples from the upper coarse calcareous layer ($\cong$ 30 cm) in core AS 6–8 (Figure 34). Here, the age of a largely shelly coarse sample (> 203 microns) is slightly younger than that of the finer grade fraction (63–203 microns) consisting primarily of foraminiferal tests. A petrographic analysis of these samples suggests that the fine fraction may have been more intensively reworked than the coarse shelly fraction.

The correlation between cores based on the carbon-14 analyses is shown in Figures 34 and 35. Cores without available radiocarbon dates were correlated by extrapolation with radiocarbon dated cores in the same environment. Lithostratigraphic distribution of sedimentary sequences was also considered in the correlation of cores (Figure 33). The isochrons in Figures 33 to 35 reveal the thicker sediment accumulations in the deep basins and also show the truncation of Holocene sections at the top of the neritic-bathyal and shallow platform cores.

The importance of volcanic activity between 5000 and 25,000 years BP in Linosa Trough is demonstrated by the radiocarbon data on cores KS 120 and KS 118 in Figure 35. Volcanism at about this time is also reported elsewhere in the Mediterranean (Keller et al., 1974).

The relation between rate of sedimentation and fault displacement can also be considered in light of the available carbon-14 dates. That deposition and faulting are contemporaneous in the neritic-bathyal environments is well displayed in 3.5 kHz records (Figures 7, 10). The development of some faults apparently stopped in the upper Pleistocene (Figure 7, arrow B). In this area, the core tops are dated at about 10,000 years BP (core LY II–4); on 3.5 kHz profiles the uppermost sediment sections are offset slightly by faults. The underlying Pliocene and Quaternary sequences also accumulated contemporaneously with fault movement as revealed by the thickening of sediments in downthrown fault blocks (see sparker profile in Figure 7, b). In some sectors faulting appears to be active at present (Figures 7, c, 8, 10), and locally the offset of identical reflectors on opposite fault scarps indicates a displacement rate in excess of the sedimentation rate. Thus, vertical displacement of certain parts of the neritic-bathyal sea floor exceeds 20 cm per 1000 years.

The nature of well-defined reflectors on 3.5 kHz records is difficult to ascertain. Core analysis (LY II–4, Figure 7; Figure 34) shows that sand layers and other distinct lithologic layers are not present in cores retrieved from this environment. As has been emphasized, the cores are characterized by their uniformity. Although many of the distinct reflectors that appear on the 3.5 kHz records could not be sampled because of core length limitations, we believe that late Quaternary deposits in this neritic-bathyal environment present a general homogeneous pattern. Thus, the lateral continuity and regional uniformity of subbottom reflectors in 3.5 kHz records suggest a lithofacies change related to some type of regional event. We exclude a tur-
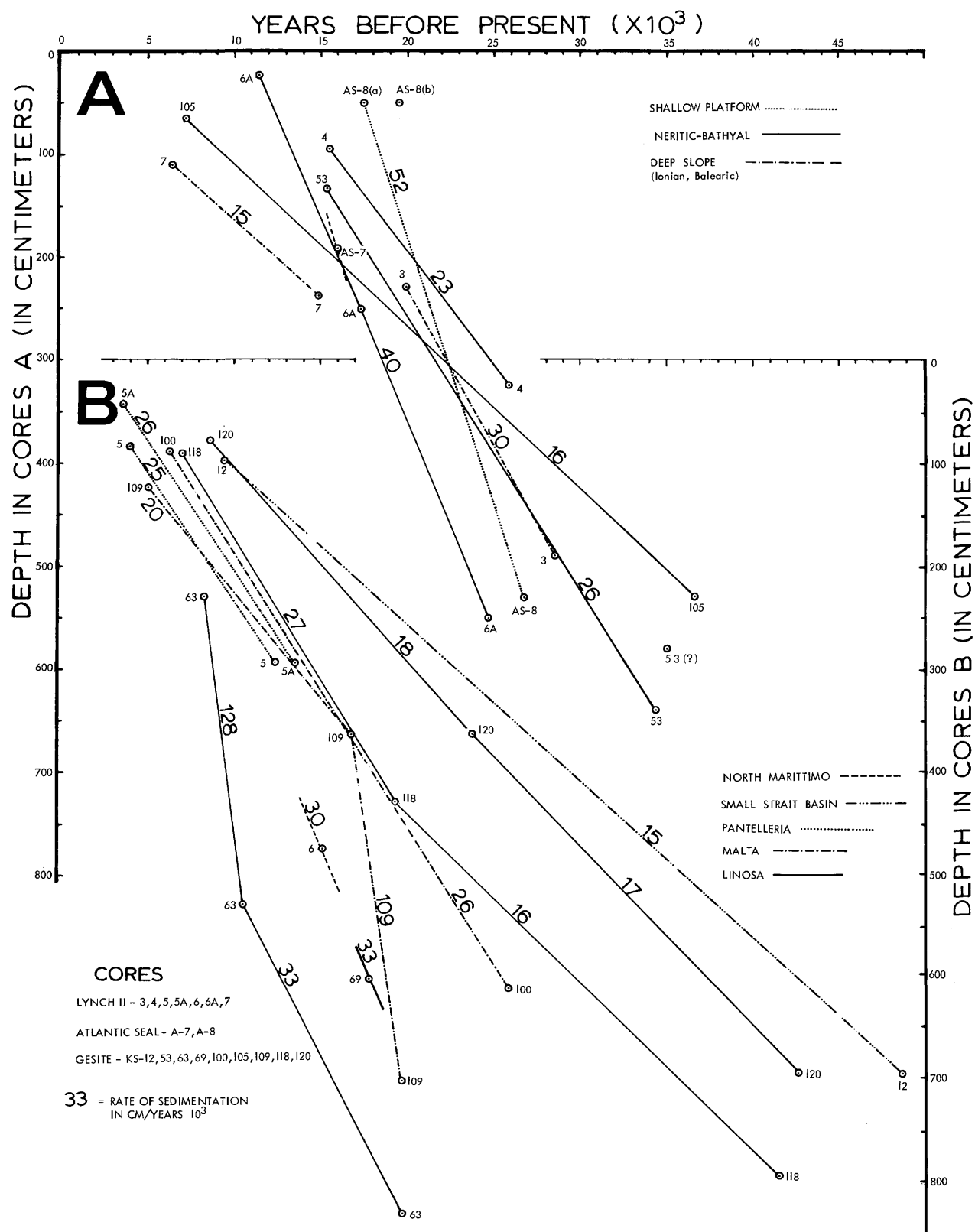
FIGURE 38.—Rates of sedimentation based on carbon-14 data from cores in the different Strait of Sicily environments: A, shallow platform, neritic-bathyal, and deep slope environments; B, deep basins and small Strait Narrows basin. (Data from core KS 69 provided by the Station de Géologie Sous-Marine de Villefranche of the University of Paris, and from LY II-7 from Rupke and Stanley, 1974.)

biditic origin for the origin inasmuch as these reflectors are continuous over a highly irregular topography. One possible origin of continuous layers are surfaces of nondeposition, perhaps related to critical sea level stands. A marked acoustic reflector also may indicate a marked change in the physical properties of the mud such as water content and porosity rather than a change in texture. Still another possible explanation for regionally extensive subbottom horizons might be concentrations of foraminiferal tests or other microfossils. An example of this, recorded in the Alboran Sea (Huang and Stanley, 1972), is attributed to a regional "bloom" related to a basin-wide event.

IMPLICATIONS OF STRAIT SEDIMENTATION TO CURRENT REVERSALS

It is noteworthy that sapropels and associated sediment types which are distributed throughout the eastern Mediterranean do not occur in the Strait of Sicily proper. Sapropel is cored only to the east on the slope trending into the Ionian Basin. Most workers are of the opinion that these dark organic-rich units are associated with water mass stratification-anaerobic conditions; they accumulated during the warming phase of the Quaternary climatic cycles, and not during the glacial maximum (Ryan, 1972; and others). We assume that the upper sapropel layer on the slope east of the Strait (core LY II–3 on Figure 34) is equivalent to the upper sapropel layer in the eastern Mediterranean, which has been dated at between 7500 and 9000 years BP (Ryan, 1972; van Straaten, 1972).

We accept the hypothesis which relates the deposition of these organic layers with phases of anaerobic conditions and water mass stratification. Whether this stratification is the result of increased outflow of low salinity waters from the Black Sea into the eastern Mediterranean coupled with decreased evaporation rates (Olausson, 1961; Ryan, 1972; Cita and Ryan, 1973; and others), or surface water warming (van Straaten, 1972), or an excess inflow of fresh water from rivers and melting ice and associated current reversals at the Strait of Gibraltar (Mars, 1963; Huang et al., 1972; Nesteroff, 1973) is not determined. Müller (1973) proposes an alternative hypothesis on the basis of nannoplankton analysis, i.e., that layering of water

masses in the eastern Mediterranean is the result of increased evaporation and less fresh water discharge or rainfall during cold periods; thus, in this case, water stratification would be produced by the influx of less saline and less dense water from the Atlantic Ocean. In any case it is apparent that repetitive phases of stratification and stagnation during the Quaternary were basin-wide phenomena. Other examples of recent sapropel and sapropel-like deposits are reported from the Cariaco Trench (Heezen et al., 1961), the Gulf of California (Byrne and Emery, 1960; van Andel and Shor, 1964), and the Black Sea (Ross and Degens, 1974).

In general the sapropel depositional models are characterized by: (a) layering of water masses; (b) stagnation of the bottom water, with formation of an H_2S rich zone; (c) seasonal (winter-summer) or periodical (eustatic changes) upwelling and vertical mixing of water. These factors favor the development and preservation of varve-like bedding (Figure 28A).

Although the depth of the three deep Strait of Sicily basin plains (1300–1700 m) is well below that at which sapropel layers are found elsewhere in the central (Adriatic) and eastern (Ionian, Levantine basins) Mediterranean, no sapropels or other distinct evidence of stagnation are noted in the basin cores. On the contrary, structures produced by benthic organisms are commonly observed, indicating that these deep narrow basins remained sufficiently oxygenated to support benthic populations throughout the late Quaternary. Thus, it appears that vertical mixing prevailed on an almost continuing basis as a result of water mass movement across the Strait of Sicily at a time when sapropels were accumulating under stagnant conditions in the adjacent eastern Mediterranean.

In this respect, core LY II–6A west of the Strait Narrows (Figure 34) is of interest. The rate of sedimentation here is higher than in many other sectors of the Strait. The mud at the top of core LY II–6A is dated as early Holocene (about 11,000 to 10,000 years BP), or well after sea level had begun to rise. Inasmuch as this core lies at a depth of 755 m, the eustatic oscillation alone is not believed to be the primary factor for erosion or nondeposition in this sector. The region just west of the Strait Narrows may be critical for interpreting Quaternary oceanographic fluctuations since it oc-

cupies a zone of particularly strong current regime (Molcard, 1972). Currents accelerate in the constricted narrows and decelerate as the Strait widens, with a probable increase in deposition away from the Narrows. Thus we would expect that cores collected in the vicinity of the Narrows would provide the best record of water mass-bottom current fluctuations during the recent geological past.

It is probably not accidental that there is an apparent correlation between the time of truncation of core tops in the Strait neritic-bathyal environments and that of the most recent protosapropel and sapropel formation (dated at about 9000 to 7500 years BP) in the eastern and central Mediterranean. Independently, other workers (Colantoni and Borsetti, 1973) record microfaunal changes in the Linosa and Malta basins at about this period. One possible explanation for these early Holocene depositional and faunal changes is a temporary short-term reversal of surface and deeper water flow (Olausson, 1961; Mars, 1963; Huang et al., 1972; Nesteroff, 1973; Huang and Stanley, 1974; and others). At present, less dense water flows (> 30 cm/sec) southeastward above northwestward flowing (32 cm/sec) Levantine water (Molcard, 1972). We propose a contrasting early Holocene short-term current reversal model in which less dense surface water flowed to the northwest in response to the early Holocene climatic evolution (Figure 39). Surface water salinity and temperature conditions (Farrand, 1971; Fairbridge, 1972) undoubtedly were modified in the Mediterranean during the warming phase of the climatic curve, but the degree of stratification resulting from this remains a point of conjecture (Letolle and Vergnaud-Grazzini, 1973).

Our core analysis shows (1) that the sea floor of the Strait of Sicily remained ventilated and swept by currents at a time when anaerobic conditions prevailed in the Ionian-Levantine basins east of the Strait, and (2) that the Strait although a broad sill apparently did not completely block circulation between the eastern and western Mediterranean basins. We conclude that the regional lithofacies distribution observed is best explained in terms of early Holocene paleooceanographic changes including possible reversal of currents. The latter concept requires further testing and we suggest that the Strait of Sicily, the major sill separating sapropel-rich eastern Mediterranean ba-

sins from nonsapropel basins in the west, is clearly one of the key sites in which to investigate this problem.

Summary

1. This marine sedimentological study defines the major Quaternary lithofacies observed in cores collected in the different sectors of the Strait of Sicily and establishes the relationship between sedimentary facies, depositional environment, structural displacement, transport processes, and late Quaternary events which affected the central Mediterranean region.

2. The major depositional environments in, and immediately adjacent to, the Strait of Sicily are as follows: slope; neritic-bathyal borderland; basin (intermediate and deep); shallow platform; marked topographic high (submarine mounts, volcanoes, diapirs); canyon; and the Strait Narrows between Cape Bon, Tunisia, and Marsala, Sicily. These environments are broadly defined on the basis of morphology, structural configuration, and thickness and attitude of the sedimentary cover as measured in seismic records. The shallow platform, neritic-bathyal borderland, and basins are the most characteristic environments in the Strait.

3. The lithologic uniformity of core sections, the high degree of bioturbation, and the importance of coarse calcareous sediments serve to distinguish the late Quaternary Strait of Sicily lithofacies from those of the adjacent deep Ionian and Balearic basins.

4. Three major Strait lithofacies assemblages are recognized: (1) coarse calcareous sand layers interbedded with mud and sandy lutite deposits prevail on shallow banks; (2) homogeneous, bioturbated light olive gray to dusty yellow muddy sequences predominate in the neritic-bathyal environments and are also found in some basins; (3) moderate-to well-stratified sand (including gravity sediment flow units and ash) alternating with hemipelagic and turbiditic mud are generally present in deep basin and Strait Narrows cores.

5. Five major sediment types are distinguished: (1) coarse calcareous sand; (2) sand- to silt-size sediments; (3) ash; (4) mud; and (5) sapropel and organic ooze (the latter type is retrieved only in cores on the Ionian margin east of the Strait). The sediment types are defined on the basis of the (a) sand fraction (> 63 microns) content and com-
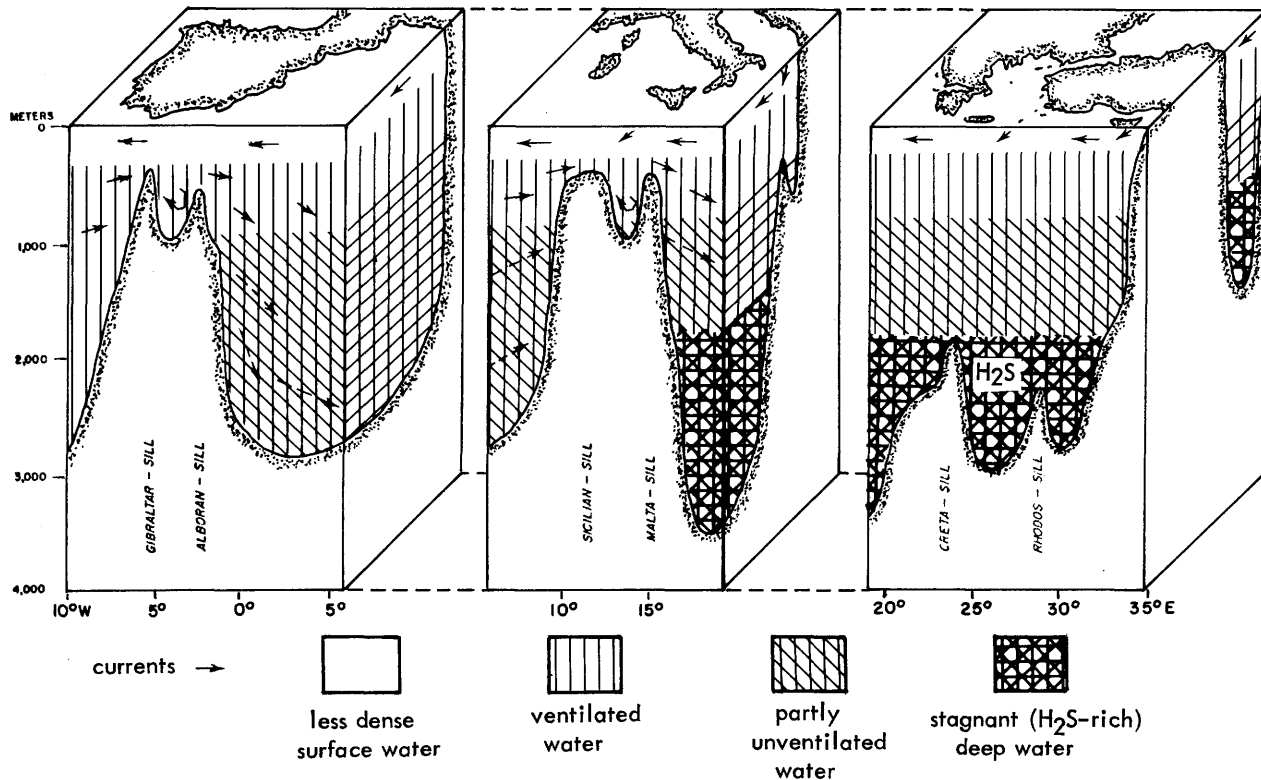
FIGURE 39.—Schematic showing possible early Holocene water mass changes in the Mediterranean. The model depicts stratification and reversal of currents during the warming phase of the climatic curve. The present study indicates that deep Strait basins remained ventilated at the time that sapropel layers accumulated in the eastern Mediterranean. (Topographic base after Wüst, 1961.)

position, (b) SEM investigation of the lutite fraction, (c) sedimentary structures observed in X-radiographs and split cores, and (d) examination of the sea floor by underwater photography.

6. The sediment types are grouped into sequences, each of which is defined on the basis of a succession of sediment types. A sequence represents deposition resulting from a specific sedimentary accident (turbidity current, mass flow, etc.) or from a regionally important, large-scale environmental event. An example of the latter: the Quaternary climatic changes which were significant enough to alter water mass stratification and movement, eustatic oscillatory patterns, and biogenic production. The four major sequences distinguished are (1) upward-coarsening and upward-fining; (2) uniform; (3) turbiditic (includes mud and sand-silt turbidites); and (4) sapropel sequences.

7. The close relation between sediment type, se-

quences, lateral distribution, and depth is demonstrated. The coarse calcareous deposits on banks, comparable to those on shallow shelves and platforms elsewhere in the Mediterranean, are typified by upward-fining and upward-coarsening sequences. Sediment facies in the shallow platform environments are directly related to Quaternary sea level oscillations. The sediments in the somewhat deeper neritic-bathyal environments are typically uniform muds devoid of marked stratification, while the more variable and well-stratified deep basin sediment sections include turbidites, volcanic ash layers, and hemipelagic mud sequences.

8. Two types of layers containing volcanic sediment are distinguished: (1) air-borne tephra layers, and (2) turbiditic ash-rich layers. The former display a vertical gradation in grain size (fining or coarsening upward), parallel lamination, or in some cases are structureless. The latter

type, composed of bioclastic as well as volcanic material, shows the vertical sequence of sedimentary structures characteristic of typical terrigenous turbidites.

9. Stratigraphic correlation of the cores is based on 41 carbon-14 analyses. The study shows that specific sediment units or sequences generally are not correlatable across the Strait or even within a single environment such as a small deep basin. It is possible, however, to recognize a general succession of sedimentation patterns in each major environment.

10. Depositional patterns in the Strait have been controlled mainly by three major factors: regional Quaternary events related to changes of climate and eustatic sea level oscillations, depth, and organisms. The Quaternary climatic and associated sea level oscillations are reflected primarily by the truncation of the upper sediment sequences on the shallow platform and in neritic-bathyal environments, and development of fining- and coarsening-upward sequences on the shallow platform. The distribution of hemipelagic and turbiditic mud lithofacies in the neritic-bathyal environments is related to the present sea level stand. In contrast, the well-stratified sections—in the deep enclosed basins show a uniform rate of sedimentation from the late Quaternary to the present, and core to core differences have resulted from variations in the number of turbiditic and volcanic ash incursions into the deep basins.

11. The close relation between sediment type and depth is well demonstrated by the inverse relation of turbiditic mud, which increases, and hemipelagic mud, which decreases with increasing depth. About three-quarters of the variance in the degree of bioturbation in the Strait cores also can be explained as a function of depth. These rela-

tions between sedimentation and depth may be applicable in the interpretation of ancient deposits.

12. Sedimentation rates in the Strait (with some exceptions) generally decrease with increasing depth and have been relatively uniform during the late Quaternary. However, there is a significant difference in the age of sediment sequences at the top of cores in the different environments: on shallow banks, the top of some cores are truncated in the late Pleistocene to early Holocene; in the neritic-bathyal environments in the early Holocene; and in the deep basins, sediments have accumulated on a fairly continuous basis from the late Pleistocene until the recent.

13. Faulting in many sectors of the Strait is of recent or subrecent origin, and correlation of reflectors on high-resolution subbottom profiles indicates that this vertical displacement is commonly in excess of the sedimentation rate, i.e., in excess of 20 cm per 1000 years.

14. No sapropel layers are noted in basin cores, although the three deep Strait of Sicily basin plains lie at a depth (1300 to 1700 m) well below that at which sapropel deposits are found elsewhere in the central and western Mediterranean. It appears that these deep basins remained ventilated during the periods when anaerobic conditions prevailed in the Ionian-Levantine basins east of the Strait. Apparently the Strait did not completely block the circulation of water masses between the eastern and western Mediterranean basins in the late Quaternary.

15. An early Holocene paleooceanographic model in which a possible reversal of currents is postulated would help explain the particular distribution of sedimentary sequences and different rates of sedimentation observed in the various Strait of Sicily environments.

Literature Cited

Akal, T.
1972. The General Geophysics and Geology of the Strait of Sicily. Pages 177–192 in T. D. Allan, T. Akal, and R. Molcard, editors, *Oceanography of the Strait of Sicily* (Conference Proceedings No. 7). La Spezia, Italy: SACLANT ASW Research Centre.

Allan, T. D., and C. Morelli
1971. A Geophysical Study of the Mediterranean Sea. *Bollettino di Geofisica Teorica ed Applicata*, 13(50): 99–134.

American Geological Institute
1972. *A Glossary of Geology*. 805 pages. Washington, D.C.: American Geological Institute.

Auzende, J. M.
1971. La marge continentale Tunisienne: Résultats d'une étude par sismique réflexion; sa place dans le cadre tectonique de la Méditerranée occidentale. *Marine Geophysical Researches*, 1:162–177.

Auzende, J. M., J. L. Olivet, and J. Bonnin
1974. Le détroit Sardano-Tunisien et la zone de fracture Nord-Tunisienne. *Tectonophysics*, 21:357–374.

Benson, R. H.
1972. Ostracodes as Indicators of Threshold Depth in the Mediterranean During the Pliocene. Pages 63–73 in D. J. Stanley, editor, *The Mediterranean Sea: A Natural Sedimentation Laboratory*. Stroudsburg: Dowden, Hutchinson & Ross, Inc.

Blanc, J. J.
1958. Sédimentologie sous-marine du détroit Siculo-Tunisien: Campagne du "Calypso." Pages 92–126 in *Résultats Scientifiques Campagne du Calypso* (III). Institut Océanographique.
1972. Observations sur la Sédimentation Bioclastique en quelques points de la Marge Continentale de la Méditerranée. Pages 225–240 in D. J. Stanley, editor, *The Mediterranean Sea: A Natural Sedimentation Laboratory*. Stroudsburg: Dowden, Hutchinson & Ross, Inc.

Blanc-Vernet, L., H. Chamley, C. Froget, D. Le Boulicaut, A. Monaco, and C. Robert
1975. Observations sur la sédimentation marine récente dans la région siculo-tunisienne. *Géologie Méditeranéene*, 2:31–48.

Boltouskoy, E.
1965. *Los Foraminiferos Recientes*. 510 pages. Buenos Aires: Eudeba.

Bouma, A. H.
1962. *Sedimentation of Some Flysch Deposits: A Graphic Approach to Facies Interpretation*. 168 pages. Amsterdam: Elsevier Publishing Company.
1964. Notes on X-ray Interpretation of Marine Sediments. *Marine Geology*, 2:278–309.

Burollet, P. F.
1967. General Geology of Tunisia. Pages 51–58 in *Guidebook to the Geology and History of Tunisia*. Petroleum Exploration Society of Libia.

Byrne, J., and K. O. Emery
1960. Sediments of the Gulf of California. *Bulletin of the Geological Society of America*, 71:983–1010.

Caputo, M., G. F. Panza, and D. Postpischl
1970. Deep Structure of the Mediterranean Basin. *XXIIe Congrès-Assemblée Plénière, Commission Internationale pour l'Exploration Scientifique de la Mer Méditerranée*. Rome.

Carter, T. G., J. P. Flanagan, C. R. Jones, F. L. Marchant, R. R. Murchison, J. H. Rebman, J. C. Sylvester, and J. C. Whitney.
1972. A New Bathymetric Chart and Physiography of the Mediterranean Sea. Pages 1–23 in D. J. Stanley, editor, *The Mediterranean Sea: A Natural Sedimentation Laboratory*. Stroudsburg: Dowden, Hutchinson & Ross, Inc.

Caulet, J. P.
1972a Les sédiments organogènes du précontinent algérien. *Mémoires du Muséum National d'Histoire Naturelle, Paris*, 25: 289 pages.
1972b. Recent Biogenic Calcareous Sedimentation on the Algerian Continental Shelf. Pages 261–277 in D. J. Stanley, editor, *The Mediterranean Sea: A Natural Sedimentation Laboratory*. Stroudsburg: Dowden, Hutchinson & Ross, Inc.

Cita, M. B., and W. B. F. Ryan
1973. Timescale and General Synthesis. Pages 1405–1416 in volume 13 in W. B. E. Ryan, K. J. Hsu, et al., editors, *Initial Reports of the Deep Sea Drilling Project*. Washington, D.C.: U.S. Government Printing Office.

Chassefière, B., and A. Monaco
1973. Relations entre sédimentogenèse, propriétés mécaniques et minéralogie: Application au détroit Siculo-Tunisien. *Comptes Rendus de l'Académie des Sciences de Paris*, 277(D):141–144.

Colantoni, P., and A. M. Borsetti
1973. Some Notes on Geology and Stratigraphy of the Strait of Sicily. *Bulletin of the Geological Society of Greece*, 10(1):31–32.

Colantoni, P., and E. F. M. Zarudzki
1973. Some Principal Sea Floor Features in the Strait of Sicily. *Bulletin of the Geological Society of Greece*, 10(1):204–205.

Dangeard, L.
1929. Observations de géologie sous-marine (Thesis). *Annales de l'Institut Océanographique*, 1: 296 pages. Paris.

Degens, E. T., and D. A. Ross
1974. *The Black Sea—Geology, Chemistry, and Biology*.

633 pages. The American Association of Petroleum Geologists (Memoir No. 20).

Emelyanov, E. M.
1972. Principal Types of Recent Bottom Sediments in the Mediterranean Sea: Their Mineralogy and Geochemistry. Pages 355–386 in D. J. Stanley, editor, The Mediterranean Sea: A Natural Sedimentation Laboratory. Stroudsburg: Dowden, Hutchison & Ross, Inc.

Emelyanov, E. M., and K. M. Shimkus
1972. Suspended matter in the Mediterranean Sea. Pages 417–439 in D. J. Stanley, editor, The Mediterranean Sea: A Natural Sedimentation Laboratory. Stroudsburg: Dowden, Hutchinson & Ross, Inc.

Emery, K. O.
1952. Continental Shelf Sediments off Southern California. Geological Society of America Bulletin, 63: 1105–1108.
1968. Relict Sediments on Continental Shelves of the World. The American Association of Petroleum Geologist Bulletin, 52:445–464.

Ewing, M., and R. A. Davis
1967. Lebensspuren Photographed on the Ocean Floor. Pages 259–302 in J. B. Hersey, editor, Deep Sea Photography. Baltimore: The Johns Hopkins Press.

Fairbridge, R. W.
1972. Quaternary Sedimentation in the Mediterranean Region Controlled by Tectonics, Paleoclimates, and Sea Level. Pages 99–114 in D. J. Stanley, editor, The Mediterranean Sea: A Natural Sedimentation Laboratory. Stroudsburg: Dowden, Hutchinson & Ross, Inc.

Farrand, W. R.
1971. Late Quaternary Paleoclimates of the Eastern Mediterranean Area. Pages 529–564 in K. K. Turekian, editor, The Late Cenozoic-Glacial Ages. New Haven: Yale University Press.

Finetti, I., and C. Morelli
1972a. Regional Reflection Seismic Exploration of the Strait of Sicily. Pages 208–216 in T. D. Allan, T. Akal, and R. Molcard, editors, Oceanography of the Strait of Sicily (Conference Proceedings No. 7). La Spezia, Italy: SACLANT ASW Research Centre.
1972b. Wide Scale Digital Seismic Exploration of the Mediterranean Sea. Bolletino di Geofisica Teorica ed Applicata, 14(56):291–342.

Flood, R. D., and C. D. Hollister
1974. Current-controlled Topography on the Continental Margin off the Eastern United States. Pages 197–205 in C. A. Burk and C. L. Drake, editors, The Geology of Continental Margins. New York: Springer-Verlag.

Frassetto, R.
1972. A Study of the Turbulent Flow and Character of the Water Masses Over the Sicilian Ridge in Both Summer and Winter. Pages 38–44 in T. D. Allan, T. Akal, and R. Molcard, editors, Oceanography of

the Strait of Sicily (Conference Proceedings No. 7). La Spezia, Italy: SACLANT ASW Research Centre.

Frazer, J. Z., G. Arrhenius, J. S. Hanor, and D. L. Hawkins
1970. Surface Sediment Distribution, Mediterranean Sea. 8 pages. Monterey: Defense Language Institute—Systems Development Agency.

Frey, R. W.
1973. Concepts in the Study of Biogenic Sedimentary Structures. Journal of Sedimentary Petrology, 43(1): 6–19.

Gennesseaux, M., J. M. Auzende, J. L. Olivet, and R. Bayer
1974. Les orientations structurales et magnétiques sous-marines au Sud de la Corse et la Dérive corso-sarde. Comptes Rendus de l'Académie des Sciences de Paris, 278(D):2003–2006.

Hampton, M. A.
1972. The Role of Subaqueous Debris Flow in Generating Turbidity Currents. Journal of Sedimentary Petrology, 42:775–793.

Hardin, F. R. and G. G. Harding
1961. Contemporaneous Normal Faults of Gulf Coast and Their Relation to Flexures. American Association of Petroleum Geologists Bulletin, 45:238–248.

Heezen, B. C., R. J. Menzies, W. S. Broecker, and W. M. Ewing
1961. Stagnation of the Cariaco Trench. Pages 99–100 in International Oceanographic Congress.

Heezen, B. C., C. D. Hollister, and W. F. Ruddiman
1966. Shaping of the Continental Rise by Geostrophic Contour Currents. Science, 151:502–508.

Heezen, B. C., and C. D. Hollister
1971. The Face of the Deep. 659 pages. New York: Oxford University Press.

Heiken, G.
1974. An Atlas of Volcanic Ash. Smithsonian Contributions to the Earth Sciences, 12: 101 pages.

Hekel, H.
1973. Late Oligocene to Recent Nannoplankton from the Capricorn Basin (Great Barrier Reef Area). Geological Survey of Queensland, 359 (Palaeontological Papers No. 33): 23 pages. Brisbane.

Hesse, R., and U. von Rad
1972. Undisturbed Large-diameter Cores from the Strait of Otranto. Pages 645–653 in D. J. Stanley, editor, The Mediterranean Sea: A Natural Sedimentation Laboratory. Stroudsburg: Dowden, Hutchinson & Ross, Inc.

Howard, J. D., and R. W. Frey
1973. Characteristic Physical and Biogenic Sedimentary Structures in Georgia Estuaries. The American Association of Petroleum Geologists Bulletin, 57(7): 1169–1184.

Howard, J. D., H. E. Reineck, and S. Rietschel
1974. Biogenic Sedimentary Structures Formed by the Heart Urchins. Senckenbergiana maritima, 6(2):185–201.

Huang, T. C., and D. J. Stanley
1972. Western Alboran Sea: Sediment Dispersal, Ponding

and Reversal of Currents. Pages 521–559 *in* D. J. Stanley, editor, *The Mediterranean Sea: A Natural Sedimentation Laboratory*. Stroudsburg: Dowden, Hutchinson & Ross, Inc.

1974. Current Reversal at 10,000 years B. P. at the Strait of Gibraltar: A Discussion. *Marine Geology*, 17: M1–M7.

Huang, T. C., D. J. Stanley, and R. Stuckenrath
1972. Sedimentological Evidence for Current Reversal at the Strait of Gibraltar. *Marine Technology Society Journal*, 6:25–33.

Isacks, B., J. Oliver, and L. R. Sykes
1968. Seismology and the New Global Tectonics. *Journal of Geophysical Research*, 73:5855–5899.

Keller, J., W. B. F. Ryan, D. Ninkovich, and A. Altherr
1974. The Deep-Sea Record of Quaternary Volcanism in the Mediterranean. In *Comité Géologie et Géophysique marines, 24ème Congrès-Assemblée pléniére de Monaco*. 4 pages.

Krinsley, D. H., and F. C. Doormkamp
1973. *Atlas of Quartz Sand Surface Textures*. 191 pages. Cambridge: University of Cambridge Press.

Krinsley, D. H., P. E. Biscaye, and K. K. Turekian
1973. Argentine Basin Sediment Sources as Indicated by Quartz Surface Textures. *Journal of Sedimentary Petrology*, 43 (1):251–257.

Kulm, L. D., R. C. Roush, J. C. Harlett, R. H. Neudeck, D. M. Chambers, and E. J. Runge
1975. Oregon Continental Shelf Sedimentation: Interrelationships of Facies Distribution and Sedimentary Processes. *The Journal of Geology*, 83(2):145–175.

Lacombe, H., and P. Tchernia
1960. Quelques traits généraux de l'hydrologie Méditerranéenne. *Cahiers Océanographiques*, 12(8):527–547.

1972. Caractères hydrologiques et circulation des eaux en Mediterranée. Pages 25–36 *in* D. J. Stanley, editor, *The Mediterranean Sea: A Natural Sedimentation Laboratory*. Stroudsburg: Dowden, Hutchinson & Ross, Inc.

Leclaire, L.
1972. Aspects of Late Quaternary Sedimentation on the Algerian Precontinent and in the Adjacent Algiers-Balearic Basin. Pages 561–582 *in* D. J. Stanley, editor, *The Mediterranean Sea: A Natural Sedimentation Laboratory*. Stroudsburg: Dowden, Hutchinson & Ross, Inc.

Letolle, R., and C. Vergnaud-Grazzini
1973. Essai sur l'évolution générale de la Méditerranée pendant les époques glaciaires. *Colloques Internationaux du Centre National de la Recherche Scientifique*, 219:231–238.

Maldonado, A.
1975. Sedimentation, Stratigraphy and Development of the Ebro Delta, Spain. Pages 311–338 *in* M. L. Broussard, editor, *Delta Models for Exploration*. Houston: Houston Geological Society.

Maldonado, A. and D. J. Stanley
1975. Nile Cone Lithofacies and Definition of Sediment Sequences. Pages 185–191 *in* volume 6 in *IXth International Congress of Sedimentology* (Nice).

Margolis, S. V., and D. H. Krinsley
1974. Processes of Formation and Environmental Occurrence of Microfeatures on Detrital Quartz Grains. *American Journal of Science*, 274:449–464.

Mars, P.
1963. Les faunes et la stratigraphie du Quaternaire méditerranéen. *Recueils des Travaux de la Station Maritime d'Endoume*, 28:61–97.

McIntyre, A., and A. W. H. Be
1967. Modern Coccolithophoridae of the Atlantic Ocean: I, Placoliths and Cyrtoliths. *Deep-Sea Research*, 14:561–597.

Middleton, G. V., and M. A. Hampton
1973. Sediment Gravity Flows: Mechanics of Flow and Deposition. Pages 1–38 *in* G. V. Middleton and A. H. Bouma, editors, *Turbidites and Deep Sea Sedimentation*. Pacific Section, Society of Economic Paleontologists and Mineralogists.

Milliman, J. D.
1974. *Marine Carbonates*. 375 pages. New York: Springer-Verlag.

Milliman, J. D., and J. Müller
1973. Precipitation and Lithification of Magnesian Calcite in the Deep-Sea Sediments of the Eastern Mediterranean Sea. *Sedimentology*, 20:29–45.

Milliman, J. D., Y. Weiler, and D. J. Stanley
1972. Morphology and Carbonate Sedimentation on Shallow Banks in the Alboran Sea. Pages 241–259 *in* D. J. Stanley, editor, *The Mediterranean Sea: A Natural Sedimentation Laboratory*. Stroudsburg: Dowden, Hutchinson & Ross, Inc.

Molcard, R.
1972. Preliminary Results of Current Measurements in the Strait of Sicily in May 1970. Pages 82–95 *in* T. D. Allan, R. Akal, and R. Molcard, editors, *Oceanography of the Strait of Sicily* (Conference Proceedings No. 7). La Spezia, Italy: SACLANT ASW Research Centre.

Moore, D. G., and P. C. Scruton
1957. Minor Internal Structures of Some Recent Unconsolidated Sediments. *Bulletin of the American Association of Petroleum Geologists*, 41(12):2723–2751.

Moore, D. G.
1969. Reflection Profiling Studies of the California Continental Borderland: Structure and Quaternary Turbidite Basins. *Geological Society of America, Special Paper*, 107: 142 pages.

Moore, J. C.
1967. Base Surge in Recent Volcanic Eruptions. *Bulletin Volcanologique*, 30:337–363.

Morel, A.
1972. The Hydrological Characteristics of the Waters Exchanged Between the Eastern and the Western Basins of the Mediterranean. Pages 193–207 *in* T. D.

Allan, T. Akal, and R. Molcard, editors, *Oceanography of the Strait of Sicily* (Conference Proceedings No. 7). La Spezia, Italy: SACLANT ASW Research Centre.

Müller, C.
1973. Calcareous Nannoplankton Assemblages of Pleistocene-Recent Sediments of the Mediterranean Sea. *Bulletin of the Geological Society of Greece,* 10(1): 133–144.

Nesteroff, W. D.
1973. Petrography and Mineralogy of Sapropels. Pages 713–720 *in* volume 13 *in* W. B. F. Ryan, K. J. Hsu, et al., *Initial Reports of the Deep Sea Drilling Project.* Washington, D.C.: U.S. Government Printing Office.

Ninkovich, D., and J. D. Hays
1972. Mediterranean Island Arcs and Origin of High Potash Volcanoes. *Earth and Planetary Science Letters,* 16:331–345.

Ninkovich, D., and B. C. Heezen
1965. Santorini Tephra. Pages 413–453 *in* volume 17 in *Proceedings of the Seventeenth Symposium of the Colston Research Society* (The Colston Papers). London: Butterworths Scientific Publications.

Olausson, E.
1961. Sediment Cores from the Mediterranean Sea and the Red Sea. Pages 335–391 *in* number 6 *of* volume 8 in *Reports of the Swedish Deep-Sea Expedition, 1947–1948.*

Oomkens, E.
1970. Depositional Sequences and Sand Distribution in the Post-Glacial Rhone Delta Complex. Pages 198–212 *in* J. P. Morgan, editor, *Deltaic Sedimentation Modern and Ancient.* Society of Economic Paleontologists and Mineralogists (Special Publication 15).

di Paola, G. M.
1973. The Island of Linosa (Sicily Channel) *Bulletin Volcanologique,* 37(2):149–174.

Parker, F. L.
1958. Eastern Mediterranean Foraminifera. Pages 219–283 *in* number 4 *of* volume 8 in *Report of the Swedish Deep-Sea Expedition, 1947-1948.*

Pierce, J. W., and D. J. Stanley
1975. Suspended Sediment Concentration and Composition in the Central and Western Mediterranean and Mineralogic Comparison with Bottom Sediments. *Marine Geology,* 19:M15–M25.

Piper, D. J. W.
1973. The Sedimentology of Silt Turbidites from the Gulf of Alaska. Pages 847–867 *in* volume 17 *in* L. D. Kulm, R. von Huene, et al., *Initial Reports of the Deep Sea Drilling Project.* Washington, D.C.: U.S. Government Printing Office.

Poizat, C.
1970. Hydrodynamisme et sédimentation dans le Golfe de Gabès (Tunisie). *Tethys,* 2(1):267–296.

Reineck, H. E.
1973. Schichtung und Wuhlgefuge in Groundproben vor der ostafrikanischen Kuste. *Meteor,* 16:67–81.

Reineck, H. E., and I. B. Singh
1973. *Depositional Sedimentary Environments.* 439 pages. New York: Springer-Verlag.

Rickard, D. T.
1970. The Origin of Framboids. *Lithos,* 3:269–293.

Rittmann, A.
1967. Studio Geovulcanologico e Magmatologico dell'isola di Pantelleria. *Revista Mineraria Siciliana,* 1967: 106–108.

Ross, D. A., and E. T. Degens
1974. Recent Sediments of Black Sea. Pages 183–199 *in* E. T. Degens and D. A. Ross, editors, *The Black Sea—Geology, Chemistry and Biology.* The American Association of Petroleum Geologists (Memoir No. 20).

Rupke, N. A., and D. J. Stanley
1974. Distinctive Properties of Turbiditic and Hemipelagic Mud Layers in the Algéro-Balearic Basin, Western Mediterranean Sea. *Smithsonian Contributions to the Earth Sciences,* 13: 40 pages.

Ryan, W. B. F.
1972. Stratigraphy of Late Quaternary Sediments in the Eastern Mediterranean. Pages 149–169 *in* D. J. Stanley, editor, *The Mediterranean Sea: A Natural Sedimentation Laboratory.* Stroudsburg: Dowden, Hutchinson & Ross, Inc.

Ryan, W. B. F., D. J. Stanley, J. B. Hersey, D. A. Fahlquist, and T. D. Allan
1971. The Tectonics and Geology of the Mediterranean Sea. Pages 387–492 *in* volume 4 *in* A. E. Maxwell, editor, *The Sea.* New York: John Wiley & Sons.

Sarnthein, M.
1972. Stratigraphic Contamination by Vertical Bioturbation in Holocene Shelf Sediments. Pages 432–436 *in* section 6 in *24th International Geological Congress* (Montreal).

Sarnthein, M. and C. Bartolini
1973. Grain Size Studies on Turbidite Components from Tyrrhenian Deep Sea Cores. *Sedimentology,* 20:425–436.

Scholle, P. A., and S. A. Kling
1972. Southern British Honduras: Lagoonal Coccolith Ooze. *Journal of Sedimentary Petrology,* 42(1):195–204.

Seilacher, A.
1952. Studien zur Palichnologie, I: Uber die methoden der Palichnologie. *Neues Jahrbuch für Geologie und Paläontologie Abhandlungen,* 96:421–452.

Sparks, R. S. J., S. Self, and G. P. L. Walker
1973. The Products of Ignimbrite Eruptions. *Geology,* 1:115–118.

Stanley, D. J.
1970. Fish-produced Markings on the Outer Continental Margin East of the Middle Atlantic States. *Journal of Sedimentary Petrology,* 41:159–170.

Stanley, D. J., C. E. Gehin, and C. Bartolini
1970. Flysch-Type Sedimentation in the Alboran Sea, Western Mediterranean. *Nature,* 228:979–983.

Stanley, D. J., A. Maldonado, and R. Stuckenrath
1975. Strait of Sicily Depositional Rates and Patterns, and Possible Reversal of Currents in the Late Quaternary. *Paleogeography, Paleoclimatology, and Paleoecology,* 18:279–291.

Stanley, D. J., H. Sheng, and C. P. Pedraza
1971. Lower Continental Rise East of the Middle Atlantic States: Predominant Sediment Dispersal Perpendicular to Isobaths. *Bulletin of the Geological Society of America,* 82:1831–1840.

Stieglitz, R. D.
1972. Scanning Electron Microscopy of the Fine Fraction of Recent Carbonate Sediments from Bimini, Bahamas. *Journal of Sedimentary Petrology,* 42(1): 211–226.

Sweney, R. E., and I. R. Kaplan
1973. Pyrite Framboid Formation: Laboratory Synthesis and Marine Sediments. *Economic Geology,* 68:618–634.

Swift, D. J. P.
1974. Continental Shelf Sedimentation. Pages 117–235 *in* C. A. Burk and C. L. Drake, editors, *The Geology of Continental Margins.* New York: Springer-Verlag.

U.S. Naval Oceanographic Office
1965. *Oceanographic Atlas of the North Atlantic Ocean, Section V: Marine Geology* (Publication 700). 71 pages. Washington, D.C.

U.S. Naval Oceanographic Office
1967. *Marine Geophysical Survey Program, 1965–1967: North Atlantic Ocean, Norwegian Sea, and Mediterranean Sea, Area 6.* Volume 5, 42 pages. Dallas: Texas Instruments Incorporated.

Van Andel, T. H. and G. C. Shor, editors
1964. *Marine Geology of the Gulf of California.* 408 pages. The American Association of Petroleum Geologists (Memoir No. 3).

Van Straaten, L. M. J. U.
1970. Holocene and Late-Pleistocene Sedimentation in the Adriatic Sea. *Geologische Rundschau,* 60:106–131.

Van Straaten, L. M. J. U.
1972. Holocene Stages of Oxygen Depletion in Deep Waters of the Adriatic Sea. Pages 631–643 *in* D. J. Stanley, editor, *The Mediterranean Sea: A Natural Sedimentation Laboratory.* Stroudsburg: Dowden, Hutchinson & Ross, Inc.

Villari, L.
1969. On Particular Ignimbrites of the Island of Pantelleria (Channel of Sicily). *Bulletin Volcanologique,* 33(3):1–12.

Visher, G. S.
1965. Use of Vertical Profile in Environmental Reconstruction. *The American Association of Petroleum Geologists Bulletin,* 49:41–61.

Walker, G. P. L.
1973. Explosive Volcanic Eruptions—A New Classification Scheme. *Geologische Rundschau,* 62:431–446.

Whalley, W. B., and D. H. Krinsley
1974. A Scanning Electron Microscope Study of Surface Textures of Quartz Grains from Glacial Environments. *Sedimentology,* 21:87–105.

Wüst, G.
1961. On the Vertical Circulation of the Mediterranean Sea. *Journal of Geophysical Research,* 66(10):3261–3271.

Zarudzki, E. F. K.
1972. The Strait of Sicily—A Geophysical Study. *Revue de Géographie Physique et de Géologie Dynamique,* 14(1):11–28.